Influence of biochar properties on sorption and remobilization of organic contaminants – Implications for environmental remediation

Dissertation

Doctoral thesis submitted in partial fulfillment of the requirements for the degree Doctor rerum naturalium (Dr. rer. nat.)

TECHNISCHE UNIVERSITÄT DARMSTADT

Department of Material and Earth Sciences
Technische Universität Darmstadt

Inga Johanna Schreiter (M.Sc. Angewandte Geowissenschaften)

born on 7 August 1988 in Erlangen, Germany

Supervisor: Prof. Dr. Christoph Schüth
Co-supervisor: Prof. Dr. Peter Grathwohl
Examiner: Prof. Dr. Matthias Hinderer
Examiner: Prof. Dr. Wolfgang Ensinger

Darmstadt, 2021

Schreiter, Inga Johanna

Title: Influence of biochar properties on sorption and remobilization of organic contaminants – Implications for environmental remediation

Darmstadt, Technische Universität Darmstadt

Publication on Tuprints: 2022

Thesis defense: 13 December 2021

URN: urn:nbn:de:tuda-tuprints-203914

URl: https://tuprints.ulb.tu-darmstadt.de/id/eprint/20391

Published under CC-BY-SA 4.0 International

https://creativecommons.org/licenses/

Declaration of authorship

I hereby declare that the presented dissertation is based on original research and is the result of my own work. I certify that this dissertation contains no material that has been accepted for the award of any other degree in my name, in any university or other tertiary institution and, to the best of my knowledge and belief, contains no material previously published or written by another person, except where due reference has been made in the text.

Darmstadt, 01 November 2021

Publications associated with this thesis

In the course of this thesis, several publications and conference presentations emanated from the conducted work. Four papers were published in ISI journals, whereby two were first-author papers.

Peer-reviewed articles (ISI journals)

Schreiter, I.J., Schmidt, W., Schüth, C., 2018. *Sorption mechanisms of chlorinated hydrocarbons on biochar produced from different feedstocks: Conclusions from single- and bi-solute experiments*. Chemosphere 203, 34-43.

Schreiter, I.J., Schmidt, W., Kumar, A., Graber, E.R., Schüth, C., 2020. *Effect of water leaching on biochar properties and its impact on organic contaminant sorption.* Environmental Science and Pollution Research 27, 691–703.

Kumar, A., Joseph, S., Tsechansky, L., Privat, K., **Schreiter, I.J.**, Schüth, C., Graber, E.R., 2018. *Biochar aging in contaminated soil promotes Zn immobilization due to changes in biochar surface structural and chemical properties*. Science of the Total Environment 626, 953-961.

Kumar, A., Joseph, S., Tsechansky, L., **Schreiter, I.J.**, Schüth, C., Taherysoosavi, S., Mitchell, D.R., Graber, E.R., 2020. *Mechanistic evaluation of biochar potential for plant growth promotion and alleviation of chromium-induced phytotoxicity in Ficus elastica.* Chemosphere, 125332.

Conference and book contributions

Kumar, A., **Schreiter, I.J.**, Wefer-Roehl, A., Tsechansky, L., Schüth, C., Graber, E.R., 2016. *Production and utilization of biochar from organic wastes for pollutant control of contaminated sites*. In: Prasad, M.N.V., Shih, K. (Eds.), Environmental Materials and Waste. Academic Press, pp. 91-116.

Schreiter, I.J., Wefer-Roehl, A., Graber, E.R., Schüth, C. *Biochar as a sorbent for chlorinated hydrocarbons – sorption and extraction experiments in single and bi-solute systems* (Short presentation with poster in PICO session; European Geoscience Union General Assembly 2017, Vienna).

Schreiter, I.J., Schmidt, W., Graber, E.R., Schüth, C. *Einfluss künstlicher Alterung von Biokohle auf ihre Sorption von chlorierten Kohlenwasserstoffen* (Poster; Conference of the SETAC German Language Branch „Umwelt 2018“, Münster).

Abstract

Environmental pollution is increasingly recognized as a global concern. Therefore, the development of cost-effective remediation technologies continues to be a growing topic in the scientific community. A material receiving increased attention in the field of soil and water remediation in the last decade is biochar – a carbon-rich product obtained through pyrolysis of organic materials. Biochar can be applied as a sorbent in environmental remediation for a variety of different contaminants.

In this thesis, the sorption and remobilization behavior of two model organic contaminants, trichloroethylene (TCE) and tetrachloroethylene (PCE), on different biochars was investigated to gain a better understanding of biochar-pollutant interaction mechanisms. To this end, a set of laboratory experiments was conducted that are presented in the three core chapters of this thesis. Three biochars produced from cattle manure, grain husk, and wood chips at 450°C were used in all experiments. For selected tests, an activated carbon was included to serve as a fully carbonized reference.

Single- and bi-solute batch adsorption experiments were conducted to study the effects of biochar feedstock on sorption behavior, to explore competitive and concentration-dependent effects in bi-solute systems, and to determine how sorbent properties influence partitioning and adsorption in both systems. In single-solute experiments, all biochars showed stronger sorption for TCE compared to PCE, which was attributed to steric effects. Plant-derived, carbon-rich biochars with high specific surface area and microporosity predominantly sorbed via pore-filling. Biochar produced from manure, with higher ash content and polarity, and smaller total pore volume, showed significant contribution of partitioning. In bi-solute systems, TCE and PCE showed different competition behavior depending on biochar properties. Plant-based biochars are pore-filling-dominated and show strong competition, whereby manure-derived biochar with high polarity and lower total pore volume showed significant partitioning and less competition.

When biochar is applied in remediation technologies, its properties and sorption behavior can be naturally altered by, e.g., dissolution of minerals and mobilization of leachable organic carbon (LOC). This was investigated by artificially leaching the three biochars, characterizing their leachates, determining changes in the biochars' chemical and structural properties, and relating these changes to specific differences in sorption mechanisms. The manure-derived biochar mobilized significantly more LOC and total ions, compared to the two plant-based biochars. Leaching increased external surface area, mesopore volume, and hydrophobicity of the manure-derived biochar, and decreased its polarity. This enhanced sorption via partitioning. In the plant-based biochars, micropore volume and pore size distribution were altered, most likely through the un-blocking of pores, causing increased sorption via pore-filling for both TCE and PCE.

When biochar is applied in remediation technologies, it is not only important to understand the adsorption process, but it is also vital to know if pollutants are sequestered for the long-term or if they are readily released again into the environment. To investigate the influence of biochar properties on the remobilization of organic

contaminants, the three biochars were pre-loaded with defined amounts of TCE and PCE and sequentially extracted with different solvents to analyze their remobilization behavior (water, methanol, toluene, and n-hexane). Water was only able to mobilize a comparably low fraction of the actually extractable mass. A significantly higher mobilized fraction of TCE and PCE was water-extractable from the polar, mesoporous manure-derived biochar. The more hydrophobic sorbents (grain husk biochar, wood chips biochar, and activated carbon), containing significant micropore volume, showed a lower water-extractable fraction. For all biochars, methanol contributed the highest share to the total extracted mass of all solvents at the two lowest pre-loading levels, whereby mass fractions released by toluene and n-hexane were comparably low. The non-extractable fraction appeared to be higher for PCE compared to TCE for the two plant-based biochars. Further, the fraction remaining unextracted was slightly lower at the higher pre-loading level. Overall, the results indicated that contaminant trapping in narrow micropores, especially at low concentrations, significantly influenced the release behavior of sorbed compounds. This supports the well-established hypothesis of contaminant trapping caused by swelling and deformation of the pore structure as a cause for irreversible sorption in the investigated biochars. In addition, overall matrix and pore accessibility governed by sorbent bulk hydrophobicity likely also have an impact.

The results from this thesis highlight that biochar is an excellent sorption material for organic pollutants with great potential for a variety of different applications in environmental remediation. Thereby, feedstock-governed biochar properties show a strong influence on the overall fate of pollutants, indicating that sorbents ultimately could be tailored by feedstock selection.

Zusammenfassung

Die Verschmutzung von Wasser und Boden wird zunehmend als globales Problem erkannt, weshalb die Entwicklung kostengünstiger Sanierungstechnologien im wissenschaftlichen Diskurs zunehmend an Bedeutung gewinnt. Ein Material, das in den letzten Jahren im Bereich der Wasser- und Bodensanierung zunehmend mehr Aufmerksamkeit erfahren hat, ist Biokohle. Biokohle ist ein kohlenstoffreiches Material, das durch die Pyrolyse organischen Materials gewonnen wird und in der Sanierungstechnik als Sorbent für eine Vielzahl unterschiedlicher Schadstoffe eingesetzt werden kann.

In dieser Arbeit wurde das Sorptions- und Remobilisierungsverhalten von zwei typischen organischen Schadstoffen (Trichlorethylen, TCE; Tetrachlorethylen, PCE) auf verschiedenen Biokohlen untersucht, um ein besseres Verständnis für die relevanten Interaktionsmechanismen zu erlangen. Hierzu wurde eine Reihe von Laborexperimenten mit Biokohlen, hergestellt aus den Ausgangsmaterialien Kuhdung, Getreidespelzen und Holzchips (bei 450°C), durchgeführt. In ausgewählten Versuchen diente zusätzlich eine kommerzielle Aktivkohle als Referenzmaterial.

In Einstoff- und Zweistoff-Batchexperimenten wurde das Sorptionsverhalten der beiden Stoffe sowie mögliche Konkurrenz- und Konzentrationseffekte untersucht. Außerdem wurde der Einfluss der Eigenschaften der verschiedenen Sorbenten auf die beteiligten Sorptionsmechanismen näher betrachtet. Im Einstoffsystem sorbiert TCE deutlich stärker als PCE auf allen Biokohlen. Dies kann durch sterische Hinderung erklärt werden. Stark kohlenstoffreiche Biokohle, hergestellt aus Pflanzenmaterial, besitzt eine hohe spezifische Oberfläche, sowie eine große Anzahl von Mikroporen. Daher findet Sorption hauptsächlich durch Porenfüllung statt. Im Gegensatz dazu zeigte die aus Kuhdung hergestellte Biokohle, mit hohem Aschegehalt, höherer Polarität und geringerem Porenvolumen, einen deutlichen Anteil von „Partitioning“ an der Gesamtsorption. Im Zweistoffsystem, zeigten TCE und PCE unterschiedliches Konkurrenzverhalten, welches deutlich durch die Eigenschaften der Biokohlen beeinflusst wurde. In den aus Pflanzenmaterial hergestellten Biokohlen, in denen Sorption hauptsächlich durch Porenfüllung stattfindet, konnte ein ausgeprägtes Konkurrenzverhalten der beiden Schadstoffe gezeigt werden. Im Unterschied dazu wurde in der Kuhdung-Biokohle, mit hoher Polarität und geringem Porenvolumen, eine deutlich geringere Konkurrenz zwischen TCE und PCE festgestellt. Dies wurde auf den größeren Einfluss von „Partitioning“ zurückgeführt.

Wird Biokohle in der Sanierungstechnik eingesetzt, können sich ihre Eigenschaften durch natürliche Lösungsprozesse verändern. Dazu zählen zum Beispiel die Lösung von mineralischen Phasen oder die Mobilisierung von löslichen, organischen Kohlenstoffspezies. Der Einfluss dieser Veränderungen auf die Sorptionsfähigkeit von Biokohle wurde untersucht, indem diese durch Extraktion mit Wasser einem künstlichen Lösungsprozess unterzogen wurde. Anschließend wurden die Eluate hydrochemisch charakterisiert, sowie Elementzusammensetzung, spezifische Oberfläche und Porenstruktur der eluierten Biokohlen bestimmt. Ferner wurde das Sorptionsverhalten der beiden Schadstoffe TCE und PCE an den eluierten Biokohlen in

Batchversuchen getestet. Aus der Kuhdung-Biokohle wurden große Mengen an löslichem, organischem Kohlenstoff, sowie Ionen gelöst. Die Eluate der beiden übrigen Biokohlen zeigten deutlich geringere Lösungskonzentrationen. Alle drei Biokohlen zeigen deutliche Veränderungen ihrer strukturellen und chemischen Eigenschaften. Nach der Elution konnte für die Kuhdung-Biokohle eine erhöhte Hydrophobizität, eine größere externe Oberfläche, größeres Mesoporen-Volumen, sowie geringere Polarität nachgewiesen werden. Diese Veränderungen führten gleichzeitig zu einem größeren Anteil von „Partitioning“ an der Gesamtsorption. Für die beiden Biokohlen aus Pflanzenmaterial wurde dagegen eine Veränderung des Mikroporenvolumens, sowie der Porengrößenverteilung festgestellt. Diese führte zu einem Anstieg der Sorption beider Schadstoffe, durch vermehrte Porenfüllung.

Neben dem Sorptionsverhalten von Sorbenten, ist die Frage nach einer möglichen Remobilisierung sorbierter Schadstoffe von großem Interesse. Um diesen Aspekt zu untersuchen, wurden die Biokohlen mit einer definierten Menge TCE oder PCE beladen und anschließend mit vier unterschiedlichen Lösungsmitteln sequenziell extrahiert (Wasser, Methanol, Toluol und n-Hexan). In allen Versuchen konnte mit Wasser nur eine geringe Menge der gesamtlöslichen Masse extrahiert werde. Dabei wurden von der Kuhdung-Kohle deutlich größere Anteile TCE und PCE mobilisiert als von den beiden aus Pflanzenmaterial hergestellten Biokohlen. Dies konnte auf die unterschiedlichen chemischen und strukturellen Eigenschaften zurückgeführt werden. Dabei spielt neben der Polarität der Sorbenten hauptsächlich das Mikroporenvolumen eine entscheidende Rolle. Von allen Biokohlen konnte der größte Anteil löslicher Schadstoffe mit Methanol extrahiert werden. Im Gegensatz dazu, konnten mit Toluol und n-Hexan nur geringe Mengen extrahiert werden. Im Allgemeinen scheint für die beiden Biokohlen aus Pflanzenmaterial die nicht extrahierbare Masse an PCE höher zu sein. Des Weiteren erscheint der nicht extrahierbare Anteil bei geringerer Schadstoffbeladung leicht höher. Die Ergebnisse lassen vermuten, dass besonders bei geringen Konzentrationen, Schadstoffe in engen Mikroporen festgehalten werden. Dieser Prozess kann das Elutionsverhalten von Schadstoffen deutlich beeinflussen. Das beobachtete Verhalten scheint die gängige Hypothese des Festhaltens von Schadstoff in Mikroporen durch Quellen und Deformation der Porenstruktur als Ursache für irreversible Sorption zu unterstützen. Zusätzlich scheint auch die Zugänglichkeit von Porosität und Gesamtmatrix eine Rolle zu spielen. Diese werden wiederum durch die Gesamt-Hydrophobizität des Sorbenten beeinflusst.

Insgesamt konnte in dieser Arbeit gezeigt werden, dass Biokohlen ein exzellentes Sorptionsmaterial für organische Schadstoffe darstellen, was ein großes Potenzial für den Einsatz in der Sanierungstechnik mit sich bringt. Dabei sind die Eigenschaften der Sorbenten, die stark durch die Auswahl des Ausgansmaterials beeinflusst werden, von entscheidender Bedeutung.

Table of contents

List of figures

List of tables

List of abbreviations

AC	Activated carbon
ASE	Accelerated solvent extractor
BC	Biochar
BET theory	Brunauer, Emmett, and Teller theory
CEC	Cation exchange capacity
CM	Cattle manure
C_S	Concentration of a sorbed compound on the solid phase
C_{sat}	Saturation concentration in the aqueous phase (in the BET isotherm)
$C_{S,0}$	Maximum saturated monolayer adsorption capacity of the Langmuir isotherm
C_W	Concentration of a compound in the aqueous phase
D_{mes}	Maximum of the mesopore size distribution
C_{Org}	Organic carbon content
D_{mic}	Maximum of the micropore size distribution
DOC	Dissolved organic carbon
E	Characteristic free energy of adsorption
EC	Electrical conductivity
ECD	Electron capture detector
FID	Flame ionization detector
GC	Gas chromatograph
GH	Grain husk
H/C	H/C molar ratio (indicative of the sorbent aromaticity)
IBI	International Biochar Initiative
IUPAC	International Union of Pure and Applied Chemistry
K_d	Distribution coefficient
K_{Fr}	Freundlich coefficient
K_{FR}*	Unit-equivalent Freundlich coefficient
K_L	Langmuir coefficient
K_{OC}	Organic carbon normalized partitioning coefficient
K_{om}	Organic matter normalized partitioning coefficient
K_{OW}	Octanol-water partitioning coefficient
K_p	Linear partitioning coefficient
LFER	Linear free energy relationship
LOC	Leachable organic carbon

MS	Mass spectrometer
n	Freundlich exponent
NLDFT	Non-local density functional theory
OC	Organic carbon
O/C	O/C molar ratio (indicative for the sorbent hydrophobicity)
O+N/C	O+N/C molar ratio (indicative for the sorbent polarity)
PAH	polycyclic aromatic hydrocarbons
PCE	Tetrachloroethylene/perchloroethylene
pK_a	Acid dissociation constant
PV_{mes}	Mesopore volume
PV_{mic}	Micropore volume
PV_{tot}	Total pore volume
R	Ideal gas constant
SSA	Apparent specific surface area
SSA_{ext}	External specific surface area
S_W	Water solubility
T	Temperature
TCE	Trichloroethylene
V_0	Maximum adsorbed volume of sorbate per unit mass
V_{om}	Molar volume of organic matter
W	Pore width
WC	Wood chips
ρ	Sorbate density
ρ_{om}	Density of organic matter
γ_{om}	Activity coefficient of the solute in organic matter

1. Introduction

1.1. Motivation

Widespread contamination of soil and water is a global environmental concern. Anthropogenic activities in industrial and urban areas, as well as in agricultural settings continue to cause negative effects on the environment, and negatively affect soils, surface waters, and groundwater resources all over the world.

Environmental pollution can occur through several different routes, for example diffuse or point sources, and encompasses both organic (e.g., pesticides and pharmaceuticals) and inorganic (e.g., nitrate and heavy metals) contaminants. Examples for common input pathways are the widespread use of industrial fertilizers, plant protection products and antibiotics in agriculture, the release of untreated wastewater and sewage or improper waste disposal in urban areas, or the extensive use and spillage of industrial chemicals. These activities can lead to severe risks in global environmental and human health, for instance by affecting drinking water quality or food safety.

Many authorities have implemented measures to protect and restore water resources, sediments, and soils, like the European Union's Water Framework Directive (European Comission, 2000) or the "Superfund" program of the United States Environmental Protection Agency (US EPA, 2021). Further, the United Nations have included the provision of safely managed drinking water into the UN Sustainable Development Goals (UN Environment, 2019). Therefore, the development of cost-effective and sustainable technologies to protect, remediate, and restore the different environmental compartments, and to supply clean water, continues to be a growing topic in the scientific community.

Soil, sediment, and (ground)water remediation of both inorganic and organic contaminants utilizes either *in-situ* or *ex-situ* technologies. *Ex-situ* techniques usually remove the contaminated soil/sediment or water by excavation or pumping and treat it off- or on-site. Popular technologies are groundwater pump-and-treat, soil washing, or simply "dig-and-dump" or incineration of contaminated material (Kuppusamy et al., 2016a). However, especially in populated and built-up areas or ecologically sensitive settings, these options are not always feasible. Therefore, *in-situ* technologies like adsorbent capping, bio- or phytoremediation, natural and enhanced natural attenuation, reactive barrier technologies, or advanced oxidation methods are also attractive remediation options (Kuppusamy et al., 2016b; Zhang et al., 2017).

A material receiving increased attention in the field of soil and water remediation in the last decade is biochar. Biochar is a carbon-rich product obtained through pyrolysis of organic materials such as plant residues or organic waste (Lehmann and Joseph, 2009). It is attractive for both *in-situ and ex-situ* applications as it is an excellent adsorbent for a variety of inorganic and organic contaminants. The immobilization of pollutants through sorption is one of the most commonly applied techniques in remediation and biochar could act as a low-cost and easily available alternative for materials such as, for example, commercial activated carbon in water treatment (*ex-situ*) or soil amendments used to stabilize contaminants in sediments or soils (*in-situ*).

Additional to its immobilization potential, biochar shows a number of agronomic benefits when applied to soil, for example improved soil properties (Xie et al., 2016) and crop yields (Kumar et al., 2018), enhanced microbial activity (Palansooriya et al., 2019a), and improved plant health (Kumar et al., 2018). This gives the unique opportunity to potentially improve remediation efforts, for example by boosting phytoremediation of heavy metals (Paz-Ferreiro et al., 2014) or enhancing the microbial degradation of organic contaminants (Zhu et al., 2017). One seemingly easy option to reduce environmental pollution is to minimize the release of untreated wastewater or sewage, as well as urban runoff. In this context, biochar has the potential to decrease pollutant loads in these waters, by incorporating it into on-site wastewater treatment (Dalahmeh et al., 2019) and sewage filter systems (Nguyen et al., 2020), and low impact developments (Mohanty et al., 2018) or bioreactors for stormwater treatment (Ashoori et al., 2019).

All above mentioned biochar applications have one aspect in common: a detailed knowledge of the adsorption- and remobilization-behavior of the target pollutants on biochar is essential for its safe and effective use.

Several researchers have worked on expanding the knowledge on the relevant processes over the last two decades. When looking at the number of scientific articles published in this time-period, it is evident that the interest in biochar-related topics is continuously growing (Figure 1). Since 2010, the fraction of articles listed in the Web of Science Core Collection that deal with biochar-related topics is rising exponentially (purple data set). Among these articles, the sub-topics “soil” (blue), “sorption” (yellow), and “remediation” (red) are among the most popular ones. This indicates that the application of biochar in environmental remediation is an emerging field of research that is continuously growing.

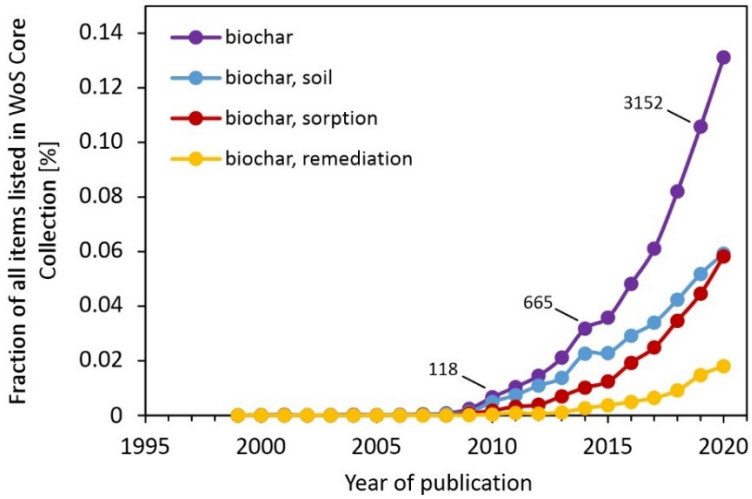

Figure 1: Bibliometric analysis of trends related to selected environmental topics in the biochar research domain. The terms were searched in the “*Topic”* field of the Web of Science Core Collection. The obtained number of items found per year was divided by the total number of items published in that year for normalization. The resulting fractions (points) were complemented by the absolute number of items in that year (black labels). More details on the search strategy and search terms used are available in Appendix A1.

1.2. Study aims and thesis outline

Although there is an undeniably large body of literature on biochar properties and its function in the environment, its influence on contaminant sorption behavior (e.g., Ahmad et al., 2014b), and its application in water and wastewater treatment (e.g., Inyang and Dickenson, 2015) as well as in soil remediation (e.g., Beesley et al., 2011), there are still several questions that remain unanswered. In order to safely apply biochar in pollution control and environmental remediation technologies, it is vital to understand the underlying mechanisms that govern both the adsorption and remobilization of contaminants.

The overall aim of this thesis is to expand the knowledge on biochar-pollutant interaction and develop a better understanding of the underlying mechanisms that drive the sorption and remobilization of organic compounds on biochar. To achieve this, different laboratory experiments were conducted that are presented in the three core chapters (chapters 3, 4, and 5) of this thesis and can be summarized as follows:

- Chapter 3: Single compound and bi-solute sorption experiments of organic contaminants on biochars prepared from three different feedstocks, in order to explore driving sorption mechanisms depending on biochar properties and the effects of competitive sorption.
- Chapter 4: Leaching of biochars and its effect on sorption mechanisms to explore long-term release behavior and resulting changes in sorption performance.
- Chapter 5: Accelerated extraction experiments with pre-loaded biochars to study remobilization behavior of organic contaminants depending on biochar properties.

Preceding to these three core-chapters describing original research, chapter 2 provides a general overview on biochar research and gives a theoretical background on the topic of sorption. The final chapter 6 presents an overall conclusion and highlights implications for future research in the biochar field.

2. Theoretical background

2.1. Biochar: A definition and historical considerations

Biochar is a form of pyrogenic carbon that is intentionally produced through the thermochemical conversion of biomass. Lehmann and Joseph (2009) define biochar as a "carbon-rich product obtained when biomass, such as wood, manure or leaves, is heated in a closed container with little or no available air". They put special emphasis on the fact that biochar is intended to be applied to soil to improve its quality and sequester carbon (Lehmann and Joseph, 2009). Although this definition is widely accepted, a variety of descriptions appear in the published literature and reflect biochar's overall complex nature and range of possible applications (Ahmad et al., 2014b; Ok et al., 2015). In 2015, the International Biochar Initiative (IBI) introduced a broader definition, calling biochar "a solid material obtained from the thermochemical conversion of biomass in an oxygen-limited environment" (IBI, 2015) with a variety of possible applications, including remediation and protection against environmental pollution.

Considering its porous nature, chemical composition, and atomic structure, biochar is similar to activated carbon and charcoal. Although all three materials are produced through the thermochemical conversion of biomass, their intrinsic history and originally intended applications are distinct (Hagemann et al., 2018).

Activated carbon is a highly-porous form of carbon that is produced at relatively high temperature (> 700°C) and treated after production to "activate" its surface (Pignatello, 2013). Common feedstock materials include coal, peat, wood, coconut or nut shells, or synthetic polymers (Çeçen and Aktas, 2011; Chen et al., 2011). Activation after pyrolysis is usually done by thermal or chemical treatment, with the goal of removing impurities, oxidizing the surface, and enhancing its sorptive properties (Bansal and Goyal, 2005; Çeçen and Aktas, 2011). Today, activated carbon is extensively used in water treatment and environmental pollution control, as well as in general liquid and gas phase purification (Bansal and Goyal, 2005).

Charcoal is mostly produced from wood and is historically used as fuel and for industrial purposes (Hagemann et al., 2018; Ok et al., 2018). However, its application as a soil amendment also dates back several centuries (Glaser, 2006) and represents a close link to today's biochar research.

Modern-day **biochar** research arose from the discovery of the highly fertile "*Terra Preta di indo*" soils in the Amazonian basin (Schimmelpfennig and Glaser, 2012). Several studies reported the occurrence of charred materials or charcoal in these soils (e.g., Sombroek et al., 1993; Glaser et al., 2001). Glaser et al. (2001) suggested that it originates from the "enrichment with black carbon from residues of incomplete burning produced by the early Amerindian population" (Glaser et al., 2001), and was intentionally added as a soil amendment (Glaser et al., 2002). This pyrogenic carbon is chemically and biologically recalcitrant, and is assumed to be stable in the environment over centuries because of its aromatic structure (Glaser et al., 2002). These findings sparked great interest in soil-charcoal-interaction, and specifically in charcoal (later called biochar) as a soil amendment for sustainable agriculture. The term biochar seemed to first appear in the literature in 1998 (Bapat and Manahan,

1998) describing the solid residual of biomass pyrolysis. However, Lehmann et al. (2006) were the first to systematically introduce the concept of biochar as a soil amendment for carbon sequestration in terrestrial ecosystems and thereby shaped the understanding of biochar as it is mostly referred to in recent literature.

Despite their different applications and (historic) definitions, it is evident that a distinct differentiation between pyrogenic carbon materials is challenging (Hagemann et al., 2018). This is also apparent in the rapidly growing field of biochar research (see Figure 1 and also Wu et al., 2019), where different research domains increasingly overlap. Examples for this overlap are studies on biochar as a precursor of activated carbon (Tan et al., 2017), biochar as an alternative solid fuel source (Yadav et al., 2019), or biochar in functional material development (Liu et al., 2015; Huang et al., 2019).

2.2. Biochar production

As mentioned above, biochar is produced by a controlled pyrolysis process in an oxygen-free atmosphere at moderate temperatures (< 700°C; Lehmann and Joseph, 2009; Pignatello, 2013). Besides biochar as the solid product, pyrolysis also produces bio-oil and syn-gas. The proportions of these three products and the properties of the resulting biochar strongly depend on the chosen pyrolysis process and its conditions, i.e., temperature, heating rate, holding time, as well as the feedstock material (e.g., Ahmad et al., 2014b; Zhang et al., 2019).

Generally, biochar can be produced via different forms of pyrolysis, including slow pyrolysis, fast pyrolysis, flash pyrolysis, and pyrolytic gasification (Manyà, 2012; Liu et al., 2015).

Slow pyrolysis, the traditional carbonization method, is characterized by low heating rates and long vapor residence times (Manyà, 2012). With a yield of 35-50 %, it shows a high biochar production efficiency (Liu et al., 2015) and is usually the preferred method for producing biochar. In contrast, fast pyrolysis with high heating rates and much shorter residence times favors the formation of bio-oil and therefore shows much lower biochar yields (Liu et al., 2015) (see Figure 2). Flash pyrolysis, developed by Antal et al. (2003), produces biochar utilizing a flash fire in a pressurized packed bed of biomass. It promises very fast reaction times (< 30 minutes) and a high fixed-carbon yield in the produced biochar (Antal et al., 2003).

According to Mohan et al. (2011) gasification should be differentiated from pyrolysis, because the biomass is intentionally reacted with air or steam as an oxidizing agent at high temperatures (Mohan et al., 2014). This method is designed to produce syn-gas as the main product and therefore its biochar yield is only about 10 % (Zhang et al., 2019).

Moreover, techniques such as torrefaction and hydrothermal carbonization are reported in the biochar context. Torrefaction is performed at relatively mild temperatures (around 290°C, Zhang et al., 2019) and is therefore also called mild pyrolysis (Kambo and Dutta, 2015). It is mainly applied to produce (bio)char with increased heating value and combustion characteristics (Chen et al., 2015). Therefore, it gained increasing attention in the

bioenergy field. Torrefaction represents the beginning of the pyrolysis process, hence its product represents an in-between stage of the original biomass and biochar (Kambo and Dutta, 2015).

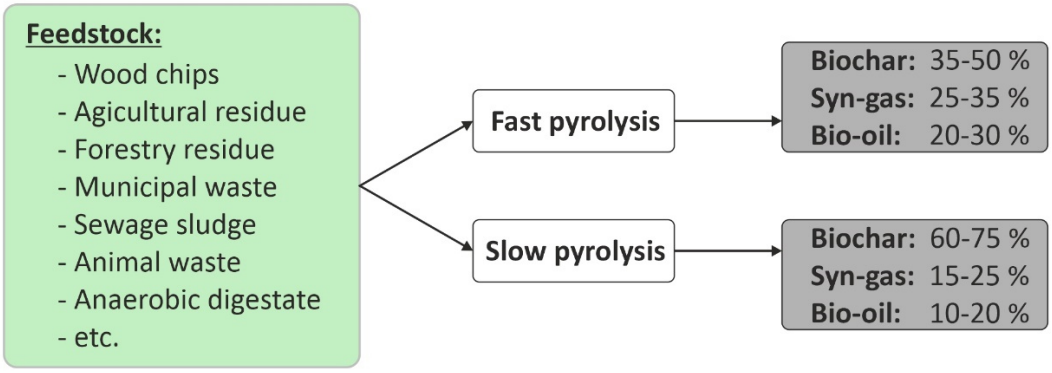

Figure 2: Two modes of pyrolysis commonly applied in biochar production (fast and slow pyrolysis) and their typical product distributions (biochar, syn-gas, and bio-oil) (modified after Al-Wabel et al., 2018).

In the process of hydrothermal carbonization, the solid feedstock material is submerged in water and heated in a closed container (at 180-260°C) under pressure (e.g., Libra et al., 2011; Kambo and Dutta, 2015). It produces a char-water-slurry that is further dried and filtered to yield "hydrochar" as the final product (Kambo and Dutta, 2015). Hydrochar differs from biochar in important properties like the arrangement of the aromatic structure and its elemental composition. This is owed to the different reaction mechanisms during the decomposition process of the biomass (e.g., Libra et al., 2011; Taskin et al., 2019).

2.3. Biochar feedstock and pyrolysis mechanisms

Most biochars are produced from lignocellulosic biomass, like different types of wood (e.g., pine, bamboo, spruce, poplar, hickory) and plants, agricultural wastes (e.g., almond or pecan shells, wheat straw, cottonseed hull, corn stover, rice husk), and weeds (e.g., buffalo weed), but also bagasse, for example from sugar cane or orange pomace. Recently, also non-lignocellulosic biomass has gained increasing attention, due to its unique structure and chemical composition (Li and Jiang, 2017). This includes, for instance, various types of manure and litter, sewage sludge, algae, or bones (Li and Jiang, 2017). A selection of typical feedstocks is also listed in Figure 2.

Most precursory biomass is a combination of cellulose, hemicellulose, and lignin, together with some organic extractives (e.g., fatty acids, proteins) and mineral matter (Brown, 2009). During the pyrolysis process, these components undergo a series of thermochemical reactions, each at different rates and under different temperature regimes (e.g., Liu et al., 2015; Zhang et al., 2019). Despite a lot of research on different pyrolysis techniques, these reaction mechanisms are only partially understood because of the wide variety of possible feedstock materials (Libra et al., 2011) and their unique compositions.

Studies by Yang et al. (2006a) and Yang et al. (2007) investigated the pyrolysis behavior of the three major biomass components cellulose, hemicellulose, and lignin. By utilizing thermogravimetric analysis of the pure synthetic compounds, they revealed that these three main components decompose in specific temperature regimes. Hemicellulose decomposes between 220 and 315°C, whereas cellulose decomposition mainly occurs between 315 and 400°C. In contrast, lignin does not show a specific temperature window, but rather decomposes slowly over a wide temperature range (150-900°C).

Liu et al. (2015) and Zhang et al. (2019) summarized the main processes involved in the decomposition of cellulose and hemicellulose: dehydration, depolymerization, decarboxylation, aromatization, and intramolecular condensation. For lignin, the so-called "free radical reaction" is proposed as the main decomposition pathway (e.g., Kosa et al., 2011; Cho et al., 2012; Chu et al., 2013), however exact mechanisms are still partly unclear (Liu et al., 2015). All reaction mechanisms occur simultaneously during the pyrolysis process and can be influenced by the interaction between the different biomass components (Wang et al., 2011) or affected by inherent mineral species (Hu et al., 2015).

Generally, biochar formation and all related mechanisms are controlled by a number of variables in the pyrolysis process, like the pyrolysis peak temperature, heating rate, vapor residence time, and type of reactor used (e.g., Cha et al., 2016; Zhang et al., 2019).

These parameters together with the feedstock material are the main factors influencing biochar yield and physicochemical properties. As detailed in the previous paragraphs, temperature is a main factor controlling the degradation process of biomass. Increasing the pyrolysis temperature usually results in reduced biochar yield, nutrient content, cation exchange capacity, and extractable cations (Ronsse et al., 2013). It also leads to increased biochar pH, structural aromatization, specific surface area, porosity, ash, and fixed carbon content (e.g., Uchimiya et al., 2011; Suliman et al., 2016). Further, the amount of surface functional groups tends to decrease with increasing pyrolysis temperature (Suliman et al., 2016). However, these trends can significantly vary, depending on feedstock material, as the development of biochar properties is a complicated interplay of biomass composition and the production conditions applied in the pyrolysis process.

2.4. Biochar molecular structure

Biochar is a complex, multi-phase material and, as mentioned previously, its structure is highly variable, depending on the composition of the feedstock material and the different production conditions (e.g., Gwenzi et al., 2017). Lu et al. (2020) described biochar "(…) as a super complex which contains various molecular weight compounds connected which different strength of chemical bonds".

Generally, biochar's structure can be divided into three main phases, the amorphous organic phase, the carbonized organic phase, and the inorganic (mineral) phase. In biochar, these main phases are usually intimately interlaced and a differentiation is rather challenging (Xiao et al., 2018). The distribution of these main

phases is strongly dependent on the relative distribution of cellulose, hemicellulose, and lignin in the original feedstock material (Zhang et al., 2019), as well as on the pyrolysis conditions.

The major elements building the organic phase that can be considered the skeleton of biochar are carbon, hydrogen, and oxygen (Lu et al., 2020). Carbon as the most abundant element in the organic phase, can form aliphatic and aromatic structures, or be incorporated in surface functional groups. With increasing temperature during pyrolysis, the organic carbon phase transitions from its original, crystalline form (as present in cellulose, hemicellulose, and lignin) towards aliphatic carbon and further towards increasingly aromatic composition (Xu and Chen, 2013). Similar to carbon, hydrogen can be incorporated in aliphatic and aromatic structures, or be present in functionalized form (Xiao et al., 2018). With increasing pyrolysis temperature, hydrogen as well as oxygen are lost as volatile products through dehydration and depolymerization of the biomass (Keiluweit et al., 2010). Oxygen tends to redistribute from the interior of the biochar towards its surface at temperatures of about 300 to 400°C (Lian and Xing, 2017). In the organic phase, oxygen is mostly attached to carbon, building a variety of surface functional groups (Xiao et al., 2018). These surface functionalities can dissociate and act as electron donors or acceptors, making them highly important for biochar's reactivity in the environment (see section 2.5.6).

Keiluweit et al. (2010) proposed a dynamic molecular model with four characteristic stages, which illustrates the transformation of the organic phase along a temperature gradient during the formation of wood- and grass-derived chars (Figure 3):

- Stage 1: "Transition char" - initial volatile dissociation products are forming an amorphous center, but most of the crystalline structure of the feedstock material is still intact.
- Stage 2: "Amorphous char" - heat-altered aliphatic elements and initial small aromatic units build a randomly mixed amorphous carbon phase.
- Stage 3: "Composite char" - poorly-ordered, stacked graphene sheets (turbostratic crystallites) are mixed in an amorphous matrix composed of aliphatic and oxygen-containing components.
- Stage 4: "Turbostratic char" - all amorphous carbon is converted into aromatic rings, building increasingly ordered turbostratic crystallites.

This dynamic molecular evolution leads to the development of diverse biochar properties, depending on feedstock composition and pyrolysis conditions (Kleber et al., 2015).

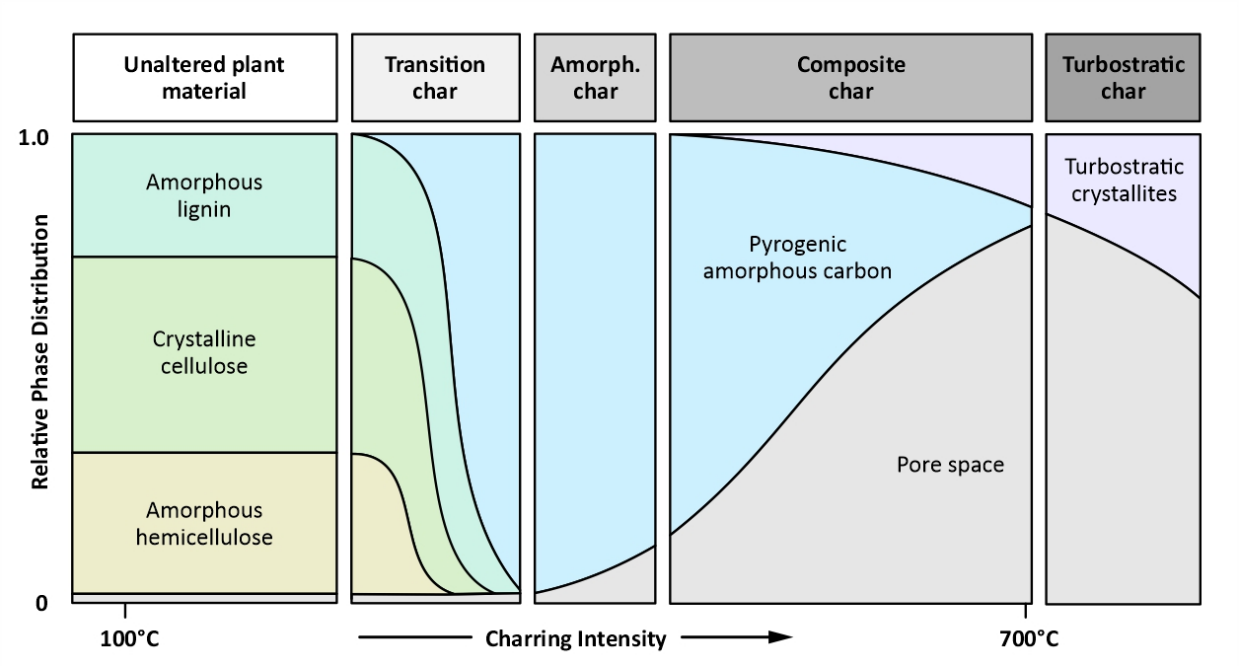

Figure 3: Evolution of the molecular structure of plant biomass-derived biochar along a charring gradient and schematic representation of the four proposed char categories/stages with their physical and chemical characteristics (modified after Keiluweit et al., 2010).

Additional to the organic phase, biochar contains an inorganic fraction that is closely interlaced with the carbon structure (Xiao et al., 2018). It influences and interacts with the organic phase of the biochar, for example by influencing the pyrolytic behavior of biomass (Vijayaraghavan, 2021 and references therein). The inorganic elements can either exist as amorphous or crystalline structures scattered on the surface or in pores, or be associated with the surface functional groups (Wang et al., 2015). This fraction is usually called the ash or mineral content and its composition strongly depends on feedstock material and pyrolysis conditions (refer to section 2.5.3.).

2.5. Biochar properties

The physical and chemical properties of biochar play an important role in its function in the environment and are crucial for its application. As highlighted in the previous section, biochar is a multi-phase material with a complex molecular structure and its properties are highly variable depending on multiple factors, i.e., feedstock material and processing conditions.

The following section presents a selection of biochar properties that are important for its function in environmental applications and an overview of typical measurement techniques. This is not an exhaustive list, but rather highlights a selection of characteristics that are deemed important in biochar-pollutant interaction. Although the properties are presented as individual characteristics, one has to keep in mind that most of these properties are interrelated and influence each other.

2.5.1. Bulk elemental composition

One of the fundamental characteristics of biochar is its bulk elemental composition, comprised of the amounts of carbon (C), hydrogen (H), oxygen (O), nitrogen (N), and sulfur (S) in the sample. These elements are usually determined with an elemental analyzer by dry combustion and reported in percent [%] on dry weight basis. In most biochars, C is the most abundant element. However, its amount varies from as low as 15 % for manure and sewage sludge biochars (Lu et al., 2013) to about 90 % in biochars prepared from wood (Mukome et al., 2013). Considering the pyrolysis temperature, biochar C content usually increases with increasing production temperature (Suliman et al., 2016). The remaining elements (H, O, N, and S) are usually less abundant, whereby O, N, and S are mostly present in the form of a variety of surface functional groups (see section 2.5.6). The amount of O and H usually decreases with increasing production temperature (Keiluweit et al., 2010), whereas the trend for N is less consistent (Xie et al., 2015).

Although the elements are often reported as bulk fractions, one has to keep in mind that they occur in different molecular forms in biochar, having different functions in the overall structure (see section 2.4). While the bulk elemental composition does not consider this functionality, it is still a useful tool as it is easy to measure and allows to gain some basic understanding of the material.

2.5.2. Molar elemental ratios

The molecular properties of biochar can be approximated by calculating typical molar elemental ratios that are based on the bulk elemental composition (see section 2.5.1). The aromaticity ratio H/C is a measure of the amount of C=C bonds (Leng et al., 2019) and therefore allows to estimate the degree of carbonization of the biochar (high ratio represents low aromaticity). The O/C ratio as a measure of hydrophobicity is also frequently reported (high ratio represents low hydrophobicity). Both H/C and O/C ratios usually decrease with increasing pyrolysis temperature as a result of dehydration and depolymerization and the development of a more condensed biochar structure (Keiluweit et al., 2010). Additionally, the polarity ratio (O+N)/C is often reported as a proxy for the abundance of oxygen-containing functional groups (high ratio suggest high polarity and abundant functional groups). It usually shows decreasing values with increasing production temperature, as functional groups are continuously lost during pyrolysis (Suliman et al., 2016).

2.5.3. Ash content

Beside the elements reported in the bulk composition, biochar contains other mineral elements, which can be summarized as the so-called “ash content”. It is determined gravimetrically after decomposition of the organic portion of the sample, usually in a muffle furnace at 750°C, and reported in percent [%] of total dry mass. Generally, biochars produced from plant materials yield distinctly less ash compared to biochars derived from sludge or manure (Mukome et al., 2013; Zhao et al., 2013a). Biochars produced at higher pyrolysis temperatures often yield more ash (Cao and Harris, 2010), as mineral species concentrate while large parts of the organic

portion are lost through volatilization during pyrolysis (Xu et al., 2017). The ash content is an important fraction, as it influences other biochar properties, like biochar pH, surface chemistry, and porosity (Xu et al., 2017). It also determines the nutrient value of biochar, as it can contain soluble nutrients like potassium (K), magnesium (Mg), or manganese (Mn) that can be released into the soil.

Therefore, besides the amount of ash, its composition is also of interest. It is usually measured by ICP-AES or ICP-MS after dry ashing and wet digestion (using different acids or hydrogen-peroxide) of the sample and reported by weight [mg g^{-1} or mg kg^{-1}] or percent [%] of element of the dry mass. Besides digestion methods, also X-ray fluorescence (XRF) analysis is commonly applied for elemental analysis. Biochars can contain a variety of elements including alkali metals (K and Na) and alkaline earth metals (Ca and Mg), and a variety of trace elements including different heavy metals (Mn, Fe, Cr, etc.). The ash composition is highly variable and depends mostly on the elements in the feedstock and only moderately on the pyrolysis temperature (Zhao et al., 2013a). Liu et al. (2015) showed that biochars produced from wood-based biomass contain significantly lower inorganic matter compared to biochars derived from herbaceous or hydrophyte biomass, and Zhao et al. (2013a) highlighted that plant-residue-derived biochars contain less minerals compared to sludge- or manure-derived biochars.

Besides total element determination, X-ray diffraction (XRD) is often applied to determine discrete mineral species. Typical minerals in biochar include, but are not limited to, quartz, carbonates, phosphates, sulfates, sylvite, or other potassium salts (e.g., Yuan et al., 2011; Prakongkep et al., 2015). With increasing pyrolysis temperature, mineral elements in biochar tend to become more crystallized (Yuan et al., 2011), significantly affecting their solubility, which usually decreases with increasing temperature (Xu et al., 2017).

2.5.4. Specific surface area, pore volume, and pore size distribution

The specific surface area of biochars is usually determined by gas adsorption and reported in [m^2 g^{-1}]. Besides the specific surface area, the pore volume and its distribution among the different pore sizes is equally important. The total pore volume and the micropore volume are also derived from gas sorption measurements and both reported in [cm^3 g^{-1}]. According to the recommendations of the International Union of Pure and Applied Chemistry (IUPAC), pores are classified into three groups by their respective size: Micropores with a diameter < 2 nm, mesopores with a diameter of 2 - 50 nm, and macropores > 50 nm (Sing et al., 1985). Their distribution is displayed in a plot of the size-weighted pore volume [cm^3 $(g\ nm)^{-1}$] or the incremental pore volume [cm^3 g^{-1}] against the pore width [nm].

The traditional and widely used method to measure surface area, pore volume, and pore size distribution of porous samples has been nitrogen (N_2) adsorption at 77K (Thommes and Cychosz, 2014). However, in recent years the application of other probing gasses like krypton (Kr at 77K), carbon dioxide (CO_2 at 273K), or argon (Ar at 87K) has gained increasing attention. Kr is only utilized for samples with very low surface area and rarely applied in biochar studies. By contrast, CO_2 sorption (at 237K) attracted attention in the biochar community

(Igalavithana et al., 2018), because it allows to characterize very narrow micropores as small as 0.4 nm in width. Further, diffusion of CO_2 (at 273K) into the pores is much faster compared to N_2 or Ar (at cryogenic temperature) enabling much shorter measurement times. Despite these advantages, measurements performed with CO_2 at 273K only cover a maximum pore size of 1 nm (Thommes et al., 2015), requiring a complementary analysis with N_2 or Ar to achieve full sample characterization. Additionally, several studies have reported that because of their large quadrupole moment, both CO_2 and N_2 are prone to exhibit specific interactions with surface functional groups (Thommes and Cychosz, 2014; Thommes et al., 2015). This impacts the micropore filling pressure resulting in incorrect pore size distributions. Therefore, a recent IUPAC report recommends Ar at 87K for the pore size analysis of microporous solids with polar functional groups (Thommes et al., 2015), which includes biochars (e.g., Xiao et al., 2018) as well as activated carbons (e.g., Heidarinejad et al., 2020).

In general, it is important to keep in mind that the results obtained with different probing gases are not readily interchangeable as they target different pore size ranges and therefore data comparison should be done with great care. Pituello et al. (2015) characterized 20 different biochars with both N_2 and CO_2 gas sorption, revealing that values obtained with CO_2 can be more than 200-fold higher compared to values from N_2 measurements.

The specific surface area and pore volume of biochars is highly variable. Values measured by N_2 sorption range from as low as 0.5 $m^2 g^{-1}$ for poultry litter biochar (Pituello et al., 2015) to over 600 $m^2 g^{-1}$ for biochar produced from pine wood (Chen et al., 2017).

Thereby, both feedstock and pyrolysis temperature have significant influence on the development of surface area and porosity (Aller, 2016). Generally, surface area and pore volume increase when the pyrolysis temperature increases (Chia et al., 2015; Weber and Quicker, 2018). Keiluweit et al. (2010) attributed the rise in N_2 surface area at high temperatures to the lateral growth of graphene sheets during the conversion of amorphous carbon to graphitic crystallites (see Figure 3). Because the resulting graphene sheets are significantly denser, this phase transition leads to the development of small pores, especially in the micro- and nanopore range (Keiluweit et al., 2010), where the majority of biochar surface area is located (Pignatello, 2013). However, some studies observed a decrease in surface area at very high pyrolysis temperatures. Brown et al. (2006) produced biochars from pine wood at temperatures from 450 to 1,000°C and found the highest surface area at 750°C. Weber and Quicker (2016) concluded that the maximum surface area is usually reached between 650 and 850°C, depending on feedstock material and heating rate. Chia et al. (2015) hypothesized that this is the result of the collapse of some parts of the biochar pore structure at high temperatures. Fu et al. (2012) suggested structural ordering, pore widening, coalescence of neighboring pores, or pore blocking as possible reasons for reduced porosity in high temperature chars. A data set compiled by Ippolito et al. (2020) in the course of a meta-analysis illustrates the trend of increasing biochar surface area with increasing pyrolysis temperature (Figure 4). It also indicates the decrease of surface area at very high temperatures, however only supported by a small number of data points.

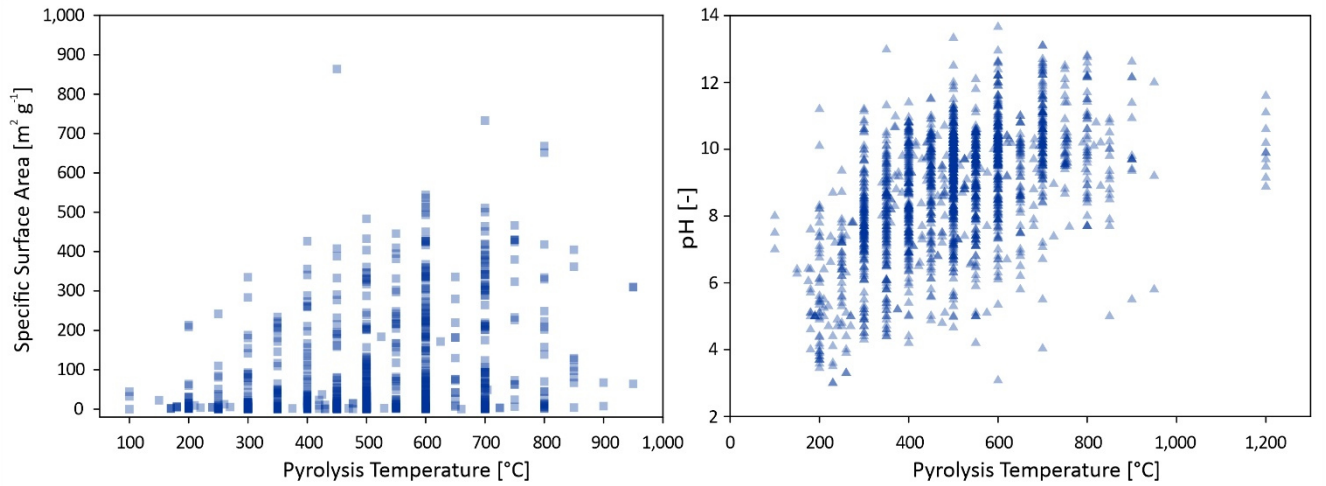

Figure 4: Exemplary data illustrating the increasing trend of specific surface area (left) and pH (right) of biochars with increasing pyrolysis temperature. Note the apparent decrease of surface area at very high temperatures, however only supported by a small number of data points. Data compiled and kindly provided by Ippolito et al. (2020).

Generally, biochars produced from wood exhibit larger surface area and porosity compared to other feedstock types (Ippolito et al., 2020). Lima et al. (2010) and Zhao et al. (2013a) attributed differences in structural properties to varying proportions of hemicelluloses, cellulose, and lignin in the precursory materials. Biochars produced from manure often feature lower porosity and surface area (Ippolito et al., 2020), probably because of their higher initial ash content (Tomczyk et al., 2020).

Surface area and porosity are among the most important properties that influence the ability of biochar to adsorb organic compounds (Ahmad et al., 2014b). Further, studies have also shown that high porosity biochar can increase the field capacity and plant-available water in coarse-grained soils (Wang et al., 2019).

2.5.5. pH and electrical conductivity

Two basic yet important properties are the pH and the electrical conductivity (EC) of biochars. Both pH and EC, the latter reported in [µS cm^{-1}], are usually measured in aqueous extracts obtained at a defined biochar to water ratio (often a 1:10 or 1:50 ratio). Most biochars are basic in nature (pH > 7), making them a valuable option for ameliorating soil acidity (Wan et al., 2014). Their pH is influenced by two different factors, being the amount of soluble salts (e.g., carbonates) in the ash content and the presence of oxygen-containing functional groups (Mukome et al., 2013), which can donate protons into solution. Biochar pH tends to increase with increasing pyrolysis temperature (e.g., Li et al., 2017; Ippolito et al., 2020), which likely is due to the loss of acidic functional groups and the formation of carbonate mineral phases (Cao and Harris, 2010; Ippolito et al., 2020). Figure 4 displays a data set collected by Ippolito et al. (2020) for a meta-analysis that nicely illustrates this trend. The EC of biochars can vary from only a few µS cm^{-1} to several mS cm^{-1}. It is a measure of soluble ions in the sample and therefore mostly influenced by the amount and nature of the ash content.

Both, pH and EC are mostly important for the agricultural application of biochar, for example as an indicator of their nutrient value or their applicability as a soil liming agent (Al-Wabel et al., 2018). However, pH and EC are also important characteristics that can influence the fate of organic and inorganic contaminants. Examples are the influence of biochar pH and EC on the sorption of heavy metals (Thomas et al., 2020) and ionizable organic compounds (Sigmund et al., 2016).

2.5.6. Surface functional groups

The surface chemistry of biochars is manifold and complex, and is an important property influencing biochars' chemical interaction with the environment. Generally, biochar surfaces can be hydrophilic, hydrophobic, acidic, or basic, and their nature strongly depends on feedstock material and production conditions (Amonette, 2009). Amongst these, surface functional groups (basic and acidic) are one of the most important surface properties. They include, but are not limited to, hydroxyl, epoxy, carboxyl, acyl, carbonyl, ether, ester, amido, sulfonic, and azyl groups (Xiao et al., 2018). While there is a large variety of surface functionalities, research has mostly focused on oxygen-containing functional groups (phenolic, carboxyl, carbonyl, and ester groups), as they are the most abundant type on biochar (Xiao et al., 2018 and references therein). However, recently other functional groups, for instance nitrogen-containing functionalities have received increasing attention (e.g., Leng et al., 2020).

Surface functionalities can be measured with several chemical or spectroscopic methods. Traditionally, the Boehm titration (Boehm et al., 1964) is used to quantify acidic functional groups on black carbon or activated carbon, and has also been widely adopted for biochar characterization (Fidel et al., 2013; Tsechansky and Graber, 2014). It allows the determination of three main groups of functionalities that are determined by their acid dissociation constants (pK_a values): carboxylic, lactonic, and phenolic. Complementary, there are several spectroscopic methods that can identify a variety of surface functionalities. The most commonly applied techniques are Fourier transform infra-red spectroscopy (FTIR) and X-ray photoelectron spectroscopy (XPS), but also the application of more sophisticated methods like ^{13}C nuclear magnetic resonance (NMR) or near-edge X-ray adsorption fine structure spectroscopy (NEXAFS) have been reported.

Under different environmental conditions, surface functional groups can dissociate and act as electron donors or acceptors (Xiao et al., 2018 and references therein). Therefore, understanding the nature and behavior of biochar functional groups is essential, for example for the retention of charged ions and the influence of biochar on nutrient cycling in soil (Al-Wabel et al., 2018 and references therein), or the sorption of metals (Li et al., 2017 and references therein) and ionizable organic compounds (Kah et al., 2017 and references therein).

Generally, biochars produced at higher temperatures contain fewer surface functional groups, because O and H are increasingly lost from the biochar structure when the pyrolysis temperature increases, and condensation occurs (Keiluweit et al., 2010). Further, the type and composition of the feedstock material can have a pronounced influence on the nature of surface functionalities (e.g., Antonangelo et al., 2019), which is mainly

due to the different decomposition mechanisms of cellulose, hemicellulose, and lignin (Hassan et al., 2020 and references therein; see also section 2.3). For example, Qiu et al. (2014) and Wang et al. (2016b) found higher surface polarity (O/C and (O + N)/C ratios indicative for polar surface functional groups; see section 2.5.2) for animal waste-derived biochars compared to biochars produced from plant residues. Qiu et al. (2014) suggested that the higher mineral content in animal waste biochars protects the polar functional groups from being removed during the pyrolysis process.

2.6. Biochar application

Biochar has a wide range of possible applications. As previously discussed, Lehmann et al. (2006) introduced the concept that biochar can serve as an amendment to sequester carbon in soils and thereby contribute to climate change mitigation. Biochar serves as a carbon sink for atmospheric CO_2 that is transferred into the soil system and can be stored for long periods of time (Lehmann et al., 2006). Through the conversion of the biomass to biochar, its immediate decay is prevented (Woolf et al., 2010), resulting in less greenhouse gas emission into the atmosphere. Several researchers also report that biochar application can reduce the release of other greenhouse gasses, i.e. N_2O (Cayuela et al., 2014) and CH_4 (Jeffery et al., 2016). However, the effect of biochar on the carbon and nitrogen cycle in soil is not straightforward, as it also seems to depend on soil type and biochar properties.

The agricultural use of biochar is another highly relevant application domain. Biochar amendment not only changes soils' elemental composition by adding organic carbon, but can also alter a variety of other important soil properties. By increasing the soil pH and the cation exchange capacity (CEC), biochar can alleviate soil acidity, increase the retention and availability of nutrients, and decrease the accessibility of toxic elements to plants (e.g., Dai et al., 2017; Kavitha et al., 2018). Additionally, biochar itself can supply essential nutrients like C, N, P, and K to low fertility soils (e.g., Faria et al., 2018). Its application can also benefit the soil microbial community by providing a viable habitat for bacteria, increase the soil stability, water holding capacity, and soil texture (e.g., Anyika et al., 2015; Gul et al., 2015).

These immediate effects can improve the overall productivity of plants in above ground biomass and crop yield (e.g., Graber et al., 2010; Biederman and Harpole, 2013) and increase their resistance to diseases (e.g., Kumar et al., 2018). Therefore, biochar is suggested as a valuable tool to restore degraded soils and improve their agricultural productivity.

However, most of the reported benefits can be strongly dependent on factors like biochar type, soil type, and also climatic conditions. Several studies are mostly observational, and a more in-depth mechanistic understanding is needed to effectively predict biochar behavior in the field. Further, a potential downside of biochar application might be a reduced efficacy of pesticides used in agriculture (Nag et al., 2011; Graber et al., 2012).

Despite the reported positive effects of biochar on soils and plants, several researchers have also raised concerns with biochar application to agricultural soils. If produced from contaminated feedstock or under uncontrolled conditions, biochar can contain high amounts of contaminants, for example heavy metals or polycyclic aromatic hydrocarbons (PAHs) (Lian and Xing, 2017). By applying contaminated biochar to soil, contaminants can be mobilized into the environment and potentially pose risks to plants and organisms in soil and water (Bastos et al., 2014), or even human health (Wang et al., 2018; Liu et al., 2019c).

Besides its use in agriculture, biochar gained a lot of attention in the soil remediation field. It can be applied to soil and act as a sorbent for a variety of contaminants, strongly influencing their fate in the environment (e.g., Beesley et al., 2011; Xie et al., 2015). These include heavy metals like arsenic, zinc, chromium, copper, lead, or cadmium. Several pot-based laboratory studies have shown that biochar application to contaminated soil can immobilize heavy metals and reduce their bioavailability, phytoavailability, and phytotoxicity (e.g., Beesley et al., 2010; Karami et al., 2011; Park et al., 2011; Herath et al., 2015). By promoting plant growth, biochar also has the potential to enhance the phytoextraction of several heavy metals (Břendová et al., 2015; Gascó et al., 2019). Although the majority of studies is laboratory-based, a growing number of plot and field trials have been published over the last years, investigating heavy metal fate under different land use and climatic conditions. A recent review by O'Connor et al. (2018) concluded that the main influencing factor in reducing heavy metal bioavailability is the increase in soil pH after biochar application. However, effectiveness can strongly vary depending on site-specific conditions, application period, or biochar type, and the positive effect can decrease with time due to biochar aging (O'Connor et al., 2018). Most importantly, the authors found that the majority of field trials was undertaken in the humid subtropical regions of China. Therefore, data might be biased towards this climatic region (O'Connor et al., 2018).

Besides heavy metals, the fate of a variety of organic contaminants in soil can be influenced by biochar amendment. A variety of laboratory and pot studies suggest that biochar application can enhance the immobilization of a wide range of contaminants, for instance, PAHs (Beesley et al., 2010; Gomez-Eyles et al., 2013), petroleum hydrocarbons, antibiotics such as sulfamethazine (Vithanage et al., 2014) and sulfamethoxazole (Srinivasan and Sarmah, 2015), pesticides like atrazine (Cao et al., 2011) and diuron (Yang et al., 2006b), chlorinated compounds (Song et al., 2012; Song et al., 2013), and polychlorinated biphenyls (PCBs) (Denyes et al., 2012). Biochar can also significantly impact the leaching behavior, bioavailability, and bioaccumulation of contaminants (e.g., Yang et al., 2006b; Xu et al., 2012; Rajapaksha et al., 2014). Further, some studies suggested that biochar can potentially enhance the natural degradation of contaminants in soil by stimulating the growth of degrading soil microorganisms (e.g., Qin et al., 2013; Zhu et al., 2017). However, other researchers proposed that immobilization by biochar can decrease degradation, as it limits the availability of the compounds for microorganisms (e.g., Zhang et al., 2004; Jones et al., 2011).

Nevertheless, only a limited number of field studies have been conducted to date. Denyes and colleagues conducted two different field trials in soils historically contaminated with PCB (Denyes et al., 2013) and DDT

(Denyes et al., 2016), and reported reduced bioavailability for both compounds after biochar application. One long-term field study with PAH contaminated soil confirmed that biochar addition can reduce bioaccumulation and additionally promote plant growth (Oleszczuk et al., 2017). Gámiz et al. (2016) showed in a field trial with artificially spiked soil that biochar application reduces leaching of the fungicides tebuconazole and metalaxyl, but slowed down their degradation. Stefaniuk and colleagues applied sewage sludge together with biochar in several field experiments and confirmed that the addition of biochar reduces freely available PAHs, their leaching and toxicity, and additionally stimulates PAH degradation in the soil (Stefaniuk and Oleszczuk, 2016; Stefaniuk et al., 2017; Stefaniuk et al., 2018). In general, more long-term field studies are needed in order to understand the multifaced effects that biochar has on both heavy metal and organic contaminant fate in soil, especially to understand long-term effects.

Besides soil remediation, biochar has also been intensively studied for the remediation of contaminated water (e.g., Ahmad et al., 2014b; Mohan et al., 2014). A large database of laboratory-based studies confirms that biochar can act as a sorbent for a variety of contaminants that may be present in surface water, groundwater, drinking-water, or wastewater. Contaminants studied include organic compounds like dyes (e.g., methyl violet and methylene blue; Xu et al., 2011; Liu et al., 2012), PAHs (e.g., naphthalene and phenanthrene; Chen and Chen, 2009; Qiu et al., 2014), and chlorinated compounds (e.g., trichlorobenzene; Han et al., 2016). In recent years, the focus has shifted towards emerging micro-pollutants, like personal care products (e.g., sulfamethoxazole and diclofenac; Zheng et al., 2013; Lonappan et al., 2018), agrochemicals (e.g., atrazine, simazine, imidacloprid; Zheng et al., 2010; Mandal et al., 2017), and fluorinated compounds (Xiao et al., 2017). Studies investigating sorption of inorganic contaminants have intensely focused on the removal of heavy metals (Inyang et al., 2016). However, also other inorganic compounds of concern have been studied, including fluoride (Mohan et al., 2012), nitrate (Gai et al., 2014), ammonium (Gao et al., 2015), and phosphate (Hollister et al., 2013). While early studies were more descriptive, over the last decade several sorption mechanisms were identified (discussed in detail in section 2.7.1), and studies grew to be more mechanistic in nature. Generally speaking, sorption mechanisms for both inorganic and organic compounds are complex, because they depend on both the compound of interest and the properties of the utilized biochar.

Until today, most studies have focused on batch- or small-scale column studies that do not allow direct predictions for long-term applications in water treatment, and an understanding of important engineering aspects, like relevant process parameters, is still lacking (Palansooriya et al., 2019b).

Multiple efforts have been made to enable biochar for storm water treatment in low impact developments (Reddy et al., 2014; Mohanty et al., 2018), the treatment of drinking and reuse water (Inyang and Dickenson, 2015; Gwenzi et al., 2017), tertiary wastewater treatment (Huggins et al., 2016; Thompson et al., 2016), as well as sewage treatment (Dalahmeh et al., 2018). However, only a very limited number of studies have tested biochar in real-world applications for water treatment (Gwenzi et al., 2017). Klasson et al. (2013) successfully tested a small-scale column with an activated almond shell biochar for the removal of dibromochloropropane

from municipal well water. Kuoppamäki et al. (2019) conducted lysimeter studies to evaluate the impact of biochar addition on contaminant retention in artificial biofilter structures, containing sewage sludge-derived compost, that are used for stormwater infiltration.

Besides environmental applications, biochar is gaining increased interest in engineering and material science, for example for its use in construction material (Gupta and Kua, 2017), in engineered nano-composites (Premarathna et al., 2019), in different functional materials (Liu et al., 2015; Huang et al., 2019), or its application as a catalyst (Lyu et al., 2020). This is not an exhaustive list as the research domain around biochar is continuously evolving.

2.7. Sorption of organic compounds on carbonaceous materials

2.7.1. Sorption mechanisms of organic contaminants

Mechanisms driving the sorption of organic molecules on carbonaceous sorbents are manifold and usually depend on both the properties of the sorbent itself and the characteristics of the organic compound. In recent years, numerous review papers have summarized important interaction mechanisms of both non-polar and ionizable organic compounds with carbonaceous sorbents (e.g., Pignatello, 2011; Kah et al., 2017; Pignatello et al., 2017; Tong et al., 2019).

The following chapter does not aim to provide an in-depth discussion of all possible driving forces, but rather highlights some important mechanisms that influence organic contaminant sorption.

Generally, intermolecular forces that characterize the interaction of the sorbate and the sorbent can be divided into three categories: chemisorption, ion exchange, and physisorption (Pignatello, 2011).

Chemisorption involves the formation of covalent bonds and is generally not considered as a sorption mechanism (in a strict sense), as it is irreversible (Kah et al., 2017). However, it has been suggested to play a role in ionizable organic compound sorption, for example in the sorption of aniline on carbon nanotubes (Wu et al., 2013).

Ion exchange is a significant process in the environmental system and an important interaction mechanism of ionizable organic compounds with functionalized carbonaceous sorbents (see section on electrostatic interactions below).

The force most prevalent in hydrophobic organic contaminant sorption is physisorption. It describes the formation of weak intermolecular bonds, where the nature of the molecule is preserved. It is in principle reversible and may be further subdivided into adsorption and absorption. According to Tong et al. (2019), adsorption describes the “attachment” of a molecule to a solid phase, whereas absorption describes the process of partitioning into a solid phase and should not be called a “sorption mechanism”. However, several researchers include partitioning as a prevalent “interaction or sorption mechanism” between biochar and organic compounds and often describe sorption as a combination of a partitioning and adsorption processes (e.g., Chen

et al., 2008). Pignatello (2011) noted that *per se* a distinction between adsorption and absorption is more phenomenological and might not always be useful at a molecular scale.

Dissolution-type sorption or "partitioning" is the historic paradigm of organic compound sorption to natural organic matter in soils and sediments (Pignatello, 2011). It can be described as the dissolution of an organic compound into the bulk phase (Chefetz and Xing, 2009) or the "intermingling of a molecule within the atomic/molecule lattice of a solid" (Pignatello, 2011). Absorption via partitioning is usually concentration-independent, i.e. linear, described by linear sorption isotherms and can be estimated via empirical equations from solubility or K_{OW} data (e.g., Allen-King et al., 2002 and references therein) (see also section on the K_{OC}-K_{OW} concept in chapter 2.7.3). In carbonaceous sorbents (e.g., biochar), partitioning usually takes place in the non-carbonized, amorphous phase that is mostly composed of aliphatic and polyaromatic compounds (Abbas et al., 2018). In order for the solid phase to accommodate the incoming molecule, a "cavity" needs to be created, requiring a sorption free energy depending on parameters such as, for example, molecular size (Pignatello, 2011 and references therein).

In contrast, adsorption encompasses a variety of different interaction mechanisms that "act simultaneously and additively in combinations appropriate to the structures of the interacting species" (Pignatello, 2011).

Weak molecular interactions via "London-van der Waals" forces are expected to occur to a certain extent in all types of sorptive interaction, although they remain hard to quantify (Kah et al., 2017). They arise when non-ionic, uncharged molecules interact with uncharged surfaces via permanent or induced dipole-dipole interactions (Pignatello, 2011), mostly via dispersion (Schwarzenbach et al., 2003). Together with solvophobic effects, also called hydrophobic effects or hydrophobic interactions, they sometimes are referred to as "nonspecific or hydrophobic sorption" (Kah et al., 2017).

As a large part of the surface of carbonaceous materials is hydrophobic in nature (e.g., Pignatello, 2013), one might easily conclude that hydrophobicity is the main driving force in organic contaminant sorption. Indeed, the so-called "hydrophobic effect" or "hydrophobic interaction" is a phenomenon that is frequently described in the literature in the context of hydrophobic contaminant sorption. Pignatello (2011 and 2013) describes the hydrophobic effect as "the sum of forces that limit the solubility of a-polar molecules or parts thereof in water" and gives a comprehensive overview of its causes. According to Pignatello (2013), the tendency of a-polar molecules to "escape" the water phase is not caused by direct repulsion between the hydrophobic molecule and the water molecule, nor by any special attractive forces towards the sorbent. It rather is the effect of "the disruption of the cohesive energy of water as a result of bringing the a-polar entity into solution" (Pignatello, 2013). This disruption is the result of the greater ordering of the water molecules and the reduced number of water-water hydrogen bonds that exist in the hydration shell that surrounds the hydrophobic, a-polar molecule, compared to the bulk water phase (e.g., Pignatello, 2011; Pignatello, 2013; Kronberg, 2016). This causes an increased "entropy and/or enthalpy penalty" for the solution of the a-polar molecule in water (Pignatello, 2011). This highlights that the "hydrophobic effect" is not driven by intermolecular forces (Tong et al., 2019). Therefore,

the often used terms “hydrophobic interaction” or “hydrophobic bonding” are actually not appropriate (Pignatello, 2011).

Although hydrophobic effects certainly contribute to organic compound sorption to a significant extent, several studies have demonstrated that it is not the sole cause of sorption. When sorption data were normalized for the hydrophobic effect with the aid of the octanol-water coefficient, hexadecane-water coefficient, benzene-water coefficient, or the water solubility (e.g., Kleineidam et al., 2002; Zhu and Pignatello, 2005), there still was considerable difference in the sorption of different organic compounds. Therefore, other forces than purely hydrophobicity clearly contribute to organic compound sorption.

One important type of interaction between carbonaceous sorbents and organic molecules are π-interactions (Pignatello et al., 2017). This mechanism traditionally describes the interaction of the π-electron clouds of two arenes with differing π-electron densities (Pignatello, 2013), but can also involve the interaction of the π- cloud of one arene with cations, anions, or proton-donor molecules (Pignatello et al., 2017). According to Pignatello (2013), the most prominent force in these types of interaction seems “to be attraction between quadrupole moments of the opposing ring systems, resulting in a sandwich or parallel-displaced alignment”. In the context of carbonaceous sorbents, the polyaromatic or fused rings that form upon carbonization can serve as both electron-donors or electron-acceptors (Keiluweit and Kleber, 2009). Zhu and Pignatello (2005) demonstrated π-π-interactions between charcoal and π-accepting molecules (nitroaromatic compounds) and π-donating molecules (PAHs). Another special type is the π^{+}- π-interaction, where the π- π electron donor-acceptor complex is further supported by a cation-π interaction. This was observed, for instance, by Teixidó et al. (2011) as one force contributing to the sorption of cationic-sulfamethazine to biochar. Although large efforts were made in recent years, the nature of these π-interactions is not fully understood (Pignatello, 2013).

“Coulombic forces”, also called “electrostatic interactions”, occur between two charged moieties (Tong et al., 2019). This type of specific interaction can play an important role in the sorption behavior of ionizable organic compounds, like organic dyes, pesticides, and pharmaceuticals (Kah et al., 2017). These compounds can interact with the (mostly negatively) charged surfaces of functionalized carbonaceous sorbents, like biochar. The surface charge mostly originates from the deprotonation of acidic functional groups. Thereby, it is important to note that electrostatic interactions can be attractive or repulsive in nature. Xu et al. (2011) observed the electrostatic attraction between methyl violet, a cationic dye, and the carboxylate and phenolic hydroxyl groups of biochar. Sigmund et al. (2016) suggested that electrostatic repulsion between the dissociated form of aromatic acids and deprotonated carboxy groups hindered sorption. As both, the deprotonation of the surface functionalities (and therefore the surface charge) and the ionic state or the sorbing compounds are pH-dependent, electrostatic interactions are strongly influenced by experimental and environmental conditions, like solution pH and ionic strength.

Another type of specific interaction is the formation of hydrogen (H)-bonds between a hydrogen donor and a hydrogen acceptor (Tong et al., 2019). These are usually represented by an electronegative atom (e.g., F, N, or

O) and the electropositive center of a functional group (e.g., -OH and -NH) (Kah et al., 2017). As functional groups are plentiful on biochar surfaces, the formation of H-bonds is quite likely. Li et al. (2020) have suggested that H-bonding between (non-ionized) sulfamethoxazole and polar functional groups on biochar contributed to sorption. However, ordinary H-bonding remains hard to prove experimentally and only little direct evidence has been presented until now (e.g., Kah et al., 2017; Pignatello et al., 2017). Further, in an aqueous environment it is likely that bulk water will outcompete solute molecules that are present at a much lower concentration (Pignatello, 2013). Therefore, clusters of water molecules forming at polar surface groups can thermodynamically block specific sorption sites (Pignatello, 2013). However, Pignatello and co-workers have recently presented evidence for a charge-assisted H-bond, which is stronger in nature and is able to outcompete water (Pignatello et al., 2017). Studies by Teixidó et al. (2011) and Ni et al. (2011) found this type of interaction between weak organic acids (sulfamethazine and allelophatic aromatic acids) and surface carboxylate or phenolate groups on biochar.

An important driving force in organic compounds sorption, which is not technically classified as a sorption mechanism as it does not describe attachment (Tong et al., 2019), is (micro)pore-filling. Carbonaceous sorbents like biochar exhibit a significant portion of their surface area in meso- and micropores (see section 2.5.4) that are highly attractive for sorption. Pelekani and Snoeyink (1999) attributed this to a larger free energy change as a result of enhanced adsorption associated with multiple contact points of the adsorbate with the pore walls. Therefore, attractive forces are stronger in pores compared to adsorption on a two-dimensional surface. Further, sorption increases in smaller pores, because the sorption potentials of the pore walls increasingly overlap (Lastoskie et al., 1993) and sorption involves more contact points (Lattao et al., 2014). Pignatello (2013) further explained preferential sorption in pores with the lack of a “cavity penalty”, making pore-filling thermodynamically more attractive than partitioning. Thereby, it should be noted that molecules can be sterically hindered to sorb via pore-filling because of steric effects, like size exclusion (Pignatello, 2013 and references therein). Nguyen et al. (2007) identified pore-filling as an important mechanism in aromatic hydrocarbon sorption on a natural wood char. They also reported an increase in sorption capacity with decreasing molecular diameter (Nguyen et al., 2007), highlighting the importance of steric effects. Further, Lattao et al. (2014) found that size exclusion becomes more prominent, when porosity is dominated by small micropores.

Selected sorption mechanisms of organic compounds are illustrated in Figure 5, together with properties of carbonaceous sorbents that are considered important in the sorption process.

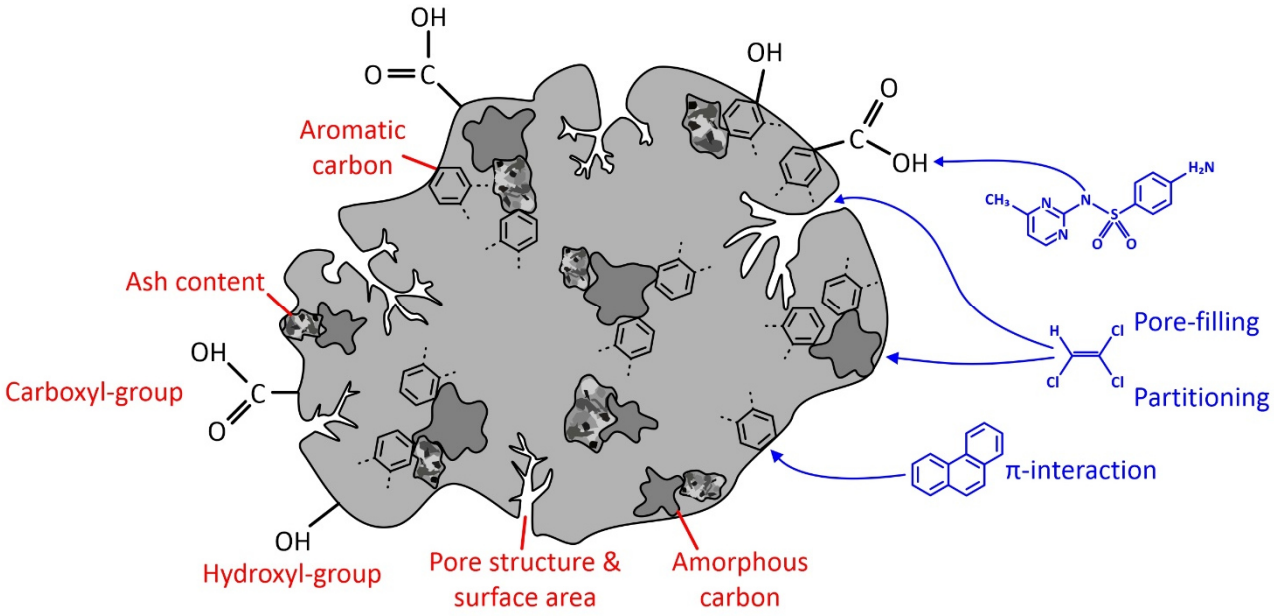

Figure 5: Graphical representation of important biochar properties (in red) and selected sorption mechanisms of different organic molecules on carbonaceous sorbents (in blue).

2.7.2. Sorption kinetics

Sorption kinetics are an important aspect of the overall sorption process. They describe the time-dependent sorptive uptake in a solid/solution system until a thermodynamic equilibrium between adsorption and desorption is reached. This process can take from only a few seconds to up to several months or even years (e.g., Limousin et al., 2007). Generally, the sorption process can be described as a mass transfer of the solute to the sorption site, followed by the solute-sorbent interaction (Tong et al., 2019). Weber (1984) proposed the following four steps associated with the sorption of molecules in porous sorbents: (1) "Bulk transport" of the sorbate in the solution, (2) "film-diffusion" of the sorbate through the immobile water coating surrounding the sorbent, (3) "intra-particle or intra-sorbent diffusion" of the sorbate within the porous matrix of the sorbent, and (4) "adsorptive-attachment". A simplified graphical representation is displayed in Figure 6 below.

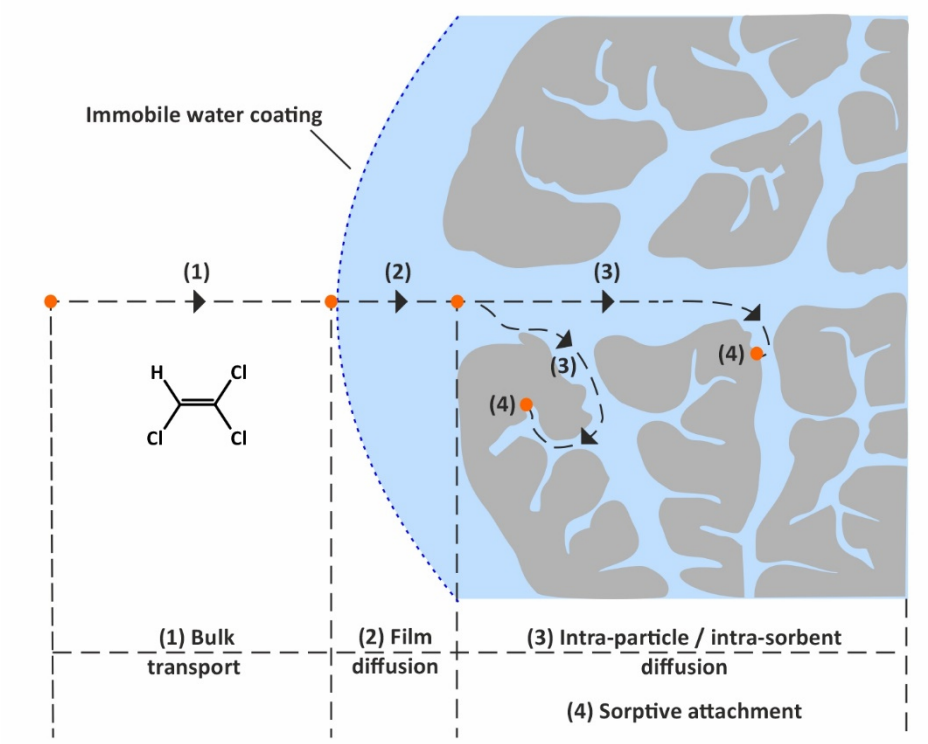

Figure 6: Illustration of sorption kinetics comprising of the four steps (1) bulk transport, (2) film diffusion, (3) intra-particle/intra-sorbent diffusion, and (4) sorptive attachment (adapted from Weber, 1984).

In theory, any of these four steps can be rate-limiting, i.e., retarding in the sorption process. Transport in the bulk solution is usually rapid, especially in well-controlled laboratory experiments (e.g., due to mixing). Therefore, several authors mainly distinguish between diffusion- and reaction-controlled kinetics (e.g., Tong et al., 2019). Brusseau et al. (1991) highlighted that specifically for hydrophobic organic compounds the sorption process is usually fast and Pignatello (1989) showed that interaction energies involved in physisorption are too low to effectively slow down the sorption process. Therefore, the actual sorption process ("sorptive-attachment") is not considered rate-limiting for hydrophobic organic compounds. However, it has to be noted that this might be the case for ionizable organic compounds containing polar functional groups, like pesticides and pharmaceuticals, where specific interactions, for example ion exchange, are of high importance (Ho and McKay, 1998). Film-diffusion through the liquid boundary layer surrounding the sorbent can be rate-limiting, especially in the fast initial stage of sorption (Brusseau et al., 1989; Pignatello and Xing, 1996 and references therein). However, in well-mixed batch systems the concentration gradient controlling diffusion through the liquid film is assumed to be low (Tong et al., 2019), making it a non-rate limiting process. This leaves intraparticle/intrasorbent diffusion as the main rate-limiting step in hydrophobic contaminant sorption (Brusseau et al., 1989). Pignatello and Xing (1996) described this step as diffusion of the molecule in "pores within the particle (pore diffusion), and penetrable solid phase (matrix diffusion)", which well reflects the physical and chemical characteristics of carbonaceous sorbents, like biochar. Chen et al. (2012a) found that naphthalene sorption rates were strongly dependent on pyrolysis temperature-controlled biochar properties.

Biochar produced at low and high temperatures displayed fairly high sorption rates; whereby, biochar produced at intermediate temperatures displayed comparably low sorption rates, caused by slow diffusion into highly condensed organic partitioning phases (Chen et al., 2012a). Chen et al. (2017) observed decreasing carbamazepine sorption rates with increasing degree of carbon condensation in biochar. These findings illustrate that sorption kinetics can be strongly influenced by sorbent properties and their characterization is an important step in understanding the overall sorption process.

2.7.3. Sorption isotherms

When sorption equilibrium is reached in a system, the relationship between the aqueous concentration of a compound (C_W) and the concentration of the sorbed compound on the solid phase (C_S) at a fixed temperature can be described with an empirical relationship, called a sorption isotherm. Generally, isotherm models are a useful tool to elucidate sorption mechanisms, to compare different sorbates and sorbents to each other, or to derive input parameters for environmental fate and transport models (Pignatello, 2013).

The relationship between C_W [mg L^{-1}] and C_S [mg kg^{-1}] at any point of the isotherm is defined by the distribution coefficient K_d [L kg^{-1}].

$$K_d = \frac{C_S}{C_W} \qquad \text{(Eq. 1)}$$

If sorption is independent of the aqueous concentration, K_d becomes the partitioning coefficient K_p [L kg^{-1}] and sorption can be described by a linear isotherm following Henry's law:

$$C_S = K_p\, C_W \qquad \text{(Eq. 2)}$$

Figure 7 (left panel) shows an example plot of C_W versus C_S illustrating a linear isotherm with a constant slope representing the linear partitioning coefficient K_p.

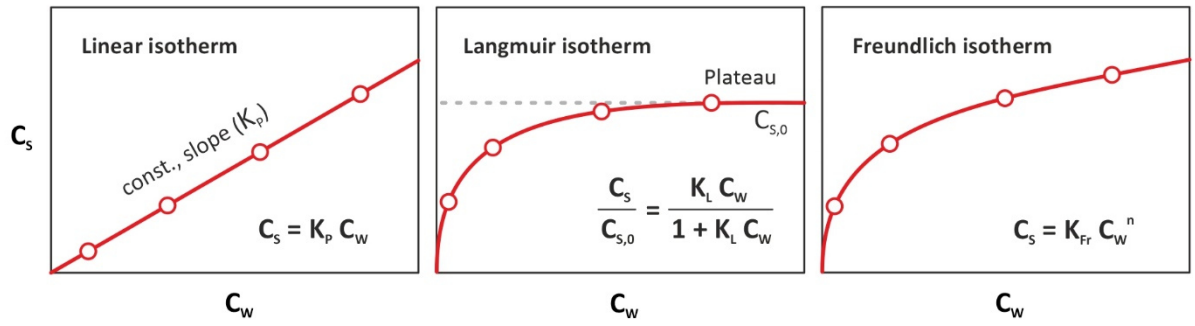

Figure 7: Illustration of the three most commonly applied adsorption isotherm models: the linear isotherm model (Eq. 2), the Langmuir model (Eq. 7), and the Freundlich model (Eq. 9).

In natural environmental materials, like soils and sediments, linear sorption is mostly attributed to the partitioning of (hydrophobic) organic compounds into natural organic matter (Chiou et al., 1979; Karickhoff et al., 1979). Therefore, the partitioning coefficient K_p is often normalized to the organic matter or more frequently

to the organic carbon content of the sorbent (f_{OC} *or* C_{Org}), resulting in the organic carbon normalized partitioning coefficient K_{OC} [L kg^{-1}]:

$$K_{OC} = \frac{K_d}{f_{OC}} \qquad \text{(Eq. 3)}$$

If required, the K_{OC} can be easily converted into the organic matter normalized partitioning coefficient K_{om} (Olsen and Davis, 1990 as cited in Fetter et al., 2017):

$$K_{om} = \frac{K_{OC}}{1.724} \qquad \text{(Eq. 4)}$$

The partitioning process of an organic compound between the water and organic matter phase can be treated similarly to the partitioning between water and an organic solvent (e.g., Chiou et al., 1982; Allen-King et al., 2002). This can be described by Raoults's law (after Schwarzenbach et al., 2003):

$$K_p = \frac{1}{\gamma_{om} V_{om} \rho_{om} S_W} \qquad \text{(Eq. 5)}$$

where γ_{om} is the activity coefficient of the solute in the organic matter [-], V_{om} the molar volume of the organic matter [L mol^{-1}], ρ_{om} the density of the organic matter [kg L^{-1}], and S_W the aqueous solubility of the solute [mg L^{-1}]. This equation illustrates that K_{om} is in theory inversely proportional to the sorbate's aqueous solubility (Allen-King et al., 2002) and can be predicted from sorbent and sorbate properties. However, as organic matter is a heterogenous material and its properties are mostly not known, empirical equations, known as linear free energy relationships (LFERs) are used to estimate K_{OC} values. According to Kleineidam et al. (2002) and Allen-King et al. (2002), the octanol-water partitioning coefficient K_{OW} is more reliable compared to S_w, especially for low solubility compounds. Therefore, LFERs are usually relationships between K_{OC} and K_{OW} (after Schwarzenbach et al., 2003).

$$\log K_{OC} = a \log K_{OW} + b \qquad \text{(Eq. 6)}$$

In this equation *a* and *b* are empirical constants that are dependent on solute properties, as well as on the characteristics of the organic matter (Allen-King et al., 2002). Over the last decades, several researchers have estimated K_{OC} - K_{OW} correlations from own experimental or previously published data for a variety of organic compound classes and different sorbents (e.g., Karickhoff et al., 1979; Chiou et al., 1983; Seth et al., 1999; Schwarzenbach et al., 2003). A comprehensive overview can be found in Allen-King et al. (2002) or in textbooks by Schwarzenbach et al. (2003) and Fetter et al. (2017).

While sorption via linear partitioning into organic matter can be well described by the K_{OC} - K_{OW} concept, sorption on carbonized sorbents, like biochar, is often found to be more complex and does not follow a linear isotherm. Over the last century, a variety of different isotherm models were developed in order to better describe the observed non-linear sorption behavior.

A popular model that is able to describe non-linear sorption is the Langmuir model (Langmuir, 1918). It was developed for the adsorption of gases on solid surfaces (Tran et al., 2017 and references therein), but is also frequently applied to describe adsorption from the liquid phase. Its commonly utilized form is given in Eq. 7.

$$\frac{C_S}{C_{S,0}} = \frac{K_L\, C_W}{1 + K_L\, C_W} \qquad \text{(Eq. 7)}$$

where $C_{S,0}$ [mg kg^{-1}] is the maximum saturated monolayer adsorption capacity and K_L [L mg^{-1}] is the Langmuir coefficient, a constant related to the affinity between the adsorbent and adsorbate. The Langmuir model assumes the formation of a monolayer, where adsorption takes place at a fixed number of sorption sites of the same affinity and no lateral interaction or steric hindrance between the adsorbed molecules occurs (Foo and Hameed, 2010; Tran et al., 2017 and references therein). Graphically, this is represented in the formation of a plateau at high concentrations (Figure 7).

An extension of the Langmuir model is the BET model (Eq. 8), named after their inventors Brunauer, Emmett, and Teller (Brunauer et al., 1938). The BET theory takes the possibility of sorption in multiple layers into account. It assumes that there is no interaction between each adsorption layer and that the Langmuir theory can be applied to each layer (Fetter et al., 2017).

$$C_S = \frac{K_L\, C_{S,0} C_W}{(C_{sat} - C_W)\left[1(K_L - 1)\frac{C_W}{C_{sat}}\right]} \qquad \text{(Eq. 8)}$$

In the aqueous phase, C_{sat} [mg L^{-1}] is equivalent to the water solubility S_W. The BET model is commonly applied in the analysis of gas adsorption measurements for the determination of the specific surface area and pore size distribution of solid samples (see section 2.5.4).

A third popular model, which is one of the earliest empirical equations developed to describe equilibrium sorption on heterogeneous surfaces, is the Freundlich isotherm (Freundlich, 1907; Freundlich, 1909).

$$C_S = K_{Fr}\, {C_W}^n \qquad \text{(Eq. 9)}$$

where K_{Fr} [(mg kg^{-1})/(mg L^{-1})^n] and n [-] are the Freundlich coefficient and Freundlich exponent, respectively (Figure 7). The Freundlich model is the first equation describing non-ideal and reversible adsorption that is not restricted to monolayer adsorption. Therefore, it is widely applied in studies on organic compound sorption to heterogenous sorbents such as activated carbons or molecular sieves (Foo and Hameed, 2010).

However, Carmo et al. (2000) noted that the use of K_{Fr} values for the comparison of sorbates with different aqueous solubilities (S_W) might be misleading. Therefore, aqueous concentrations can be normalized to the water solubility to obtain a unit-equivalent Freundlich coefficient K_{Fr}* [mg kg^{-1}] with units that are independent of the Freundlich exponent n (Carmo et al., 2000):

$$C_S = {K_{Fr}}^* \left(\frac{C_W}{S_W}\right)^n \qquad \text{(Eq. 10)}$$

The unit-equivalent Freundlich coefficient K_{Fr}* can also be calculated from the Freundlich coefficient K_{Fr}:

$$K_{Fr}{}^{*} = K_{Fr}\, S_W{}^{n} \qquad \text{(Eq. 11)}$$

As described previously (see section 2.7.1), several authors found evidence that sorption of organic compounds on carbonaceous sorbents follows a pore-filling process (e.g., Nguyen et al., 2007; Chen et al., 2008; Ahmad et al., 2013b). This process can be described by Polanyi's potential theory (Polanyi, 1916) and non-linear sorption isotherms can be captured by the Polanyi-Dubinin-Manes model (Allen-King et al., 2002). A commonly applied form is given in Eq. 12 (Kleineidam et al., 2002) :

$$C_S = V_0\, \rho\, exp\left[-\left[\frac{RT\left(-ln\frac{C_W}{S_W}\right)}{E}\right]\right]^{b} \qquad \text{(Eq. 12)}$$

where V_0 [cm³ kg^{-1}] is the maximum adsorbed volume of sorbate per unit mass, ρ [g (cm^3)$^{-1}$] the sorbate density, E [J mol^{-1}] the characteristic free energy of adsorption, R [J (mol K)$^{-1}$] the ideal gas constant, and T [K] the absolute temperature. To minimize the number of fitting parameters, b [-] is usually set to an integer between 1 and 5 (Roque-Malherbe, 2000). With b fixed to 2 the Dubinin-Raduskevich equation is obtained (Allen-King et al., 2002), which is used in the following chapters.

As biochar is a highly heterogeneous material, sorption can be a combination of several processes. Therefore, a combined adsorption-partitioning model was proposed with K_p [L kg^{-1}] being the linear partitioning coefficient (Xia and Ball, 1999):

$$C_S = V_0\, \rho\, exp\left[-\left[\frac{RT\left(-ln\frac{C_W}{S_W}\right)}{E}\right]\right]^{b} + K_p C_W \qquad \text{(Eq. 13)}$$

3. Sorption mechanisms of chlorinated hydrocarbons on biochars produced from three different feedstock materials

As highlighted in chapter 2.6, numerous studies have demonstrated that biochar can sorb a wide range of organic contaminants. Due to the heterogeneous nature of biochar, sorption mechanisms are complex and often follow a combined partitioning-adsorption process (Chen et al., 2008; Chen and Chen, 2009; Chiou et al., 2015; Chen et al., 2017). Adsorption mainly takes place in the well carbonized, aromatic structure, whereas partitioning can occur in the non-carbonized phase (Chun et al., 2004). Depending on feedstock and pyrolysis conditions, biochars can contain a significant fraction of this not fully carbonized portion (Mohan et al., 2014).

Although several studies have investigated sorption mechanisms of organic compounds on biochars, most studies focused on effects of biochar pyrolysis temperature on its sorption ability. With a focus on chlorinated hydrocarbons, Ahmad and colleagues investigated buffalo-weed, soybean stover, and pine needle biochars and could show that sorption is positively correlated with surface area, hydrophobicity, and pore volume, which are properties that are strongly influenced by the pyrolysis temperature (Ahmad et al., 2012; Ahmad et al., 2013a; Ahmad et al., 2013b; Ahmad et al., 2014a).

However, only little attention has been paid to the influence of biochar feedstock materials on sorption mechanisms. Especially how feedstock-governed properties influence the distribution of different sorption mechanisms, for example partitioning and pore-filling, has only received little attention. Further, how these sorption mechanisms are interlinked and modified by the properties of the target compound, for instance through the effect of size exclusion, has not been fully understood.

Another important aspect in sorption studies is the effects that occur when multiple compounds are present in the system. Many studies have investigated sorption of organic contaminants in bi-solute systems, including experiments with different biochars. Diverse effects were reported, ranging from strong competition between compounds (e.g., Schaefer et al., 2000; Sander and Pignatello, 2005a; Wang et al., 2006; Zheng et al., 2010; Jung et al., 2015; Wang et al., 2016a) to enhanced sorption of the target compound in the presence of a co-solvent (Chen et al., 2012b). Wu et al. (2017) proposed that competition of two pharmaceuticals (ketoprofen and triclosan) is weaker in a low-temperature, partitioning-dominated biochar than in biochar produced at higher pyrolysis temperature from the same material. However, the effect of biochar feedstock on sorption in bi-solute systems has not been explored in detail. Also, most studies focus on isotherm-effects for the primary solute while adding the competing compound at a fixed concentration. Therefore, information on concentration-dependent effects in bi-solute systems are scarce.

In this chapter, the aim was to (1) study the effects of different biochar feedstocks on the sorption of the two model compounds, trichloroethylene (TCE) and tetrachloroethylene (PCE), (2) explore competitive and concentration-dependent effects in bi-solute experiments, and (3) determine how sorbent properties influence partitioning and adsorption in both systems.

3.1. Materials and methods

3.1.1. Test compounds

In this thesis, two chlorinated hydrocarbons, TCE and PCE, were selected as model organic contaminants, as they are still among the most detected contaminants in soil and groundwater (e.g., Damgaard et al., 2013; Huang et al., 2014), especially in industrialized countries. Both compounds were extensively used for metal degreasing, in dry cleaning, the textile industry, and in the production of chemicals (ATSDR, 2014; Matteucci et al., 2015; ATSDR, 2016) and are therefore of widespread environmental concern. As TCE and PCE have similar physical-chemical properties and applications, they show a similar environmental fate behavior and are often found together on contaminated sites. They are hydrophobic organic molecules and are classified as dense non-aqueous phase liquids (DNAPL). Both compounds are considered probable human carcinogenic (ATSDR, 2014, 2016) and are hence of high environmental concern. Selected physical and chemical properties of both compounds are listed in Table 1.

Table 1: Selected physical-chemical properties of the investigated compounds TCE and PCE.

	Molar mass [g mol^{-1}] [a]	Liquid density ρ [g cm^{-3}] [a]	Water solubility S_W [mg L^{-1}] [a]	Log K_{OW} [-] [a, b]	Molar volume [cm^3 mol^{-1}] [c]	Second largest dimension [Å] [d]
TCE	131.4	1.46	1,093	2.42	90	6.2
PCE	165.9	1.62	141	2.88	102	6.6

[a] All properties at 20°C; obtained from Schwarzenbach et al. (2003).
[b] log K_{OW} represents the octanol-water partitioning coefficient.
[c] Calculated from molar mass and liquid density.
[d] Second largest dimension of the molecule as limiting for size exclusion (1 Å = 0.1 nm). Data obtained from Karanfil and Dastgheib (2004) and Bembnowska et al. (2003).

3.1.2. Sorbent materials and characterization

Three biochars produced via slow pyrolysis at 450°C as the highest treatment temperature were used in the experiments. They were derived from different feedstock materials - cattle manure (BC-CM), grain husk (BC-GH), and wood chips (BC-WC). BC-CM was produced at the Volcani Center (Bet Dagan, Israel) in a batch-pyrolysis unit under nitrogen atmosphere. BC-GH and BC-WC were supplied by the company Sonnenerde (Austria). Additionally to the three biochars, one commercially available powdered activated carbon (AC; Aquasorb G9, Jacobi Carbons, Germany) was included as a fully-carbonized, microporous reference. All sorbents were dried (105°C) for 24 hours in a drying cabinet and the biochars were ground to a fine powder with a vibratory disk mill (Siebtechnik, Germany) before use.

The ash content was determined gravimetrically after heating (750°C, 6 hours) in a muffle furnace (triplicate determination) according to method ASTM D 1762-84 (2013). Elemental composition (C, H, N, and S) was determined in duplicates by combustion (1,000°C) in an oxygen stream using an elemental analyzer (vario EL cube, Elementar, Germany; analysis performed by Zeta Partikelanalytik, Mainz, Germany). The oxygen content

was calculated by mass balance: O = 100 - (C + H + N + S + ash) in weight-% (similar to Kah et al., 2016). Organic carbon content (C_{Org}) was measured in triplicate with a carbon analyzer equipped with an infrared detector (LiquiTOC II, Elementar, Germany). Molar ratios describing aromaticity (H/C), hydrophobicity (O/C), and polarity ((O+N)/C) were calculated from bulk elemental composition.

Specific surface area (SSA), external specific surface area (SSA_{ext}), total pore volume (PV_{tot}), micropore volume (PV_{mic}), and pore size distribution were determined by argon sorption using a Micromeritics 3Flex sorption analyzer (Micromeritics Instrument Co., Norcross, USA) at the Max-Planck-Institut für Kohlenforschung, Mülheim, Germany. Prior to the measurement, the samples were outgassed and dehydrated, first at 110°C for 2 hours followed by 250°C for 9 hours under vacuum. All sorption isotherms were recorded at 87K (temperature of liquid argon as cryogen). The SSA was determined from multiple points using the BET model (Brunauer et al., 1938). The linear data range used for analysis was determined by the method proposed in Rouquerol et al. (2007). PV_{tot} was calculated from the adsorbed volume at a relative pressure close to $P/P_0 = 0.995$. PV_{mic} and SSA_{ext} were determined with the t-plot method using the Statistical Thickness Surface Area (STSA) equation as the reference thickness curve. Analysis of pore size distribution and cumulative pore volume was carried out using the non-local-density function theory (NLDFT) method with the model for argon adsorption in slit-shaped pores on carbon materials at 87K, implemented in the Micromeritics 3Flex software package (Olivier, 1995). Argon (at 87K) was chosen as the adsorbate, because it is non-polar and therefore does not suffer from polar interactions with the surface functional groups of the microporous sample material (Thommes et al., 2015), as detailed in section 2.5.4.

3.1.3. Batch experiment set-up

Equilibrium sorption experiments were conducted in 50 mL glass headspace vials with Teflon-lined crimp top caps in a 0.01 M $NaClO_4$ aqueous background solution (prepared from $NaClO_4$ monohydrate, CAS 7791-07-3, Merck Millipore, Germany) to maintain a constant ionic strength. Appropriate amounts of sorbent (0.4 mg - 0.5 g) were added to the vials to achieve a decrease in solute concentrations of 20 to 90 %. Samples > 15 mg were weighed on an analytical balance (Ohaus Explorer Pro; precision ± 0.1 mg) directly into the headspace vials. Amounts < 15 mg were weighed in tin boats on a micro-balance (Sartorius Micro M 500 P; precision ± 0.01 mg) and transferred to the vials. TCE and PCE were spiked dissolved in methanol. The added volume never exceeded 0.5 % to exclude co-solvent effects (Nkedi-Kizza et al., 1987). All experiments were run in triplicate, accompanied with blank and sorbent-free control samples.

Vials were placed on a horizontal shaker and agitated for 7 days in the dark under ambient conditions (20°C ± 1). Preliminary kinetic experiments had shown that this period is sufficient to reach sorption equilibrium (example data shown in Appendix A2, Figure A 1). Aqueous phase concentrations were determined using static headspace sampling with gas chromatographic (GC) separation, and flame ionization (FID) or electron capture (ECD) detection as detailed in the following section.

3.1.4. Analytical conditions for headspace gas chromatography

Aqueous concentrations of both TCE and PCE were determined via static headspace gas chromatography utilizing an Agilent Technologies Gas Chromatograph GC 6890 equipped with a flame ionization detector (FID) and an electron capture detector (ECD). Sample separation was achieved using a Zebron ZB-5 column (30 m x 250 µm x 0.25 µm) connected to the ECD and an Agilent HP-5 column (30 m x 320 µm x 0.25 µm) connected to the FID. Depending on sample concentration the appropriate detector was chosen (ECD: 0.05 - 2.5 mg L^{-1}; FID: 2.5 - 150 mg L^{-1}). An isothermal oven temperature of 120°C and a constant carrier gas flow of 1.5 mL min^{-1} helium was chosen. Both injection ports were operated in split mode and set to 220°C (Split ratio ECD 1:70; FID 1:50). The ECD was operated at 280°C and constantly flushed with 60 mL min^{-1} N_2 as a make-up gas. The FID flame was run at 150°C with 350 mL min^{-1} air and 35 mL min^{-1} H_2 flow. For sample application, 250 µL of headspace was withdrawn from the sample vials and manually injected using a 500 µL gas-tight glass syringe (Pressure Lock®, VICI Precision Sampling, Baton Rouge, Louisiana, USA). All sample concentrations were quantified utilizing external standards.

3.1.5. Data analysis

For data evaluation, the Freundlich model (Eq. 9), the Polanyi-theory-based pore-filling model (Eq. 12), and the combined adsorption-partitioning model (Eq. 13) were fitted to the data obtained from the batch experiments (see section 2.7.3). Additionally, the unit-equivalent Freundlich coefficients were calculated according to Eq. 11. Sorption coefficients including standard errors and confidence intervals were derived by dynamic curve fitting in the software SigmaPlot 12.0 (Sysstat Software Inc., USA). Sorption coefficients of different data sets were considered to be significantly different when their 95 % confidence intervals did not overlap.

Pearson correlation analysis between sorption coefficients, as well as the contribution of partitioning and sorbent properties was conducted using the software SigmaStat 4.0 (Sysstat Software Inc., USA).

3.2. Results and discussion

3.2.1. Sorbent properties

As all biochars were produced at the same pyrolysis temperature, the results of the sorbent characterization show that biochar properties are strongly feedstock-dependent (Table 2).

Table 2: Chemical and structural properties of the four sorbents.

	BC-WC	BC-GH	BC-CM	AC
C [%]	73.7	55.8	22.7	89.8
H [%]	2.5	3.3	1.1	2.4
N [%]	0.5	1.5	1.3	0.6
S [%]	0.4	0.4	0.7	0.4
Ash content [%]	12.5	26.6	62.8	4.8
C_{Org} [%]	68.7	53.7	23.5	84.4
O [%] [a]	10.5	12.4	11.4	1.9
H/C [b]	0.40	0.71	0.55	0.32
O/C [b]	0.11	0.17	0.38	0.02
(O+N)/C [b]	0.11	0.19	0.43	0.02
SSA [$m^2 g^{-1}$] [c]	341	215	6	921
SSA_{ext} [$m^2 g^{-1}$] [d]	58	60	6	n.d.
PV_{tot} [$cm^3 g^{-1}$] [e]	0.173	0.136	0.023	0.540
PV_{mic} [$cm^3 g^{-1}$] [f]	0.109	0.061	n.d.	0.265
PV_{mes} [$cm^3 g^{-1}$] [g]	0.064	0.075	0.023	0.275
D_{mic} [nm] [h]	0.64	0.78	n.d.	0.55; 1.2
D_{mes} [nm] [h]	2.8	2.9	n.d.	2.9

[a] O determined by difference.
[b] Molar ratios describing aromaticity (H/C), hydrophobicity (O/C), and polarity ((O+N)/C) of the sorbents (ratios based on bulk elemental composition).
[c] Apparent specific surface area (BET method).
[d] Specific external surface area (t-plot method).
[e] Total pore volume determined at P/P_0=0.995.
[f] Micropore volume (t-plot method).
[g] Mesopore volume (PV_{tot} - PV_{mic}).
[h] Maxima of micropore and mesopore size distribution (NLDFT method).
n.d. Not determined.

BC-CM shows the highest ash content (62.8 %), followed by BC-GH (26.6 %) and BC-WC (12.5 %). This is consistent with previous studies, suggesting that wood- and crop-derived biochars show lower ash contents than biochars produced from materials like manure or sludge (Mukome et al., 2013; Zhao et al., 2013a). Cao and Harris (2010) identified minerals including quartz and calcite in dairy-manure biochar. Other researchers attributed the higher ash content in manure and grass biochars to silica from mixed-in soil in the precursory material (Mukome et al., 2013). Consequently, BC-CM shows low amounts of total C and C_{Org} in the bulk mass (22.7 % and 23.5 %, respectively). BC-WC shows a high C value, as does AC. Due to different feedstock composition, biochars produced from animal waste and sewage sludge typically show lower C contents than plant-based chars (Cao and Harris, 2010; Qiu et al., 2014; Zielińska et al., 2015; Wang et al., 2016b).

The molar ratio H/C indicates the degree of carbonization or aromaticity of a sample. Low H/C for AC and BC-WC suggest high amounts of aromatic carbon structures (Chun et al., 2004). Despite the lower C and higher ash content of BC-CM, H/C indicates higher carbonization compared to BC-GH (BC-GH: 0.71; BC-CM: 0.55). Its low

aromaticity suggests that more residue of the original organic material is present (Chun et al., 2004; Wang et al., 2006). The molar O/C and (O+N)/C ratios describe the bulk hydrophobicity and polarity of the sorbents (Chun et al., 2004; Chen et al., 2008). The polarity of the sorbents increases with ash content (Sun et al., 2016). BC-CM is highly polar ((O+N)/C = 0.43) and shows lower hydrophobicity than plant-derived chars. Its high ash content may protect the oxygen-bearing functional groups during pyrolysis (Qiu et al., 2014). These functionalities result in low hydrophobicity and high polarity, and facilitate accumulation of water clusters on the biochar surface (Chun et al., 2004).

The SSA and PV_{tot} of all sorbents increase with C_{Org} and C content ($p < 0.01$; following BC-CM < BC-GH < BC-WC < AC). BC-GH, BC-WC, and AC show high micropore volume whereas BC-CM lacks micropores. The differential pore size distribution (Figure 8) shows that pore volumes in AC, BC-WC, and BC-GH are predominantly present in the micropore range (< 2 nm; AC: about 53 %, BC-WC: 61 % and BC-GH: 46 %).

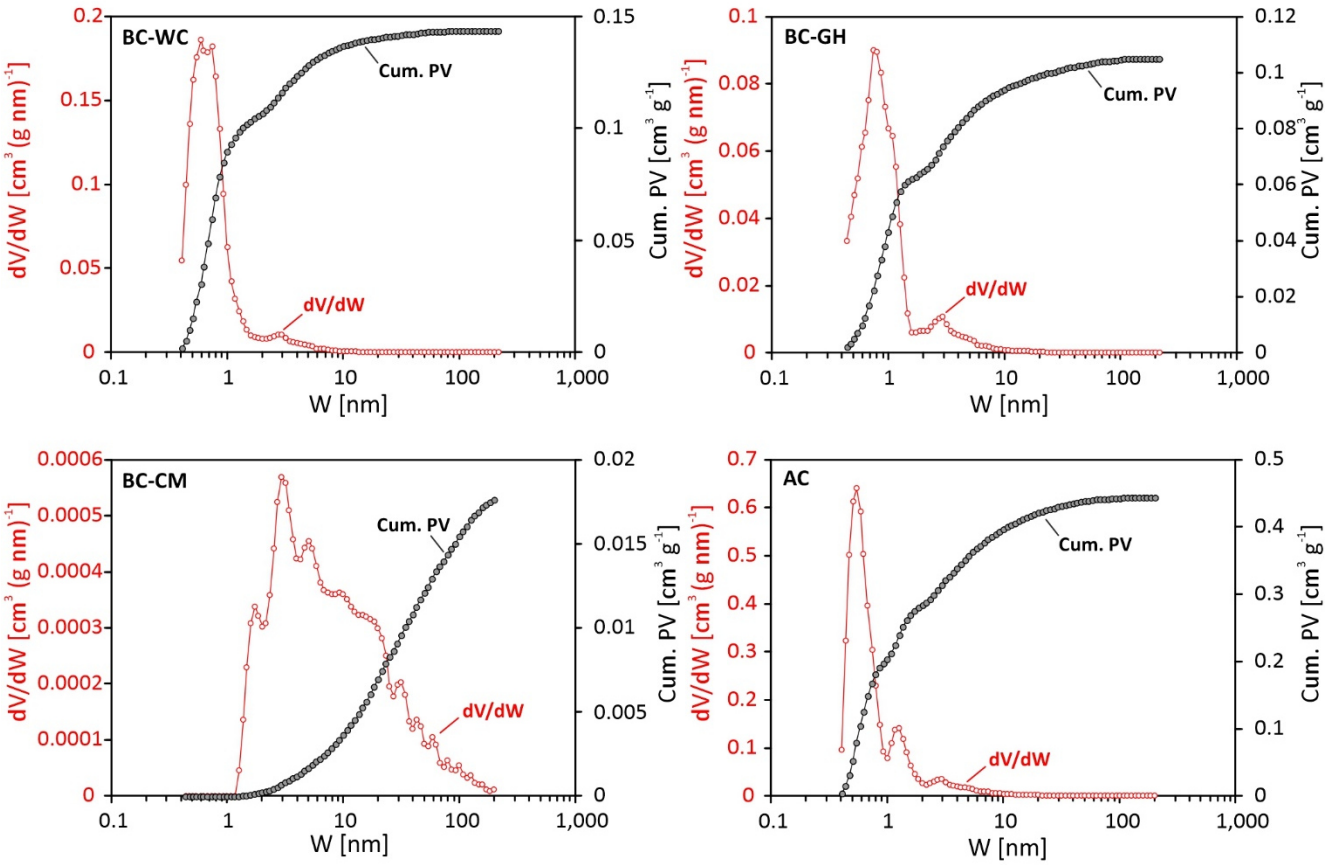

Figure 8: Differential pore size distribution and cumulative pore volume (Cum. PV) of the four sorbents determined by argon sorption. The data were analyzed using a NLDFT model for argon in slit-shaped pores. W [nm] corresponds to the pore width.

Both plant-based chars show a sharp pore diameter maximum of 0.78 and 0.64 nm for BC-GH and BC-WC, respectively. Two maxima are detected in AC at 0.55 and 1.2 nm pore width. Several studies show that feedstock strongly influences biochar surface area (e.g., Cao and Harris, 2010; Zhao et al., 2013a), explaining the very high variability observed in the samples. Zhao et al. (2013a) hypothesize that varying proportions of hemicellulose,

cellulose, and lignin in precursory materials cause differences in pore volume. Further, Lima et al. (2010) state that specifically the development of microporosity is feedstock-dependent.

3.2.2. Single-compound isotherms

All sorption data are well described by the Freundlich model ($r^2 > 0.95$; Table 3 and Figure 9). The linearized log K_{Fr} values range from 3.29 to 5.05 for TCE, and from 3.19 to 5.40 for PCE. For both contaminants all sorbents show significant difference in sorption and rank BC-CM < BC-GH < BC-WC < AC. TCE sorbs as good as or stronger than PCE to all biochars, despite TCE's lower log K_{OW} (see Table 1). In contrast, AC sorbs significantly less TCE than PCE, with log K_{Fr} being 5.05 and 5.40, respectively.

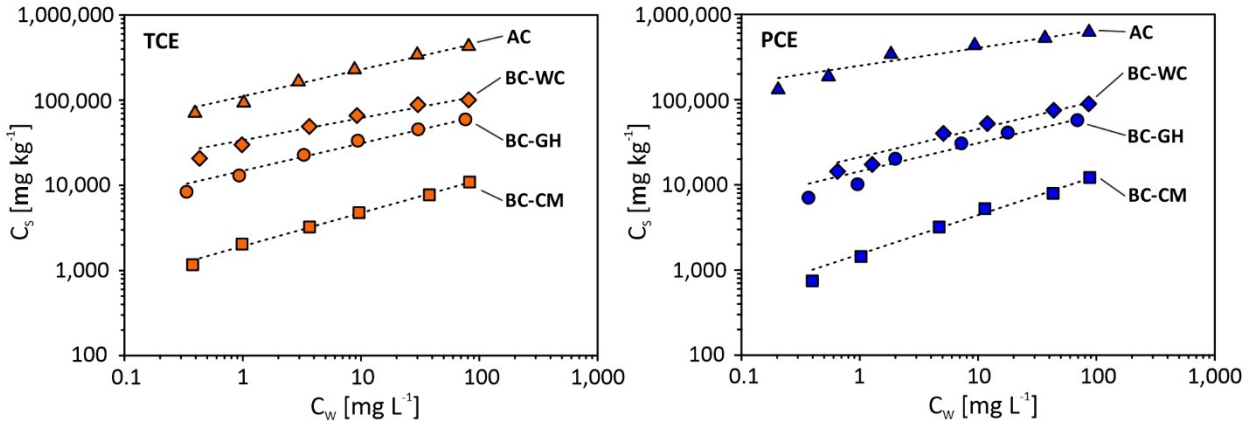

Figure 9: Single-compound isotherms of TCE (left) and PCE (right) fitted with the Freundlich isotherm model (dashed lines) plotted on a log-log scale. Different symbols refer to the four tested sorbents as follows: ▲ AC, ♦ BC-WC, ● BC-GH, and ■ BC-CM. Data points represent the mean of triplicate samples. All error bars are within symbol size.

Table 3: Freundlich isotherm parameters and unit-equivalent Freundlich coefficients of TCE and PCE sorption experiments.

		K_{Fr} [a] [(mg kg^{-1})/(mg L^{-1})^n]	log K_{Fr} [a] [(mg kg^{-1})/(mg L^{-1})^n]	n [-] [a]	r^2 [-] [b]	p [-] [b]	log K_{Fr}* [mg kg^{-1}] [c]
TCE	**BC-WC**	33,884 ± 1,796	4.53	0.26 ± 0.02	0.96	< 0.01	5.32
	BC-GH	14,834 ± 623	4.17	0.32 ± 0.01	0.99	< 0.01	5.15
	BC-CM	1,934 ± 59	3.29	0.39 ± 0.01	0.99	< 0.01	4.47
	AC	111,046 ± 4,468	5.05	0.31 ± 0.01	0.99	< 0.01	6.00
PCE	**BC-WC**	21,182 ± 1,377	4.33	0.33 ± 0.02	0.97	< 0.01	5.03
	BC-GH	14,409 ± 935	4.16	0.33 ± 0.02	0.97	< 0.01	4.87
	BC-CM	1,540 ± 110	3.19	0.46 ± 0.02	0.99	< 0.01	4.17
	AC	250,368 ± 12,929	5.40	0.21 ± 0.01	0.95	< 0.01	5.85

[a] Freundlich coefficients K_{Fr}, log K_{Fr} (log transformed), and Freundlich exponents n calculated using non-linear curve fitting in Sigma Plot after Eq. 9.

[b] r^2 and p represent the coefficient of determination and significance of the data fit obtained from Sigma Plot.

[c] log K_{Fr}* calculated form K_{Fr} using Eq. 11.

The Freundlich exponent n ranges from 0.26 to 0.39 for TCE, and from 0.21 to 0.46 for PCE, showing that sorption is highly non-linear in all cases. Both compounds show the strongest nonlinearity for sorption on AC (TCE: n = 0.26; PCE: n = 0.21). Regarding biochar sorption, BC-WC shows the lowest and BC-CM the highest n values. Log K_{Fr} values in previous studies are in a similar range to those reported here. In all cases, sorption of TCE to different biochars was found to be nonlinear (Ahmad et al., 2012; Ahmad et al., 2013b; Ahmad et al., 2014a; Han et al., 2017).

Sorption mechanisms

Hydrophobicity, specific interactions, and influence of sorbent properties

Unit-equivalent Freundlich isotherms (Figure 10 and Table 3) allow to normalize sorption to different water solubilities. Sorption isotherms of TCE and PCE on AC "collapse" to a single isotherm (individual isotherms are not statistically different), showing that sorption is mainly driven by the compounds' hydrophobicity. The three biochars behave distinctly different. Instead of collapsing, TCE and PCE isotherms show even higher differences in sorption (TCE about 2-fold higher than PCE).

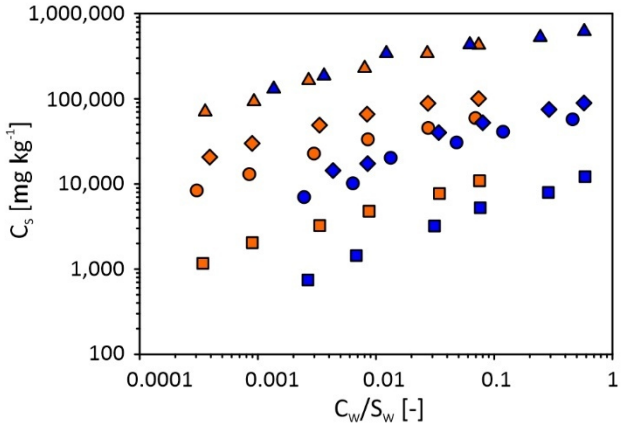

Figure 10: Sorption isotherms of TCE (orange) and PCE (blue) normalized to the water solubility S_W plotted on a log-log scale. Different symbols refer to sorbents as follows: ▲ AC, ♦ BC-WC, ● BC-GH, and ■ BC-CM. Data points represent the mean of triplicate samples. All error bars are within symbol size.

This illustrates that sorption of hydrophobic compounds on biochars is not exclusively governed by their hydrophobicity. Chen and Chen (2009) attributed differences in isotherms of naphthalene and 1-naphtanol, after solubility normalization, to multiple sorption mechanisms, for instance, surface coverage and specific interactions. Other authors normalized to the hexadecane-water partitioning coefficient (Kah et al., 2016). They hypothesized that size exclusion of larger sorbates causes the differences in sorption isotherms after solubility-normalization, predominantly in plant-derived chars produced at temperatures above 350°C. However, in this study also the manure-derived biochar BC-CM shows a higher log K_{Fr}* value for the smaller sorbate (log K_{Fr}* TCE = 5.1; log K_{Fr}* PCE = 4.8), indicating that a combination of multiple sorption mechanisms causes the observed differences.

Specific interactions are a possible reason for the different sorption behavior of TCE and PCE. Because PCE has no active hydrogen atom, it is not able to interact specifically (Borisover and Graber, 1997). TCE however, could theoretically participate in hydrogen-bonding (Borisover and Graber, 1997), and therefore interact specifically with polar functional groups. All biochars show a relatively high polarity index ((O+N)/C > 0.11), suggesting a significant number of functional groups available for specific interactions.

Figure 11 shows the relationship of the calculated log K_{Fr}* to selected sorbent properties.

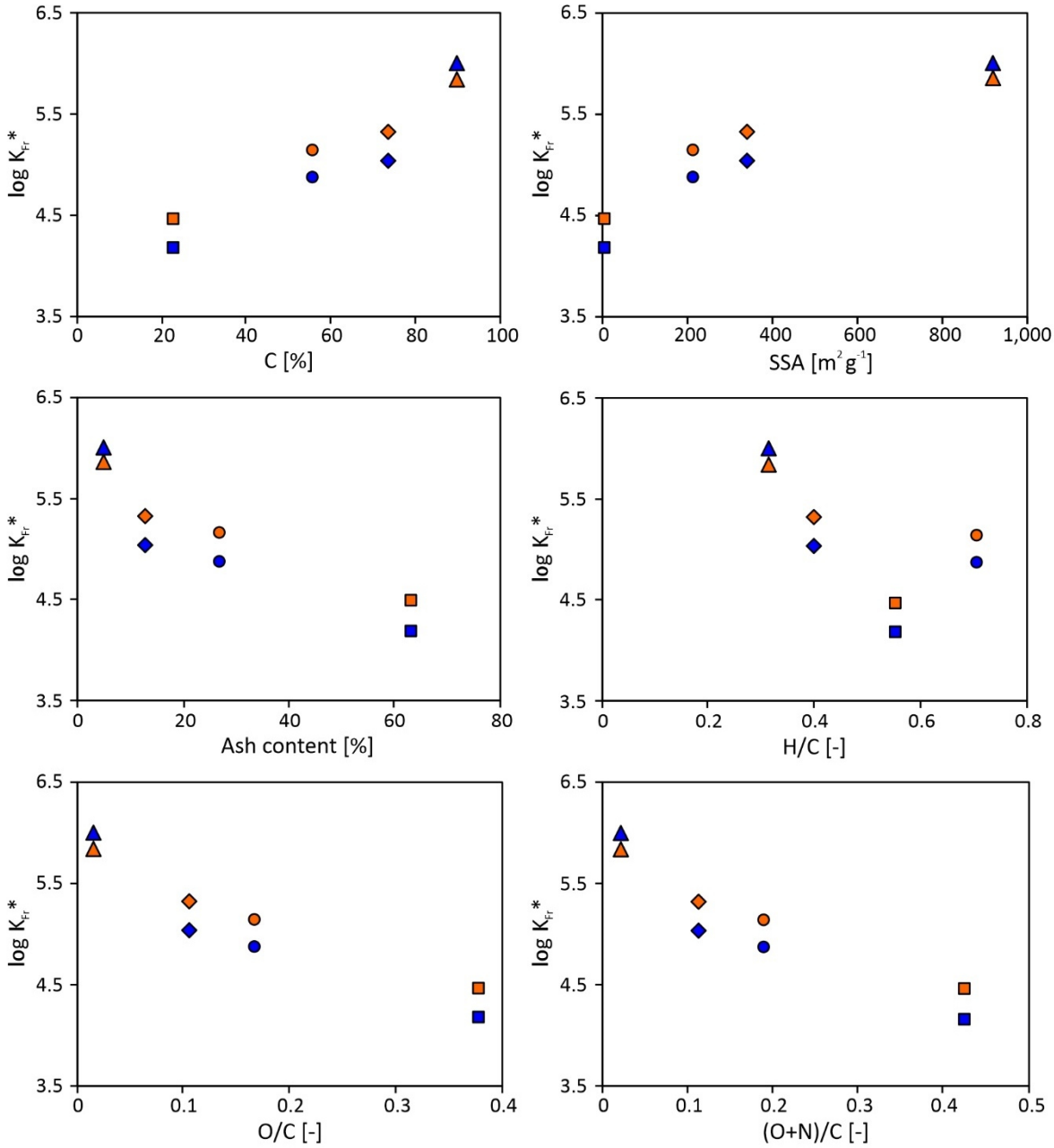

Figure 11: Relationship between log K_{Fr}* of TCE (orange) and PCE (blue) with selected sorbent properties. Different symbols refer to sorbents as follows: ▲ AC, ♦ BC-WC, ● BC-GH, and ■ BC-CM.

Sorption consistently increases with increasing C content, SSA, and PV_{tot}, and is negatively correlated with the ash content, O/C, and (O+N)/C (all $p < 0.01$). These findings are consistent with published literature (e.g., Ahmad et al., 2012; Ahmad et al., 2013b; Ahmad et al., 2014a; Hale et al., 2016; Kah et al., 2016; Kupryianchyk et al., 2016). Noteworthy, log K_{Fr}* does not correlate with the aromaticity index H/C ($p > 0.05$), which was suggested as "a smart linkage between the preparation temperatures, aromatic clusters and sorption properties of biochars" (Xiao et al., 2016). The C=C double bond in TCE and PCE is theoretically capable to participate in π=π interactions (Ma et al., 2011) with the aromatic parts of the biochar. Ahmad et al. (2014a) suggested this as one mechanism responsible for TCE sorption on a highly carbonized, high-temperature buffalo-weed biochar (H/C = 0.15). However, all biochars in this study, produced at low temperature, are only moderately carbonized (H/C > 0.4) and therefore this process appears to be of minor importance.

Pore-filling, partitioning, and steric-effects

As it was shown previously that pore-filling (e.g., Nguyen et al., 2007; Graber et al., 2012) as well as partitioning (e.g., Chen et al., 2008; Chiou et al., 2015; Kah et al., 2016) can contribute to organic contaminant sorption on biochars, the Polanyi-theory-based pore-filling model (Eq. 12) and the combined pore-filling and partitioning model (Eq. 13) was applied to resolve the contributions of the two processes to overall sorption. Isotherms are displayed in Figure 12 and a summary of the fitting parameters is presented in Table 4.

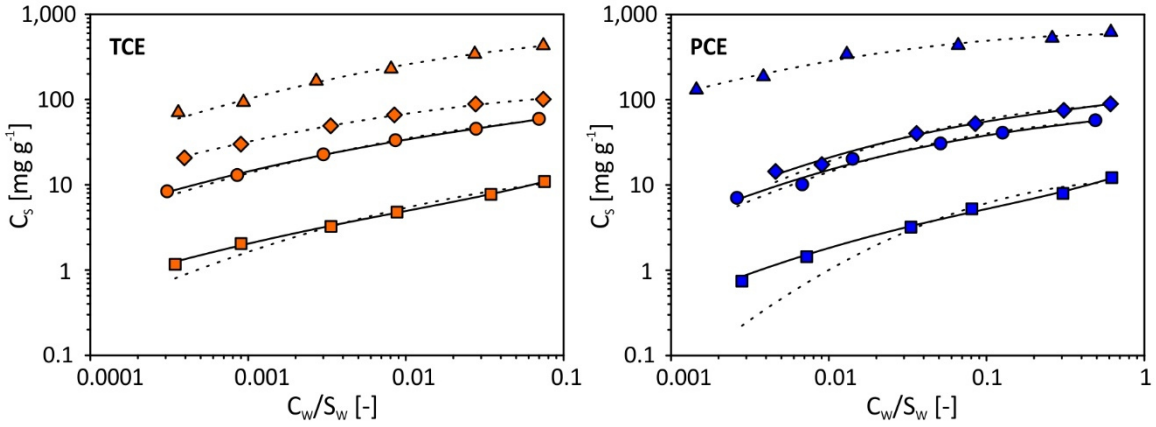

Figure 12: Single-compound isotherms of TCE (left) and PCE (right) fitted with the Polanyi-theory-based pore-filling model (dotted lines) and combined partitioning-adsorption model (solid lines). No solid lines are shown for isotherms where the partitioning coefficient K_p is not significant ($p > 0.01$). Different symbols refer to the four tested sorbents as follows: ▲ AC, ♦ BC-WC, ● BC-GH, and ■ BC-CM. Data points represent the mean of triplicate samples. All error bars are within symbol size.

Sorption of both compounds on AC, as well as TCE sorption on BC-WC, is very well described by the pore-filling model alone, without considering the partition part (K_p from combined model not statistically significant; $p > 0.01$; Figure 12, dashed lines). However, all remaining sorption isotherms show a significant contribution of partitioning to overall sorption with an increase from BC-WC to BC-CM (Figure 12), following the trend of decreasing PV_{tot} ($p < 0.05$).

Table 4: Isotherm parameters for the combined adsorption-partition model of single sorption experiments.

		K_p [L kg^{-1}] [a]	V_0 [cm³ kg^{-1}] [a]	E [J mol^{-1}] [a]	r^2 [-] [b]	p [-] [b]
TCE	**BC-WC**	n.a.[c]	85 ± 1.3	14,452 ± 193	0.96	< 0.01
	BC-GH	96 ± 35	44 ± 2.4	13,734 ± 361	0.99	< 0.01
	BC-CM	50 ± 4	6 ± 0.3	14,078 ± 355	0.99	< 0.01
	AC	n.a.[c]	369 ± 5.0	13,036 ± 142	0.99	< 0.01
PCE	**BC-WC**	218 ± 51	44 ± 2.2	10,088 ± 350	0.97	< 0.01
	BC-GH	132 ± 39	30 ± 1.5	10,266 ± 318	0.97	< 0.01
	BC-CM	73 ± 6	3 ± 0.3	10,278 ± 525	0.99	< 0.01
	AC	n.a.[c]	365 ± 7.6	13,041 ± 364	0.97	< 0.01

[a] Coefficients of the combined adsorption-partitioning model (± standard error) calculated using non-linear curve fitting in Sigma Plot after Eq. 13.

[b] r^2 and p represent the coefficient of determination and significance of the data fit obtained from Sigma Plot.

[c] Derived K_p values were not significant ($p > 0.01$).

The maximum adsorbed volume V_0, as derived from the model fit, sequentially increases, following the order BC-CM < BC-GH < BC-WC < AC, which correlates with the increasing PV_{tot} of the sorbents ($p < 0.01$). In case of AC, V_0 of the two contaminants is not statistically different (V_0^{TCE}, single ≈ V_0^{PCE}, single). This supports the assumption that AC sorption is not selective for either of the compounds, observed differences in the isotherms solely originate from the compounds' hydrophobicity, and AC adsorption via pore-filling is the dominant process in the investigated concentration range.

Considering the biochars, V_0 is significantly higher for TCE in all cases ($V_0^{TCE, single} > V_0^{PCE, single}$), implying that TCE can access a bigger portion of the available pore volume compared to PCE. This supports the hypothesis of a steric effect, hindering PCE to access certain pores. This could be due to a size exclusion effect as reported in other studies (e.g., Lattao et al., 2014; Xiao and Pignatello, 2015; Kah et al., 2016). The molecular size of TCE is about 6.6 Å x 6.2 Å x 3.6 Å (Karanfil and Dastgheib, 2004; Lian et al., 2012), whereas PCE's effective molecular diameter and second largest dimension is 6.6 Å (Bembnowska et al., 2003). Kasaoka et al. (1989) (as cited in Li et al., 2002) state that in aqueous systems, size exclusion can occur when the pore width is smaller than about 1.7 times the second largest dimension of the target compound (1.05 nm for TCE and 1.12 nm for PCE; note: 1 Å = 0.1 nm). Both plant-derived biochars contain most of their pore volume in pores smaller than 1 nm. When comparing V_0 of TCE and PCE, it is evident that BC-WC shows greater difference between the two sorbates (BC-WC: 48 %; BC-GH: 31 %). This is probably an effect of the micropore size distribution that is dominated by smaller pores, partly unavailable for PCE sorption.

The K_p value is consistently higher for PCE ($K_p^{PCE, single} > K_p^{TCE, single}$) and decreases from BC-CM to BC-WC, however differences are not significant in all cases. BC-CM as the least hydrophobic and most polar sorbent (Table 2) also shows the highest percentage of partitioning for both compounds (At 5 % of S_W: TCE 30 %; PCE 13.1 %; Table 5).

Table 5: Calculated distribution of partitioning and pore-filling in single-compound isotherms.

		1 % of S_W [a]		5 % of S_W [a]	
		Partitioning [%]	**Pore-filling [%]**	**Partitioning [%]**	**Pore-filling [%]**
TCE	**BC-WC**	0	100	0	100
	BC-GH	3.1	96.9	9.9	90.1
	BC-CM	11.0	89.0	30.0	70.0
	AC	0	100	0	100
PCE	**BC-WC**	1.5	98.5	3.5	96.5
	BC-GH	1.2	98.8	3.1	96.9
	BC-CM	5.7	94.3	13.1	86.9
	AC	0	100	0	100

[a] Relative distribution of partitioning and pore-filling from pore-filling and combined partitioning-adsorption model calculated at 1 % and 5 % of the respective water solubility of the compound.

Polarity favors the formation of water clusters on the sorbent surface making it more hydrophilic (Li et al., 2002). This can hinder organic compounds to access high-energy sorption sites and therefore favor partitioning into the non-carbonized phase. For all biochars, partitioning becomes more important as C_{Org}, PV_{tot}, PV_{mic}, and SSA decrease, and (O+N)/C increases (all $p < 0.05$). As all these properties are closely feedstock-related, it is reasonable to state that the distribution of adsorption and partitioning is ultimately a function of the feedstock material.

3.2.3. Sorption behavior in bi-solute systems

The isotherms of TCE and PCE in bi-solute systems, fitted with the Freundlich model, are displayed in Figure 13. A summary of the fitting parameters is presented in Table 6. In Table 7, Freundlich parameters of single and bi-solute experiments are summarized, together with the competition strength calculated after Zhang et al. (2012).

Table 6: Freundlich parameters and unit-equivalent Freundlich coefficient of bi-solute sorption experiments.

		K_{Fr} [a] $[(mg\ kg^{-1})/(mg\ L^{-1})^n]$	log K_{Fr} [a] $[(mg\ kg^{-1})/(mg\ L^{-1})^n]$	n [-] [a]	r^2 [-] [b]	p [-] [b]	log K_{Fr}* $[mg\ kg^{-1}]$ [c]
TCE	**BC-WC**	28,282 ± 1,090	4.45	0.19 ± 0.01	0.95	< 0.01	5.03
	BC-GH	12,123 ± 411	4.08	0.27 ± 0.01	0.99	< 0.01	4.90
	BC-CM	1,486 ± 97	3.17	0.38 ± 0.02	0.98	< 0.01	4.32
	AC	61,430 ± 8,285	4.79	0.18 ± 0.04	0.67	< 0.01	5.33
PCE	**BC-WC**	28,665 ± 1,093	4.46	0.23 ± 0.01	0.97	< 0.01	4.96
	BC-GH	14,654 ± 563	4.17	0.30 ± 0.01	0.97	< 0.01	4.82
	BC-CM	1,276 ± 128	3.11	0.49 ± 0.03	0.98	< 0.01	4.16
	AC	190,356 ± 9,972	5.28	0.23 ± 0.02	0.96	< 0.01	5.76

[a] Freundlich coefficients K_{Fr}, log K_{Fr} (log transformed), and Freundlich exponents n calculated using non-linear curve fitting in Sigma Plot after Eq. 9.

[b] r^2 and p represent the coefficient of determination and significance of the data fit obtained from Sigma Plot.

[c] log K_{Fr}* calculated form K_{Fr} using Eq. 11.

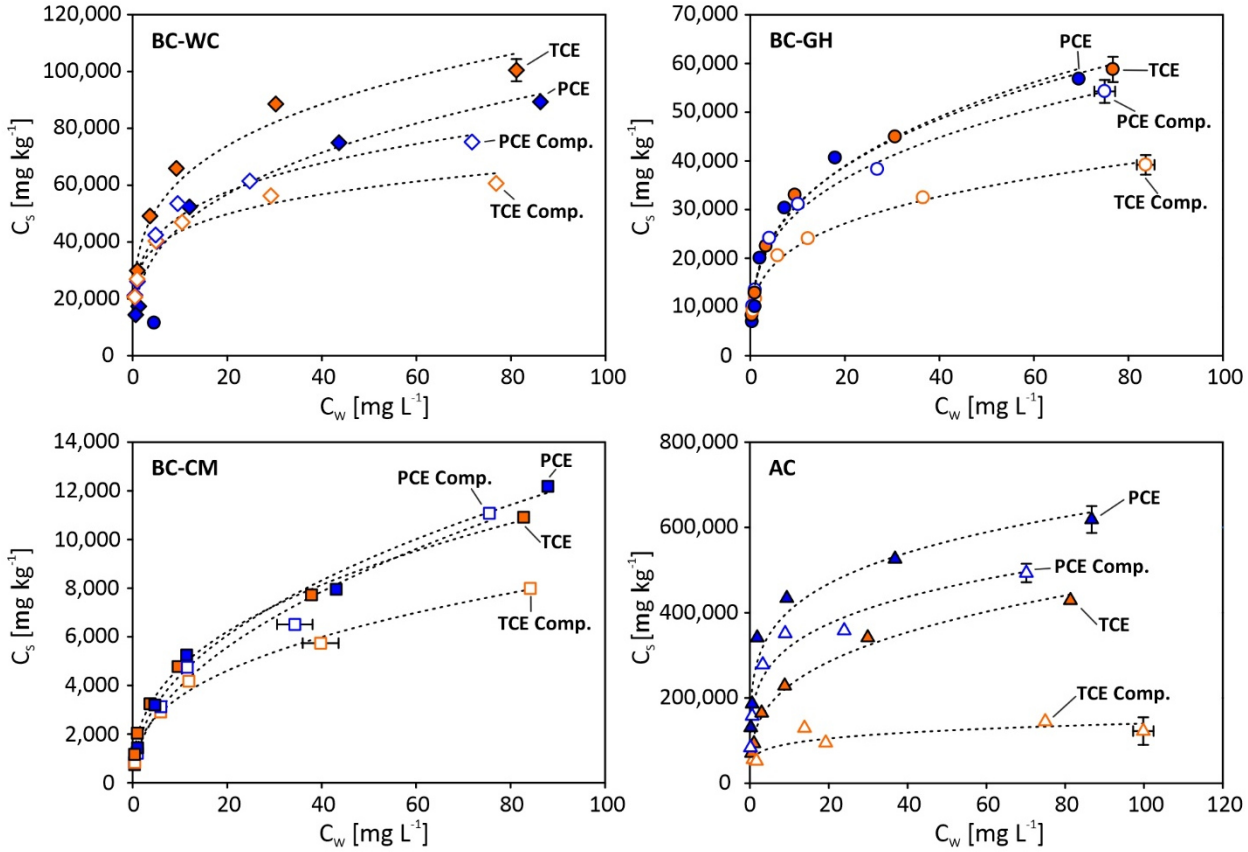

Figure 13: Results of the TCE (orange) - PCE (blue) bi-solute sorption isotherm experiments (open symbols), compared to single-compound experiments (filled symbols) on all four sorbents. Dashed lines represent the fit of the Freundlich isotherm model. Data points represent the mean of triplicate samples. Error bars show the standard deviation. Where no error bars are shown, they are within symbol size.

Table 7: Comparison of non-linearized Freundlich coefficients (K_{Fr}) and unit-equivalent Freundlich coefficients (K_{Fr}*) of single and bi-solute experiments, and resulting calculated competition strength of both compounds.

		Single-compound		Bi-solute		
		K_{Fr} [a] [(mg kg^{-1})/(mg L^{-1})^n]	K_{Fr}* [b] [mg kg^{-1}]	K_{Fr} [a] [(mg kg^{-1})/(mg L^{-1})^n]	K_{Fr}* [b] [mg kg^{-1}]	Competition strength [%][c]
TCE	**BC-WC**	33,884	209,088	28,282	105,971	16
	BC-GH	14,834	140,460	12,123	79,559	12
	BC-CM	1,934	29,509	1,486	20,882	1
	AC	111,046	1,001,902	61,430	214,174	17
PCE	**BC-WC**	21,182	108,272	28,665	90,878	49
	BC-GH	14,409	74,492	14,654	65,630	43
	BC-CM	1,540	14,801	1,276	14,607	29
	AC	250,368	703,783	190,356	580,916	79

[a] Freundlich coefficients K_{Fr} calculated using non-linear curve fitting in Sigma Plot 12 after Eq. 9.

[b] K_{Fr}* calculated form K_{Fr} using Eq. 11.

[c] Competition strength calculated after Zhang et al. (2012) using K_{Fr}* (e.g., competition strength PCE = (K_{Fr}*$^{TCE, single}$ - K_{Fr}*$^{TCE, bi}$)/ K_{Fr}*$^{TCE, single}$).

In bi-solute systems, the sorption of TCE on biochars is notably reduced when PCE is added, while sorption of PCE is much less affected. For both compounds the effect of the co-solute increases in the order BC-CM < BC-GH < BC-WH, with a drop in K_{Fr}* values of about 29 %, 43 %, and 49 %, respectively.

In the AC experiments, both compounds sorb significantly less than observed in the single-compound system, although the effect on TCE is much more pronounced (K_{Fr}* reduced by 79 %), resulting in a poor isotherm fit (r^2 = 0.67, Table 6). The higher competition strength of PCE is obvious for all samples (Table 7) and is most likely an effect of its higher hydrophobicity.

To further explore the differences in bi-solute systems, the sum of the sorbed molar volumes of TCE and PCE in the individual batch samples is calculated and compared to the respective sorption isotherms in single-compound systems (Figure 14). This approach is similar to the one employed by Sander and Pignatello (2005a), Pan and Xing (2010), and Wu et al. (2017). Assuming that a specific sorbent provides a finite number of sorption sites or a certain pore volume accessible to the solutes and both compounds equally compete for them, the cumulative sorbed volume should be equal to the sorbed volume of the favored compound in single-solute experiments.

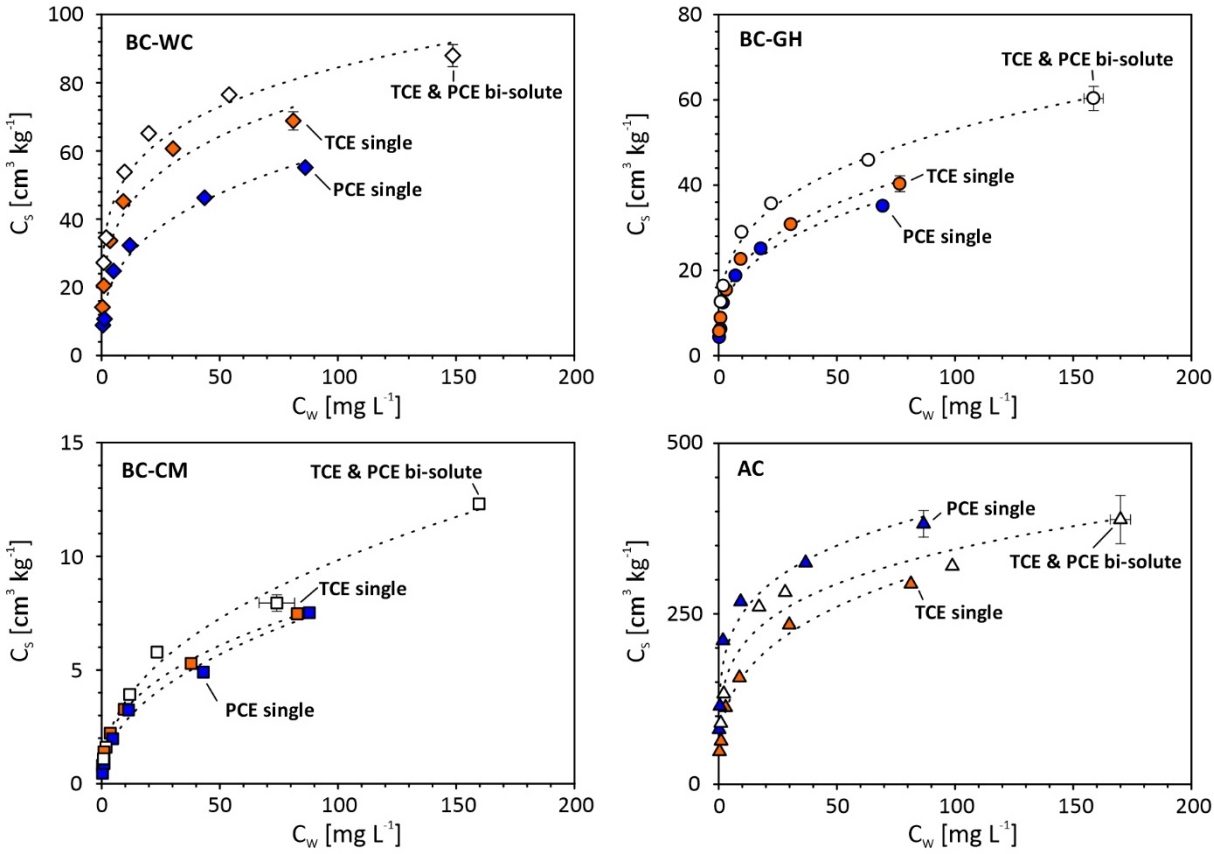

Figure 14: Cumulative TCE+PCE sorption isotherms (non-filled symbols) compared to single-compound isotherms (TCE orange; PCE blue) plotted as C_W [mg L^{-1}] vs. C_S [cm^3 kg^{-1}], the loading expressed as molar volume sorbed. Dashed lines are only for guidance and do not have numerical meaning. Data points represent the mean of triplicate samples. Error bars show the standard deviation. Where no error bars are shown, they are within symbol size.

In case of AC, the calculated cumulative isotherm plots between the PCE and TCE isotherms obtained in the single-solute system (Figure 14; PCE and cumulative sorption are not significantly different). This indicates that the overall sorption does not significantly change in the bi-solute system. TCE and PCE can replace each other and directly compete for the same sorption sites (Erto et al., 2011). The differences in the observed sorption isotherms and competition strength only originate from the different compound hydrophobicities.

For the biochars, the calculated cumulative isotherms plot above both single-compound isotherms, indicating that a higher total volume is sorbed in the bi-solute systems. TCE and PCE seem to partly compete for sorption sites but might also have compound-specific sorption domains. Two studies reported this phenomenon of complementary adsorption for chemicals with different properties on carbon nanotubes (Pan and Xing, 2010; Zhang et al., 2012). Possible reasons could be the ability of TCE and PCE to access different pores due to steric effects (as already discussed for single-compound experiments), specific interactions, or the presence of multiple sorption domains.

Applying the Polanyi-theory-based approach should help to further clarify the sorption mechanisms. Fitting parameters are summarized in Table 8 and isotherm fits are displayed in Figure 15.

As seen in single-compound experiments, the pore-filling model describes all biochar data reasonably well ($r^2 > 0.93$). However, including a partitioning domain into the model significantly improves the isotherm fits. Only in case of TCE sorption on BC-WC as well as TCE and PCE on AC, a sole pore-filling mechanism is sufficient (K_p derived from combined model not statistically significant, $p > 0.01$; Figure 15, Table 8).

Table 8: Isotherm parameters for the combined adsorption-partition model of bi-solute sorption experiments.

		K_p [L kg^{-1}] [a]	V_0 [cm^3 kg^{-1}] [a]	E [J mol^{-1}] [a]	r^2 [-] [b]	p [-] [b]
TCE	**BC-WC**	n.a.[c]	49 ± 0.7	17,327 ± 282	0.99	< 0.01
	BC-GH	65 ± 21	27 ± 1.5	15,261 ± 485	0.99	< 0.01
	BC-CM	26 ± 7	5 ± 0.6	13,320 ± 728	0.99	< 0.01
	AC	n.a.[c]	105 ± 7.9	17,005 ± 1,649	0.71	< 0.01
PCE	**BC-WC**	152 ± 37	40 ± 1.3	12,793 ± 373	0.99	< 0.01
	BC-GH	232 ± 26	23 ± 0.9	12,230 ± 423	0.99	< 0.01
	BC-CM	86 ± 9	3 ± 0.3	10,840 ± 973	0.98	< 0.01
	AC	n.a.[c]	284 ± 8.3	12,841 ± 515	0.95	< 0.01

[a] Coefficients of the combined adsorption-partitioning model (± standard error) calculated using non-linear curve fitting in Sigma Plot after Eq. 13.

[b] r^2 and p represent the coefficient of determination and significance of the data fit obtained from Sigma Plot;

[c] Derived K_p values were not significant ($p > 0.01$).

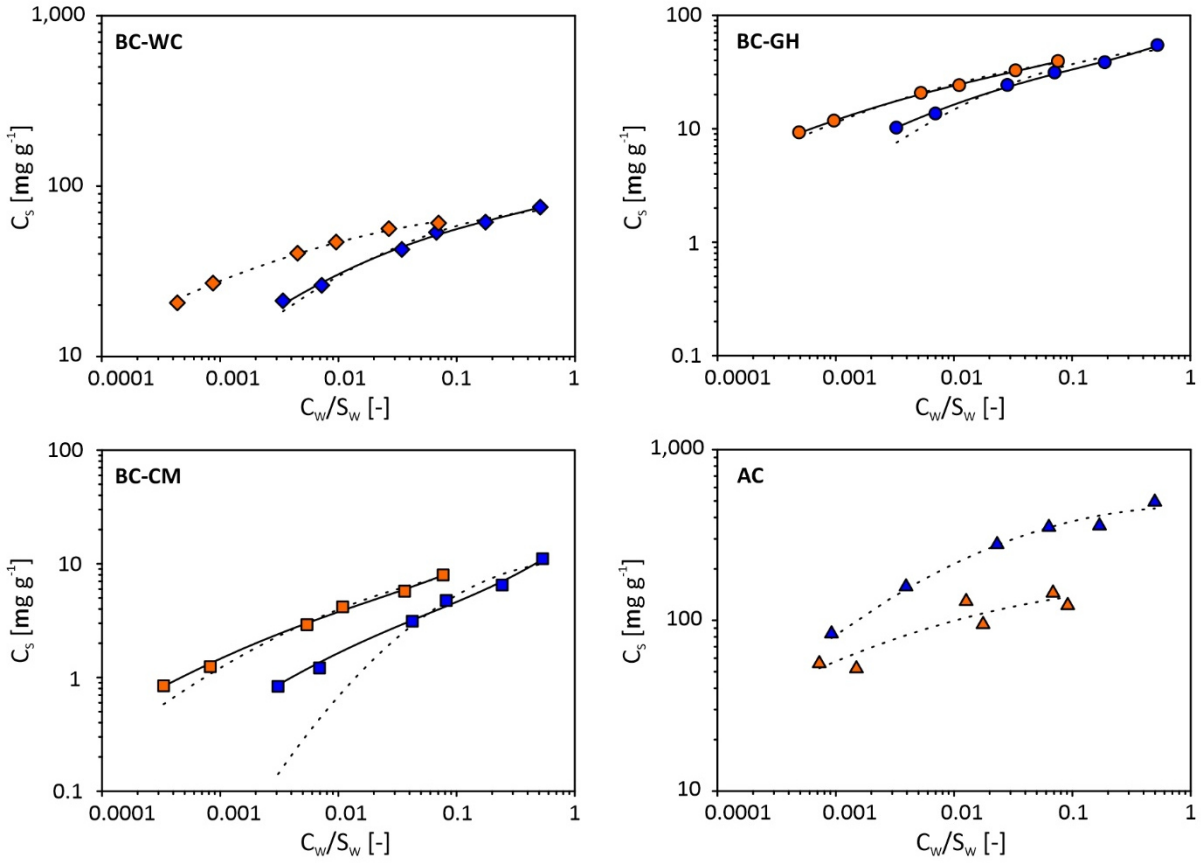

Figure 15: Bi-solute sorption isotherms of TCE (orange) and PCE (blue) with fitted Polanyi-theory-based pore-filling (dotted lines) and combined partitioning-adsorption model (solid lines). Data points represent the mean of triplicate samples. All error bars are within symbol size.

Although PCE is the stronger competitor, V_0 of the biochars BC-WC and BC-CM is significantly higher for TCE ($V_0^{TCE, bi} > V_0^{PCE, bi}$). In case of BC-GH, fitted V_0 values are also different ($V_0^{TCE, bi}$ = 27 cm³ kg^{-1} and $V_0^{PCE, bi}$ = 23 cm³ kg^{-1}), however 95 % confidence intervals slightly overlap. This indicates that TCE is more strongly attracted to sorb via pore-filling. Compared to single-compound experiments, V_0 of TCE significantly decreases ($V_0^{TCE, single} > V_0^{TCE, bi}$) for BC-WC and BC-GH. The decrease for BC-CM is not statistically significant ($V_0^{TCE, single}$ = 6 cm³ kg^{-1} and $V_0^{TCE, bi}$ = 5 cm³ kg^{-1}). This effect is much less pronounced for PCE, implying that PCE effectively competes with TCE for certain pores. However, it is not able to access all available pores. This is consistent with the hypothesis of size exclusion, hindering PCE sorption in small micropores, as discussed earlier. The sum of TCE and PCE V_0 is similar to V_0 of TCE in the single-compound system ($\Sigma V_0^{bi} = V_0^{TCE, bi} + V_0^{PCE, bi} \approx V_0^{TCE, single}$). This indicates that a limited maximum pore volume is available for pore-filling in every sorbent.

As the maximum amount of contaminant sorbed by pore-filling does not change significantly in the bi-solute system, the partitioning domain should be responsible for enhanced sorption. The K_p values are significantly higher for PCE ($K_p^{PCE, bi} > K_p^{TCE, bi}$). This supports the assumption that PCE is more attracted to the partitioning domain of the biochars, due to its higher hydrophobicity.

The role of partitioning for both compounds increases following the order BC-WH < BC-GH < BC-CM (Table 9), which correlates with the decreasing PV_{tot} and hydrophobicity, as well as with the increasing polarity of the sorbents (all $p < 0.05$). The competition strength follows the reversed trend. It decreases in the order BC-WH > BC-GH > BC-CM (Table 7), indicating that competition is stronger in hydrophobic, pore-filling-dominated biochars.

Table 9: Calculated distribution of partitioning and pore-filling in bi-solute compound isotherms.

		1 % of S_W [a]		5 % of S_W [a]	
		Partitioning [%]	**Pore-filling [%]**	**Partitioning [%]**	**Pore-filling [%]**
TCE	**BC-WC**	0	100	0	100
	BC-GH	3.0	97.0	10.1	89.9
	BC-CM	7.5	92.5	21.2	78.8
	AC	0	100	0	100
PCE	**BC-WC**	0.7	99.3	2.3	97.7
	BC-GH	2.0	98.0	5.9	94.1
	BC-CM	7.4	92.6	17.8	82.2
	AC	0	100	0	100

[a] Relative distribution of partitioning and pore-filling from pore-filling and combined partitioning-adsorption model calculated at 1 % and 5 % of the respective water solubility of the compound.

Li and Werth (2001) suggested that competition between TCE and PCE in natural solids is controlled by hydrophobic micropore spaces. Therefore, partitioning-dominated sorbents can sorb additional contaminant volume in the non-carbonized phase. This is similar to the findings by Wu et al. (2017) for the compounds ketoprofen and triclosan. They found no competition in the partitioning phase of a wheat-straw biochar prepared at 300°C. However, notable competition was present in the carbonized phase. Also, competition was stronger in the more carbonized char prepared at 700°C from the same feedstock.

When comparing the shape of single- and bi-solute isotherms and their relative position to each other (Figure 16), some additional effects are evident. In case of AC, the PCE bi-solute isotherm runs parallel to both single-compound isotherms, whereas TCE sorption is significantly suppressed over the whole concentration range. For both plant-based biochars (BC-GH and BC-WC) the difference between TCE sorption in single- and bi-solute systems increases with increasing C_W/S_W ratio. This indicates that TCE sorption in bi-solute systems is increasingly suppressed as C_W/S_W approaches one. For PCE however, sorption is higher in bi-solute systems when $C_W/S_W < 0.1$, is continuously suppressed as C_W/S_W increases, and both isotherms intersect. This further illustrates the influence of micropore-filling on competitive sorption. At low concentrations, high micropore volume is available. As TCE first sorbs in very small, high-energy pores that are partly inaccessible for PCE, only little competition occurs. When C_W/S_W increases, PCE progressively outcompetes TCE in the remaining pores. PCE

sorption is increased by additional partitioning over the whole concentration range, caused by hydrophobic effects.

For the manure-based biochar BC-CM, this concentration effect is not present. All four isotherms run almost parallel (Figure 16), indicating no concentration-dependent competition effect. Sorption is not limited by the availability of micropores, but rather influenced by the sorbent's bulk properties and partitioning phase. This illustrates that the competition behavior in bi-solute systems is on the one hand controlled by sorbent properties, on the other hand also dependent on the investigated concentration range.

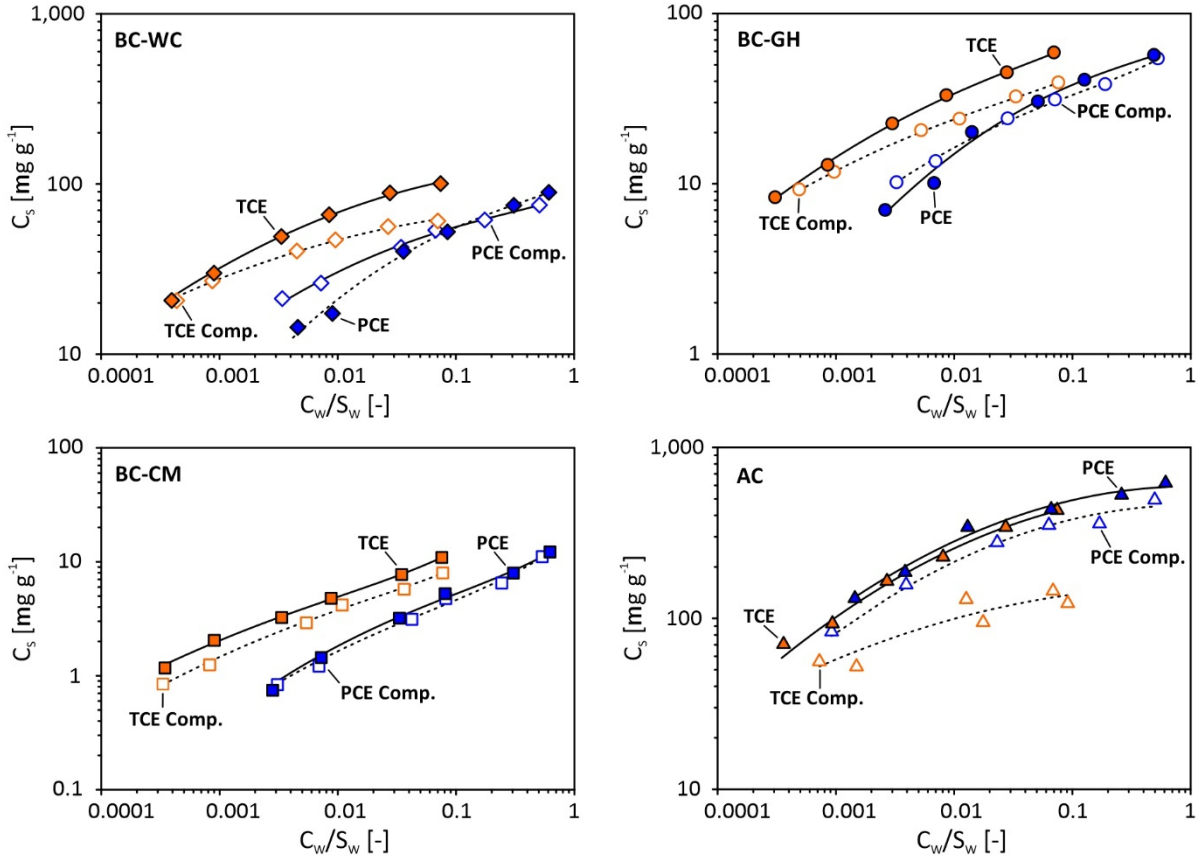

Figure 16: Bi-solute sorption isotherms (non-filled symbols) of TCE (orange) and PCE (blue) compared to single-compound sorption isotherms (filled symbols). Solid (single-compound) and dashed (bi-solute) lines represent the fitted Polanyi-theory-based adsorption-partitioning model. Data points represent the mean of triplicate samples. All error bars are within symbol size.

3.3. Conclusions

Sorption of TCE and PCE is driven by feedstock-governed biochar characteristics and the compounds' molecular properties, rather than sorbate solubility. Biochar with high C content, SSA, PV_{mic}, and PV_{tot} shows the highest sorption capacity. Besides that, the sorbent polarity plays a key role in sorption of chlorinated compounds and strongly influences the distribution of adsorption and partitioning. High-polarity biochars facilitate partitioning, while biochars with high PV_{mic} favor pore-filling of both contaminants. Size exclusion causes differences in the

sorption of TCE and PCE, especially in plant-based biochars. These points highlight the importance of feedstock when biochar is applied in remediation. Depending on the target compound, a biochar with properties tailored to the contaminant of interest needs to be selected. In bi-solute systems both compounds compete for sorption sites, but the degree of competition is strongly influenced by sorbent properties. This is again a direct effect of the feedstock material. Plant-based biochars are pore-filling-dominated and show strong competition. Chars produced from manure feedstock offer an additional partitioning phase that does not experience strong competition. This enables the sorption of additional contaminant volume in bi-solute systems, making it an attractive option for the application on mixed-contaminant sites. The described concentration effect illustrates that sorption mechanisms are complex, and the selection of feedstock plays a vital role in biochars' effective application in environmental remediation.

4. Effect of water leaching on biochar properties and its impact on organic contaminant sorption

When biochar is used in remediation technologies, the long-term effectiveness of sorption processes that reduce the mobility of contaminants is of prime interest (Ren et al., 2018a). However, biochar properties are affected by environmental exposure and interaction with the soil environment, which is summarized by the term "aging". Aging refers to several processes including leaching of minerals and organic carbon (OC) (Trigo et al., 2014), alteration of surface functional groups (Luo et al., 2017), and surface or pore blocking by organic matter (Kwon and Pignatello, 2005) and minerals (Lin et al., 2012b). These mechanisms can significantly alter biochar sorption behavior for organic contaminants. Reported effects of aging are diverse, ranging from increased sorption of herbicides (Trigo et al., 2014) to greatly attenuated sorption of non-ionic organic compounds (Luo et al., 2017), and seem to depend on multiple factors like initial biochar characteristics, as well as compound properties.

Several studies have shown that leaching of minerals and OC from biochar is one key process that occurs over the course of its aging. Studies examining leaching impact focused on nutrient release (Zhao et al., 2013b), biochars' environmental fate and stability (Spokas et al., 2014; Liu et al., 2018), potential toxicity of biochar-derived compounds (Smith et al., 2016), and the complexation between organic contaminants and biochar-released dissolved organic carbon (DOC) (Fu et al., 2018).

Two studies recently investigated the changes in sorption of organic compounds after removing leachable OC (LOC) through washing. Wang et al. (2017) reported enhanced sorption of nitrobenzene, naphthalene, and atrazine by a rice straw biochar, accelerated sorption kinetics, and reduced sorption irreversibility. This was mainly attributed to increased accessibility of micropores, due to the removal of LOC. Luo et al. (2017) also described enhanced sorption of nonionic organic compounds on two maize straw biochars after LOC removal, caused by exposure of initially blocked micropores. This suggests that the removal of LOC generally increases pore accessibility and therefore shows positive effects on contaminant immobilization. Further, Klasson et al. (2014) reported the unblocking of pores as a result of ash removal through rainwater washing. However, to date, no study has been conducted investigating both OC and mineral leaching, and linking the concomitant changes in the biochar to its contaminant sorption ability.

Knowledge about the influence of initial biochar properties on leaching and related processes is still limited, as most studies focused on only one biochar type. In particular, the impact of biochar leaching on its bulk properties, and resulting changes in sorption mechanisms of organic contaminants have received only little attention. However, previous studies have shown that element (Wu et al., 2016) and LOC (Liu et al., 2019a) leaching greatly differs with feedstock type and that structural properties and resulting sorption mechanisms are especially feedstock-dependent (see also chapter 2).

Therefore, in this chapter the aim was to link changes of biochar properties due to leaching to changes that occur in contaminant sorption, by (1) investigating what is leached from biochars produced from different feedstocks, (2) determining how leaching changes biochars' chemical and structural properties, and finally

(3) relating these changes to specific differences in sorption mechanisms. To achieve this, three biochars produced from cattle manure (BC-CM), grain husk (BC-GH), and wood chips (BC-WC), were artificially leached, the aqueous leachates were characterized, the changes in chemical and structural characteristics of the biochars were determined, and their sorption behavior for the two chlorinated compounds, TCE and PCE, was analyzed.

4.1. Materials and methods

The "original" biochars used in this section are described in chapter 3.1.2. Leaching of AC was not considered, as preliminary tests indicated negligible effects on activated carbon properties. The properties of the two chlorinated compounds TCE and PCE, again used as model compounds, are listed in Table 1.

4.1.1. Biochar leaching

Methods for the leaching of soluble ions and OC described in the literature are diverse. Numerous studies utilize simple batch-setups where biochar is shaken with deionized water (e.g., Kloss et al., 2012; Spokas et al., 2014) or acidic solutions (e.g., Klasson et al., 2014; de Figueredo et al., 2017) at varying solid to liquid ratios and shaking times. However, also repeated washing cycles (e.g., Angst and Sohi, 2013; Luo et al., 2017), continuous in-column leaching (Feng et al., 2018), and the simulation of weathering in a Soxhlet extractor (Yao et al., 2010) have been reported. As several studies suggest that leaching kinetics can be slow (Angst and Sohi, 2013; Kong et al., 2014), an accelerated leaching method utilizing an Accelerated Solvent Extractor was chosen. A similar method was previously used to extract pyrogenic water-soluble organic matter from biochars (Norwood et al., 2013). The elevated pressure and temperature applied in accelerated solvent extraction should allow rapid and complete mobilization of soluble compounds. Therefore, application of this method should yield the maximum amount of leachable compounds.

Accelerated leaching was performed with an Accelerated Solvent Extractor (ASE 300, Dionex, Germany). Stainless steel extraction cells (33 mL) were filled with 1.5 g of biochar and glass fiber filters (Thermo Scientific, Germany) at the top and bottom of the extraction cell. All biochars were extracted with deionized water (ultra-pure Millipore) at 100°C for 10 minutes under 100 bar cell pressure (for details see Table 10). Aqueous extracts were collected in 200 mL glass bottles fitted with screw caps and rubber septa. Each extraction was performed with three replicates, each yielding about 60 to 65 mL of leachate. After the extracts were cooled to room temperature, EC and pH were measured (PCE-PHD1, PCE Instruments, Germany). All leachates were stored refrigerated until further analysis. Leached biochar samples were dried for 24 hours at 105°C and stored in amber glass bottles until further use.

Table 10: ASE method details for accelerated leaching of biochar samples.

Method parameter	
Solvent	Millipore H_2O
Temperature [°C]	100
Cell pressure [bar]	100
Heating time [minutes]	5
Static time [minutes]	5
Purge time [seconds]	100
Flush volume [%]	60
Cycles	1

4.1.2. Characterization of aqueous leachates

All leachates were filtered using 0.45 µm cellulose acetate filters. Dissolved organic carbon (DOC), was determined with a carbon analyzer equipped with an infrared detector (LiquiTOC II, Elementar, Germany). Major cations (sodium (Na^+), potassium (K^+), magnesium (Mg^{2+}), calcium (Ca^{2+}), ammonium (NH_4^+)) and anions (fluoride (F^-), chloride (Cl^-), bromide (Br^-), nitrite (NO_2^-), nitrate (NO_3^-), phosphate (PO_4^{3-}), sulfate (SO_4^{2-})) were determined by ion chromatography (882 Compact IC plus, Metrohm, Switzerland).

4.1.3. Characterization of leached biochars

Leached biochars were characterized utilizing the same methods as described in chapter 3.1.2. Additionally to the previously analyzed properties, also mineral elements were determined for the original and leached biochars. Samples were ashed at 1,000°C for 1 hour, the residue was fused with lithium-metaborate at 1,000°C, dissolved in 100 mL acid (4 % HNO_3/2 % HCl), and analyzed by inductively coupled plasma - atomic emission spectroscopy (ICP-AES). Results are reported as mass of element per mass bulk sample (all analysis performed by ALS Minerals, Loughrea, Ireland).

4.1.4. Batch experiments and analytical method

For consistency, equilibrium batch experiments with the leached biochars were conducted as described in section 3.1.3 and concentrations of TCE and PCE in the batch systems were quantified as detailed in section 3.1.4.

4.1.5. Data analysis

The data of leached compounds (ions and DOC) and the biochar properties were analyzed by one-way analysis of variance (ANOVA) with Tukey's post-hoc test to determine significant differences (SigmaPlot 12.0, Sysstat Software Inc., USA). Results of $p > 0.05$ are considered not significant.

The unit-equivalent Freundlich model (Eq. 10) and the Polanyi-theory-based combined adsorption-partitioning model (Eq. 13) were fitted to the data of the sorption batch experiments (see section 2.7.3).

Sorption coefficients including standard errors and confidence intervals were derived by dynamic curve fitting in the software SigmaPlot 12.0 (Sysstat Software Inc., USA). For both isotherm models, sorption coefficients of different data sets were considered to be significantly different when their 95 % confidence intervals did not overlap ($p < 0.01$), or did not overlap by more than 50 % ($p < 0.05$) (Cumming, 2009).

4.2. Results and discussion

4.2.1. Leaching of extractable ions and change in mineral content

The characteristics of the aqueous leachates of the three biochars are summarized in Table 11 below.

Table 11: Selected characteristics of aqueous leachates of the three biochars. DOC and ion content leached were calculated from the concentration measured in the leachate [mg L^{-1}], mass of biochar leached [g], and volume of leachate [mL]. Values represent the mean of three replicates ± standard deviation. Note the differing units for Ca^{2+} and Mg^{2+}.

	BC-WC	BC-GH	BC-CM
pH [-]	8.8 ± 0.05	8.3 ± 0.03	10.2 ± 0.04
EC [µS cm^{-1}] [a]	147 ± 4	599 ± 7	3,757 ± 78
DOC [mg g^{-1}]	1.5 ± 0.1	2.5 ± 0.1	27.4 ± 0.4
K^+ [mg g^{-1}]	0.6 ± 0.02	7.5 ± 0.1	31.8 ± 0.5
Na^+ [mg g^{-1}]	0.2 ± 0.01	0.3 ± 0.03	10.0 ± 0.1
Ca^{2+} [µg g^{-1}]	73 ± 4	92 ± 6	435 ± 94
Mg^{2+} [µg g^{-1}]	28 ± 1	57 ± 4	66 ± 16
PO_4^{3-} [mg g^{-1}]	0.1 ± 0.001	5.3 ± 0.1	1.5 ± 0.1
SO_4^{2-} [mg g^{-1}]	0.2 ± 0.004	1.1 ± 0.02	4.5 ± 0.1
Cl^- [mg g^{-1}]	0.1 ± 0.01	1.0 ± 0.05	24.2 ± 0.4
Total ions leached [mg g^{-1}] [b]	1.2 ± 0.03	15.5 ± 0.1	73.1 ± 1.0

[a] EC: Electrical conductivity of the leachate.
[b] Sum of all ions measured with ion chromatography. For all measured ions, refer to Table A 19.

All leachates are alkaline and pH values are similar to those determined for the original bulk biochars. The BC-CM extract shows the highest and BC-GH the lowest pH value (10.2 and 8.3, respectively). The leachate of BC-CM exhibits the highest EC, followed by BC-GH and BC-WC (3,757, 643, and 147 µS cm^{-1}, respectively; all statistically different; $p < 0.01$). EC tends to increase with increasing ash content of the original biochars. However, there is no significant linear correlation, likely because the ash composition varies and only selected minerals dissolve and contribute to the leachate EC. A similar trend as described for EC is present for the total amount of leached ions. BC-CM released the highest sum of total ions (73.1 mg g^{-1}), followed by BC-GH (15.5 mg g^{-1}), and BC-WC (1.2 mg g^{-1}) (all significantly different from each other; $p < 0.01$). K^+ and Na^+ are the dominating cations in the leachates of all three biochars. The leaching of Ca^{2+} and Mg^{2+} is comparatively low, which is similar to results reported in other studies (Yao et al., 2010; Kong et al., 2014). The anions with the highest concentrations in all

leachates are Cl^-, SO_4^{2-}, and PO_4^{3-}. However, the proportions vary depending on the leached biochar. Cl^- dominates the BC-CM leachate, whereas the leachates of BC-WC and BC-GH are characterized by high SO_4^{2-} and PO_4^{3-} concentrations, respectively. The leaching of N-species from all three biochars (in the form of NO_3^-, NO_2^-, and NH_4^+) is comparatively low, as also found by others (Graber et al., 2010), because they are likely bound in sparsely soluble form (Hollister et al., 2013).

The ion concentrations detected in the leachates are in line with the changes determined for the content of respective mineral elements in the bulk biochars before and after leaching (Table 12). Ca and Mg tend to accumulate in the bulk sample or show only small changes. Na, K, and P contents in BC-CM and BC-GH decrease notably. In BC-WC, Na tends to accumulate and changes in K and P are negligible.

Table 12: Elemental composition of original and leached biochars determined by inductively coupled plasma - atomic emission spectroscopy.

	BC-WC		BC-GH		BC-CM	
	original	**leached**	**original**	**leached**	**original**	**leached**
Si [mg g^{-1}]	38.2	54.2	69.7	69.2	172.5	175.3
Ca [mg g^{-1}]	16.0	18.3	36.9	37.7	72.2	73.6
Mg [mg g^{-1}]	3.6	3.3	3.7	3.7	14.3	14.5
Na [mg g^{-1}]	1.6	2.3	1.0	0.8	13.3	6.0
K [mg g^{-1}]	5.8	5.6	15.0	9.2	31.8	13.3
P [mg g^{-1}]	1.3	1.4	8.8	7.7	14.4	14.0

According to Wu et al. (2011) the leaching of inorganic species predominantly depends on their initial form of occurrence in biochar. Most leached ions originate from the dissolution of mineral components in the ash fraction of the biochars. Ca and Mg are often bound in hardly soluble carbonates or carboxylates (Wu et al., 2011), explaining their comparably low concentrations in all biochar leachates and accumulation in the bulk samples. The Cl^- concentrations show a positive significant ($p < 0.05$) correlation with K^+ and Na^+ in all leachates, suggesting the dissolution of sylvite (KCl) and halite (NaCl). In BC-CM leachates, the mean K/Cl molar ratio of 1.19 ± 0.01 (Table 13) suggests that sylvite dissolution is the main K^+ source. Sylvite is one of the most common minerals in biochar (Xu et al., 2017) and several studies identified sylvite in biochars produced from various feedstocks, including dairy manure (Cao and Harris, 2010), straw (Kloss et al., 2012), and plant material (Zhao et al., 2013b). For the plant-based biochars (BC-WC and BC-GH), a higher K^+ excess over Cl^- is present (K/Cl molar ratios >> 1, Table 13), suggesting an additional K^+ contribution by other soluble minerals such as phosphates, sulfates, or carbonates. Xu et al. (2017) reported that K-bearing minerals are typical for crop-residue biochar. The molar ratios of (Na + K + Mg + Ca)/(Cl + S + P) in the leachates of BC-WC (3.22 ± 0.09), and BC-CM (1.55 ± 0.02) clearly exceed unity (Table 13). This suggests that in addition to soluble salts, some of the released cations exist in other water-soluble forms in biochars, such as Na^+ and K^+ ion-exchangeable carboxylates (Wu et

al., 2011). In contrast, the corresponding molar ratio in the leachate of BC-GH (0.98 ± 0.01, Table 13) indicates no major contribution of leaching from carboxylates.

Table 13: Molar ratios of selected ions measured in biochar leachates calculated from data measured by ion chromatography.

Molar ratios [(meq L^{-1})/(meq L^{-1})]	BC-WC	BC-GH	BC-CM
Na/Cl	2.69 ± 0.29	0.50 ± 0.01	0.64 ± 0.01
K/Cl	5.93 ± 0.70	6.53 ± 0.35	1.19 ± 0.01
(K + Na)/Cl	8.62 ± 1.0	7.03 ± 0.34	1.83 ± 0.02
(Na + K + Mg + Ca)/(Cl + S + P)	3.22 ± 0.09	0.98 ± 0.01	1.55 ± 0.02

As the leachates vary depending on the biochar, it is evident that their composition greatly depends on the binding form, the ash composition, and the associated release mechanism of the different ions. These, in turn, are determined by the original feedstock composition and pyrolysis conditions. The concentrations determined in this study are within the range of values reported in the literature (Table A 20). However, one should be cautious in comparing reported results, as leaching protocols are diverse and vary greatly in extraction time, extraction temperature, and biochar to water ratio.

4.2.2. Leaching of dissolved organic carbon

The leaching procedure mobilized LOC from all biochars, which is detected as DOC in solution (Table 11). The manure-derived biochar BC-CM released the highest amount of DOC (27.4 mg g^{-1}), which is about 10-times more than determined for the two plant-based biochars. BC-GH and BC-WC leached 2.45 mg g^{-1} and 1.53 mg g^{-1}, respectively (all statistically different; $p < 0.01$). The determined DOC concentrations tend to increase with increasing O/C and (O+N)/C ratio of the original biochar, although both correlations are not statistically significant ($p > 0.05$). However, this suggests that biochars with high polarity and low hydrophobicity can mobilize more LOC. Liu et al. (2019a) found that the mobilization of LOC is positively correlated with the O and H content of biochar, as well as with its aromaticity ratio (H/C ratio). They concluded that the LOC was mainly released from biochars' labile fraction that is rich in oxygen-containing functional groups (Liu et al., 2019a). Although the data presented here do not show these correlations, the trends observed for O/C and (O+N)/C ratios indicate the importance of functional groups in LOC release, as especially (O+N)/C is a good proxy for oxygen functionalities (Chen et al., 2008). The wood-based biochar BC-WC released substantially lower DOC concentrations than BC-GH and BC-CM. This is in line with the findings by Liu et al. (2019a) that biochar produced from wood generally mobilizes less LOC than biochars from herbaceous or manure feedstock. Wood contains more lignin, which is thermally more stable than cellulose and hemicellulose (Yang et al., 2007), and therefore tends to produce biochar with less leachable bio-oil components (Liu et al., 2019a).

The DOC concentrations determined in this study are in a similar range as previously reported by Norwood et al. (2013). They examined ASE extraction of cordgrass and honey mesquite biochars and reported

concentrations of 21.5 mg g^{-1} and 16.0 mg g^{-1}, respectively. In general, the findings are in line with previous studies that the release of LOC differs for different biochars (e.g., Qu et al., 2016; Smith et al., 2016; Liu et al., 2019a), indicating that it depends on the biochar feedstock material. However, Liu et al. (2019a) also state that pyrolysis temperature is a more important factor in LOC development than feedstock material.

4.2.3. Change of biochar bulk properties after leaching

A summary of the bulk and structural properties of biochars after leaching is presented in Table 14, alongside the properties of the original biochars as determined in chapter 3 for comparison.

Table 14: Properties of original and leached biochars.

	BC-WC		BC-GH		BC-CM	
	original [a]	**leached**	**original** [a]	**leached**	**original** [a]	**leached**
EC [µS cm^{-1}] [b]	242	133	764	281	7,910	834
pH [-] [b]	9.8	7.8	8.3	7.9	10.3	9.5
C [%]	73.7	74.7	55.8	56.7	22.7	25.2
H [%]	2.5	2.6	3.3	3.1	1.1	1.6
N [%]	0.5	0.5	1.5	1.5	1.3	1.3
S [%]	0.4	0.2	0.4	0.5	0.7	0.5
Ash content [%]	12.5	9.5	26.6	25.1	62.8	61.9
C_{org} [%]	68.7	70.6	53.7	52.9	23.5	22.9
O [%] [c]	10.5	12.8	12.4	13.0	11.4	9.5
H/C [d]	0.40	0.41	0.71	0.65	0.55	0.76
O/C [d]	0.11	0.13	0.17	0.17	0.38	0.28
(O+N)/C [d]	0.11	0.14	0.19	0.19	0.43	0.33
SSA [m^2 g^{-1}] [e]	341	342	215	214	6	25
SSA_{ext} [m^2 g^{-1}] [f]	58	36	60	46	6	25
PV_{tot} [cm^3 g^{-1}] [g]	0.173	0.157	0.136	0.124	0.023	0.046
PV_{mic} [cm^3 g^{-1}] [h]	0.109	0.116	0.061	0.064	n.d.	n.d.
PV_{mes} [cm^3 g^{-1}] [i]	0.064	0.041	0.075	0.060	0.023	0.046
D_{mic} [nm] [j]	0.64	0.79	0.78	0.78	n.d.	n.d.
D_{mes} [nm] [j]	2.8	2.9	2.9	2.9	n.d.	n.d.

[a] Data also presented in Table 2 in chapter 3.2.1.
[b] Electrical conductivity (EC) and pH determined in a 1:10 biochar to water suspension.
[c] O determined by difference.
[d] Molar ratios describing aromaticity (H/C), hydrophobicity (O/C), and polarity ((O+N)/C) of biochars (ratios based on bulk elemental composition).
[e] Apparent specific surface area (BET method).
[f] Specific external surface area (t-plot method).
[g] Total pore volume determined at P/P_0=0.995.
[h] Micropore volume (t-plot method).
[i] Mesopore volume (PV_{tot} - PV_{mic}).
[j] Maxima of micropore and mesopore size distribution (NLDFT method).
n.d. Not determined.

The C content of all biochars tends to increase after leaching, however only the change in BC-CM is significant ($p < 0.05$). Simultaneously, the wood-based BC-WC shows a significant increase in C_{org} ($p < 0.05$), whereas the changes in BC-CM and BC-GH are not significant ($p > 0.05$). Several studies reported increasing C content after varying leaching protocols (Spokas et al., 2014; Qu et al., 2016; Luo et al., 2017; Wang et al., 2017), however decreasing C content after weathering or leaching was also reported (Christophe et al., 2015). The different development in C and C_{org} contents are likely a result of the relative distribution of inorganic species and mobile organic matter in the different biochars. The increase of C_{org} in BC-WC is in line with the relatively small amount of LOC mobilized and the assumption that lignin forms more stable carbon structures during pyrolysis (Yang et al., 2007). In contrast, C_{org} of BC-GH and BC-CM tends to decrease after leaching because of their higher LOC loss caused by more labile carbon formed through the pyrolysis of cellulose and hemicellulose (Yang et al., 2007). One possible reason for the increase in total C content is the effect of the low leachability of carbonates (Wu et al., 2011) as discussed earlier. This can result in the enrichment of relatively stable inorganic carbon phases compared to easily soluble labile OC and other mineral components. In line with this argument is the decrease of EC and ash content of all biochars after leaching ($p < 0.01$), as also reported in other studies (Wu et al., 2011). Additionally, all biochars exhibit decreasing pH values, which can be explained by the release of alkaline base cations (Table 11) during leaching (Yao et al., 2010).

Both plant-based biochars (BC-GH and BC-WC) show a slight increase of O in the bulk mass. In contrast, the O content in BC-CM decreases after leaching (Table 14). This is accompanied by increasing hydrophobicity (decreasing O/C ratio) and decreasing polarity (decreasing (O+N)/C ratio) of BC-CM. As the polarity ratio is a good indicator for oxygen-bearing functional groups (Chen et al., 2008), decreasing (O+N)/C and subsequent decreasing O content indicates the loss of polar functionalities during LOC leaching. Qu et al. (2016) found that the O/C ratio of biochar-released DOC was twice as high as the O/C ratio of the bulk biochar, confirming that polar functional groups are lost during the leaching process. This also results in less clustering of water molecules on the biochar surface (Chun et al., 2004), making the surface more hydrophobic. The two plant-based biochars show no relevant change in O/C and (O+N)/C ratios, which is in agreement with their significantly lower LOC leaching.

4.2.4. Change of biochar surface and pore structure after leaching

Figure 17 shows the incremental pore size distribution and the cumulative pore volume of the three biochars before and after leaching. The calculated SSA, SSA_{ext}, PV_{tot}, and PV_{mic} are listed in Table 14. The changes in SSA of BC-WC and BC-GH are negligible. However, leaching of BC-WC notably changed the pore size distribution, especially in the range smaller than 2 nm. The maximum of the micropore distribution (D_{mic}) shifted towards bigger pores, now being 0.79 nm instead of 0.64 nm, and the determined PV_{mic} slightly increased compared to original BC-WC. Figure 17 illustrates that additional pore volume developed in the range of 0.5 to 2 nm.

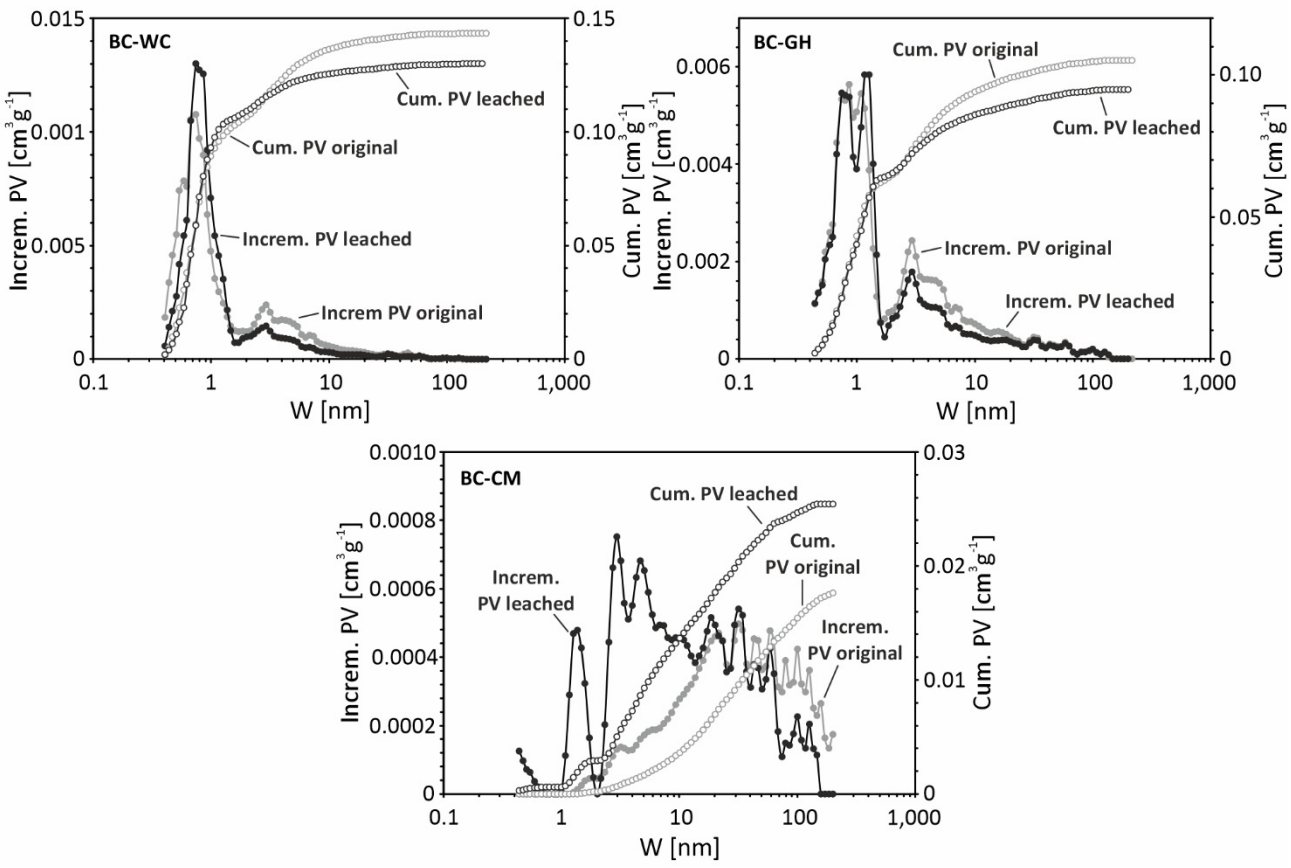

Figure 17: Incremental pore size distribution (Increm. PV [$cm^3\ g^{-1}$]; filled symbols) and cumulative pore volume (Cum. PV [$cm^3\ g^{-1}$]; open symbols) of the three biochars (BC-WC, BC-GH, and BC-CM) before (grey) and after (black) leaching. Data was obtained by argon sorption and analyzed using a NLDFT model assuming argon sorption in slit-shaped pores. W (nm) corresponds to the pore width.

The other plant-based biochar, BC-GH, shows only small changes. The pore size distribution of leached BC-GH displays a slightly higher fraction of pores around 1.2 nm pore width (Figure 17), whereas pores between 0.8 and 1 nm disappeared. Consequently, only marginal changes of PV_{mic} were detected. A reason could be the collapse of pore walls during leaching. Spokas et al. (2014) identified cracks, fractures, and "sinkhole-like" features after rinsing different biochars for 24 hours. This might also be the cause for lower SSA_{ext}, PV_{mes}, and PV_{tot} in both plant-based biochars.

The manure-derived BC-CM shows distinctly different behavior. Both original and leached BC-CM contain their entire SSA in mesopores, captured in SSA_{ext}. It is more than 4-times higher in the leached sample than determined in the original BC-CM. Consequently, PV_{mes} doubled through the development of additional pore volume mainly in the range of 2 to 10 nm pore width. Although PV_{tot} increased, no micropores are present in leached BC-CM, as well as in the original sample.

The described changes in the pore size distribution, pore volume, and SSA of the different biochars illustrate that leaching significantly affects their structural properties. However, the impact of leaching varies between the biochar types.

Although BC-WC released only a small amount of mineral components (1.2 mg g^{-1} ions) and DOC (1.5 mg g^{-1}), the effect on the micropore size distribution and pore volume is significant. In contrast, the leaching of BC-GH has only minor impact on its structural properties, despite the higher concentrations of ions (15.5 mg g^{-1}) and DOC (2.45 mg g^{-1}) released. In BC-CM, leaching of comparatively high amounts of mineral species (73.1 mg g^{-1}) and DOC (27.42 mg g^{-1}) resulted in no change in small pores but extensive alterations in the mesoporous range and SSA. This indicates that leaching does not affect all biochars equally. Depending on the initial distribution and binding of ions and LOC, the response to leaching is different.

Previous studies (Luo et al., 2017; Wang et al., 2017) have shown that LOC can be trapped in small pores and act as a pore-clogging agent. Therefore, leaching generally increased pore accessibility. Luo et al. (2017) reported that the removal of authigenic LOC from two maize straw biochars caused a slight increase in the total surface area by exposing initially blocked micropores. Wang et al. (2017) stated that the change in surface area after LOC leaching was negligible in a rice straw biochar, but total and micropore volume significantly increased. Both plant-based biochars in the present study show increasing PV_{mic} after leaching, which can be linked to the unblocking of micropores through LOC release. However, the effect is more pronounced in BC-WC compared to BC-GH. This indicates that the pore-clogging effect might be more important if a high number of small micropores is already available in the original biochar. Indeed, Luo et al. (2017) suggested that pore blockage may play a bigger role in biochars with higher surface area and porosity. Further, several researchers found that the nature and composition of the released LOC can vary greatly for different biochars (e.g., Lin et al., 2012a; Smith et al., 2013; Jamieson et al., 2014; Tang et al., 2016). Therefore, LOC in biochars derived from different feedstocks might exhibit different binding characteristics, including pore filling and pore blocking. This would result in varying release mechanisms depending on LOC properties and composition.

Similar to LOC, the release of mineral components can also alter the pore structure of biochars. Klasson et al. (2014) showed that washing of several microporous biochars produced from almond shell, removed ash and exposed surface area as well as some previously blocked small pores. Thereby, the pore structure was more affected in low-ash biochars (Klasson et al., 2014). Further, Spokas et al. (2014) confirmed that salts can be precipitated in biochar pores and limit their availability. This indicates that the change in PV_{mic} and the micropore distribution might, at least partly, be caused by the release of soluble ions.

Despite being released from pores, LOC can also be mobilized via the surface functional groups, which does not affect the structural properties. This is likely the case for BC-CM, as its decreasing (O+N)/C ratio indicates the loss of surface functionalities via LOC release. Additionally, structural changes of BC-CM are controlled by the leaching of mineral components or LOC from larger pores and the outer biochar surface. This explains the substantial increase of SSA_{ext} and PV_{mes}. Spokas et al. (2014) confirmed with scanning electron microscopy (SEM-EDS) studies that surface precipitates and organic oils coated surfaces, and concealed visible pores in fresh biochars. The removal of these precipitates and surface coatings via dissolution opened additional porosity and exposed new structural details (Spokas et al., 2014).

However, to distinguish between LOC and mineral release-driven structural changes in biochar is challenging, as the spatial arrangement and distribution of mineral and organic phases are feedstock dependent (Yang et al., 2018). Both phases are usually interlaced and interact with each other (Xiao et al., 2018). Yet, the presented results suggest that the unclogging of micropores is mainly related to LOC leaching, whereas the exposing of mesopores and SSA_{ext} is caused by mineral leaching.

4.2.5. Sorption to leached biochars

To assess the effect of the leaching and resulting changes in biochar properties on their sorption behavior, equilibrium batch experiments were conducted with the leached biochars. The unit-equivalent Freundlich model (Eq. 10) was fitted to the sorption data and the results are presented in Table 15, alongside the data obtained for the original biochars (see section 3.2) for comparison.

Table 15: Parameters of the unit-equivalent Freundlich model for TCE and PCE sorption to original and leached biochars.

			K_{Fr}* [mg kg^{-1}] [a]	n [-] [a]	r^2 [-] [b]	p [-] [b]
TCE	**BC-WC**	**original**	209,143 ± 12,730	0.26 ± 0.02	0.96	< 0.01
		leached	228,452 ± 12,813	0.26 ± 0.01	0.97	< 0.01
	BC-GH	**original**	140,467 ± 6,176	0.32 ± 0.01	0.99	< 0.01
		leached	141,489 ± 6,511	0.30 ± 0.01	0.98	< 0.01
	BC-CM	**original**	29,503 ± 806	0.39 ± 0.01	0.99	< 0.01
		leached	39,828 ± 1,496	0.43 ± 0.01	0.99	< 0.01
PCE	**BC-WC**	**original**	108,260 ± 3,345	0.33 ± 0.02	0.97	< 0.01
		leached	132,431 ± 4,695	0.30 ± 0.02	0.96	< 0.01
	BC-GH	**original**	74,484 ± 2,974	0.33 ± 0.02	0.97	< 0.01
		leached	90,228 ± 2,937	0.33 ± 0.01	0.98	< 0.01
	BC-CM	**original**	14,802 ± 365	0.46 ± 0.02	0.99	< 0.01
		leached	18,375 ± 435	0.52 ± 0.02	0.99	< 0.01

[a] Unit-equivalent Freundlich coefficients K_{Fr}* and Freundlich exponents n calculated using non-linear curve fitting in Sigma Plot after Eq. 10.

[b] r^2 and p represent the coefficient of determination and significance of the data fit obtained from Sigma Plot.

As already discussed in chapter 3.2.2, sorption affinity K_{Fr}* of both TCE and PCE increases following the order BC-CM < BC-GH < BC-WC. The same pattern is still observed after biochars are leached, although sorption of both compounds tends to increase after leaching ($K_{Fr}*_{orig.} < K_{Fr}*_{leach.}$). PCE sorption to all three biochars is significantly enhanced after leaching ($p < 0.01$). With an increase of 19 % in K_{Fr}*, BC-CM exhibits the strongest change, followed by BC-WC (18 %) and BC-GH (17 %). Considering TCE sorption, only BC-CM shows a significant increase ($p < 0.01$) in K_{Fr}* (26 %), whereas the changes in sorption to BC-GH and BC-WC are not significant. This illustrates that the changes in sorption affinity differ distinctly between compounds, but also between biochars. For both compounds, the increase in K_{Fr}* is highest for the manure-derived BC-CM that also released the highest

amount of LOC and leachable ions. However, the increasing sorption of PCE to the plant-derived biochars BC-WC and BC-GH cannot be readily explained by the amounts of leachable minerals and OC, as they are comparatively small.

The sorption nonlinearity is much less affected by the leaching procedure. Only BC-CM shows significant changes, with slightly increasing n for both TCE (original: 0.39; leached: 0.43; $p < 0.05$) and PCE (original: 0.46; leached: 0.52; $p = 0.05$). This suggests increased linear sorption, which in turn indicates stronger partitioning of both sorbates. As previously discussed, BC-CM is the only sorbent with significantly lower polarity and higher hydrophobicity after leaching. This reduces the adsorption of water molecules (Li et al., 2002; Chun et al., 2004) and therefore might increase the accessibility of the biochar matrix for partitioning.

4.2.6. Change in sorption mechanisms after biochar leaching

Sorption of organic contaminants to biochar usually comprises multiple mechanisms (e.g., Xiao et al., 2018), among which pore-filling and partitioning dominate in case of chlorinated hydrocarbons (see chapter 3). These processes are influenced by the compound properties, for example, the water solubility and molecular size of the sorbate, but also biochar characteristics. The Polanyi-theory-based adsorption-partitioning model (Eq. 13) allows to resolve the contribution of partitioning and pore-filling to the overall sorption and should help to further explore the changes in sorption mechanisms after leaching. The respective isotherms are displayed in Figure 18 and fitting parameters are reported in Table 16.

Table 16: Isotherm parameters of the combined partitioning and pore-filling model for sorption of TCE and PCE to the original and leached biochars.

			K_p [L kg^{-1}] [a]	V_0 [cm³ kg^{-1}] [a]	E [J mol^{-1}] [a]	r^2 [-] [b]	p [-] [b]
TCE	**BC-WC**	**original**	n.a.[c]	85 ± 1.3	14,452 ± 193	0.96	< 0.01
		leached	n.a.[c]	92 ± 1.0	14,849 ± 137	0.99	< 0.01
	BC-GH	**original**	96 ± 35	44 ± 2.4	13,734 ± 361	0.99	< 0.01
		leached	n.a.[c]	52 ± 0.7	13,564 ± 152	0.99	< 0.01
	BC-CM	**original**	50 ± 4	6 ± 0.3	14,078 ± 355	0.99	< 0.01
		leached	61 ± 7	7 ± 0.5	13,033 ± 403	0.99	< 0.01
PCE	**BC-WC**	**original**	218 ± 51	44 ± 2.2	10,088 ± 350	0.97	< 0.01
		leached	156 ± 51	60 ± 2.4	10,135 ± 284	0.99	< 0.01
	BC-GH	**original**	132 ± 39	30 ± 1.5	10,266 ± 318	0.97	< 0.01
		leached	214 ± 37	34 ± 1.4	10,608 ± 288	0.99	< 0.01
	BC-CM	**original**	73 ± 6	3 ± 0.3	10,278 ± 525	0.99	< 0.01
		leached	95 ± 7	4 ± 0.4	9,831 ± 755	0.99	< 0.01

[a] Coefficients of the combined adsorption-partitioning model (± standard error) calculated using non-linear curve fitting in Sigma Plot after Eq. 13.

[b] r^2 and p represent the coefficient of determination and significance of the data fit obtained from Sigma Plot.

[c] Derived K_p values were not significant ($p > 0.01$).

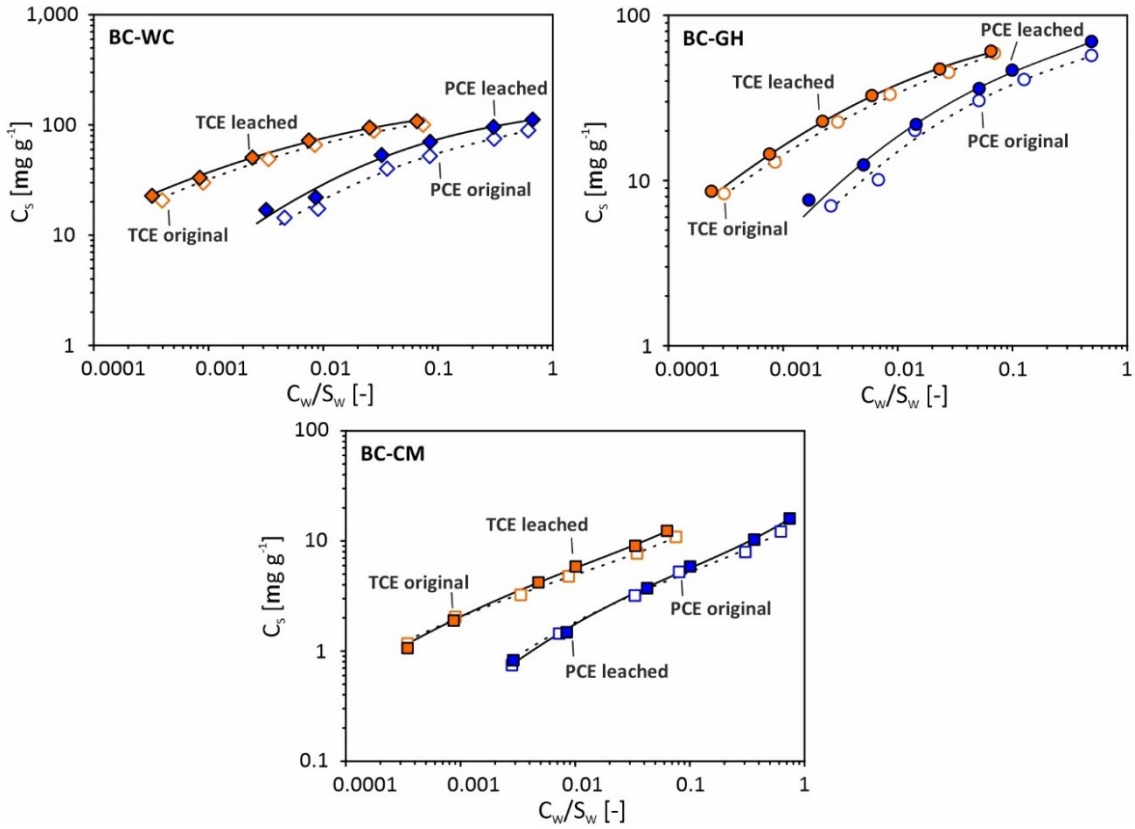

Figure 18: Sorption isotherms of TCE and PCE on the three biochars (BC-WC, BC-GH, BC-CM) before (open symbols) and after (filled symbols) leaching. Dashed (before leaching) and solid (after leaching) lines represent the fitted Polanyi-theory-based adsorption-partitioning model (Eq. 13). All data points represent the mean of triplicates. All error bars are within symbol size.

Sorption of TCE to both plant-based biochars (BC-WC and BC-GH) after leaching is well described by a sole pore-filling mechanism (K_p derived from the model fit not significant; $p > 0.01$). The partitioning component that contributed to TCE sorption to the original BC-GH is eliminated entirely after leaching (Table 16). In contrast, the manure-derived BC-CM shows significant influence of partitioning on the sorption of both compounds, as do the isotherms of PCE sorption to BC-GH and BC-WC, before and after leaching.

For all three leached biochars, the maximum adsorbed volume V_0 is significantly higher for TCE compared to PCE ($V_0^{TCE}{}_{leach.} > V_0^{PCE}{}_{leach.}$; $p < 0.01$), displaying the same trend as observed in the original biochars (see section 3.2.2). V_0 for TCE increases significantly after leaching for BC-WC and BC-GH, with 7.5 % and 15.7 %, respectively (both $p < 0.01$). The V_0 value of BC-CM also increases (about 21 %; $p < 0.05$), but is still about one order of magnitude lower than V_0 of the two other leached biochars. Considering PCE, only V_0 of BC-WC shows a significant increase (27 %; $p < 0.01$), whereas the changes for BC-GH (12.4 %) and BC-CM (5 %) are not significant ($p > 0.05$).

As discussed earlier, Figure 17 shows that BC-WC experienced significant changes in its micropore size distribution. Leaching created additional pore volume in the region between 0.5 nm and 2 nm, which is reflected by its increased PV_{mic}. The availability of additional micropores and the concomitant shift towards slightly larger pore sizes allows PCE and TCE to penetrate a larger number of sorption sites in leached BC-WC. This is reflected

in a higher V_0 of both compounds after leaching ($V_0^{TCE}_{leach.} > V_0^{TCE}_{orig.}$; $V_0^{PCE}_{leach.} > V_0^{PCE}_{orig.}$; both $p < 0.01$). However, TCE is still able to access a larger number of pores ($V_0^{TCE}_{leach.} > V_0^{PCE}_{leach.}$; $p < 0.01$). This is the result of a steric effect caused by molecular sieving, as already observed in the original BC-WC (see section 3). TCE is the slightly smaller molecule with 6.2 Å (= 0.62 nm) as its second largest dimension (TCE: 6.6 Å × 6.2 Å × 3.6 Å; Karanfil and Dastgheib, 2004), compared to PCE with 6.6 Å (= 0.66 nm) (Bembnowska et al., 2003). Both compounds can be subject to size exclusion when the pore width of the sorbent becomes smaller than 1.7 times their second largest dimension (Kasaoka et al., 1989; as cited in Li et al., 2002). The shift towards larger pores in leached BC-WC dampens this size exclusion of PCE, which is also reflected by a larger increase of V_0 after leaching (TCE: 7.5 %; PCE: 27 %). Consequently, the differences between V_0 of both compounds also decreased (original: 48 %; leached: 34 %) and sorption of PCE to leached BC-WC is now entirely taking place via pore-filling.

BC-GH experienced less obvious changes after the leaching procedure. The increase of pores around 1.2 nm width goes along with diminished pore volume between 0.8 and 1 nm width. The diameters determining size exclusion of TCE and PCE are about 1.05 nm and 1.12 nm, respectively. Therefore, the decrease in pores smaller than 1 nm should not negatively influence sorption. Instead, V_0 of TCE increases because the larger pores in the leached sample are easier to access for the molecule. PCE however, seems to still experience size exclusion from some pores, due to its bigger size. Therefore, V_0 of PCE only increases slightly and the change is not statistically significant.

Although PV_{tot} (= PV_{mes}) of BC-CM increases substantially after leaching (about 2-fold; see Table 14) and the pore size distribution experiences great changes, the effect on V_0 for both compounds is relatively small. As previously described (see section 4.2.3), leaching of BC-CM mainly opens pores in the region between 2 and 10 nm pore width. These appear to provide additional sorption sites, resulting in the increase of V_0 of TCE after leaching. However, the larger mesopores in BC-CM are likely less favorable for contaminant sorption, compared to the narrow micropores present in the two plant-based biochars (see Lastoskie et al., 1993). Therefore, the more hydrophobic molecule PCE is not highly attracted to these new sorption sites and instead favors the available partitioning domains.

The linear partitioning coefficient K_p generally experiences less obvious changes, probably because of significantly smaller contribution of partitioning to the overall sorption (Table 17). Only the K_p value of PCE sorption to BC-CM significantly increases after leaching ($K_p^{PCE}_{leach.} > K_p^{PCE}_{orig.}$; $p < 0.05$). However, also K_p for TCE sorption to BC-CM seems to increase, although the change is not significant ($p > 0.05$). These changes are consistent with the observed increasing n values determined by the Freundlich model. Both indicate enhanced partitioning into the manure-derived biochar BC-CM after leaching. As previously reported in chapter 3, increasing polarity favors partitioning, because it increases the water clustering on the surface (Li et al., 2002) and might hinder the access to pores. However, it appears that the loss of oxygen-bearing functional groups (decreasing (O+N)/C) in BC-CM through leaching enhances partitioning. This indicates that the effect of pore blocking by water clusters might not be dominating in the mesoporous BC-CM. Instead, the decreasing number

of functional groups increases the overall hydrophobicity (decreasing O/C), making the biochar matrix more attractive for partitioning of hydrophobic molecules, such as TCE and PCE. Luo et al. (2017) also concluded that oxygen-rich LOC can cover aromatic structures on biochar surfaces, which might hinder the partitioning of organic contaminants. This confirms that the high amount of mobilized LOC is responsible for the increasing K_p values of leached BC-CM by exposing additional partitioning domains. This is also reflected in the increased overall percentage of partitioning, especially for the more hydrophobic compound PCE (at 5 % of S_W: $PCE_{orig.}$ 13.1 %, $PCE_{leach.}$ 16.4 %; Table 17).

Table 17: Distribution of partitioning and pore-filling in sorption of original and leached biochars.

			1 % of S_W [a]		5 % of S_W [a]	
			partitioning [%]	**pore-filling [%]**	**partitioning [%]**	**pore-filling [%]**
TCE	**BC-WC**	**original**	0	100	0	100
		leached	0	100	0	100
	BC-GH	**original**	3.1	96.9	9.9	90.1
		leached	0	100	0	100
	BC-CM	**original**	11.0	89.0	30.0	70.0
		leached	11.8	88.2	30.3	69.7
PCE	**BC-WC**	**original**	1.5	98.5	3.5	96.5
		leached	0.8	99.2	1.9	98.1
	BC-GH	**original**	1.2	98.8	3.1	96.9
		leached	1.6	98.4	4.2	95.8
	BC-CM	**original**	5.7	94.3	13.1	86.9
		leached	7.7	92.3	16.4	83.6

[a] Relative distribution of partitioning and pore-filling from the combined partitioning-adsorption model calculated at 1 % and 5 % of the respective water solubility S_W of the compound.

For both plant-based biochars, no significant changes are evident for K_p and generally the role of partitioning in sorption decreases (Table 17). This is the case, because no significant change in O/C and (O+N)/C occurred for these biochars, and consequently both compounds are attracted to the newly accessible micropores in the leached samples.

4.3. Conclusions

The present results illustrate that accelerated leaching of biochars can significantly impact their properties and sorption behavior for chlorinated hydrocarbons. Biochars produced from different feedstocks show unique changes in their structure, which results in distinct changes in sorption mechanisms. In the plant-based biochars, leaching of small amounts of ions and LOC exposed additional micropores and notably changed their size distribution. This increases the accessibility of sorption sites in small micropores and enhanced pore-filling of TCE and PCE. In contrast, the release of high ion and DOC concentrations from the manure-based biochar only

modified external surface area and mesopore volume, which showed little effect on sorption. Instead, the removal of oxygen-containing functional groups, and resulting increasing hydrophobicity and lower polarity, enhanced the accessibility of partitioning domains, and therefore increased its contribution to overall sorption. This highlights that both LOC and minerals can play an important role in modifying the chemical and structural characteristics of biochar, and thus influence organic contaminant sorption. Thereby, the impact on sorption is not mainly driven by the mass leached, but rather by the release mechanism and spatial distribution of leachable constituents.

5. Impact of sorbent properties on the remobilization of organic contaminants

As highlighted in the previous chapters, biochar can potentially serve as a long-term sink for environmental contaminants. Therefore, when applied in remediation technologies, it is not only important to understand the adsorption process, but it is also vital to know if pollutants are sequestered for the long-term or if they are readily released again into the environment.

A widely applied approach to evaluate the ability of sorbed contaminants to be remobilized after sorption is to conduct desorption experiments. This is mostly done by the decant-refill method. After reaching adsorption equilibrium, desorption is initiated by removing a defined amount of the bulk solution and replacing it with an equivalent volume of sorbate free background solution. If sorption is fully reversible, the adsorption and desorption branch of the isotherm should be identical, which equates to the entire mass previously adsorbed being released. However, very frequently the "chemical released by dilution of the solute in the fluid phase is less than predicted by the isotherm constructed in the "forward" (uptake) direction" (Pignatello, 2011). This phenomenon is called sorption hysteresis or irreversible sorption (e.g., Pignatello, 2013 and references therein). Sorption hysteresis and/or irreversible sorption have been reported for a variety of sorbents, including natural organic matter (e.g., Sander and Pignatello, 2005b; Sander and Pignatello, 2009), different soils and sediments (e.g., Weber et al., 1998), and selected activated carbons (e.g., Tanthapanichakoon et al., 2005; ElHaddad et al., 2013). Braida et al. (2003) were among the first to describe sorption hysteresis in charcoals, a material very similar to biochar (see section 2.1). They attributed sorption hysteresis of benzene to swelling of the sorbent and pore deformation caused by the sorbate. This pore deformation can cause the polyaromatic structure of the sorbent to collapse during desorption, ultimately trapping some of the sorbate (Braida et al., 2003).

In recent years, several researchers described hysteretic behavior or irreversible sorption in biochars. Yu et al. (2010) observed irreversible sorption of the pesticide pyrimethanil in red gum wood chip biochars, and Jing et al. (2018) found sorption hysteresis of phthalic acid esters in peanut hull and wheat straw biochars. In both cases, the authors attributed the hysteretic behavior to pore deformation.

Besides pore deformation, Wang et al. (2017) highlighted another possible reason for irreversible sorption of nitrobenzene, naphthalene, and atrazine in rice straw-derived biochars, called the "ink-tank effect". It can occur when LOC clogs the entrance of pores and therefore hinders desorption, because the activation energy for desorption from the ink-tank pore is greater than the energy for the molecule to enter the pore (Pignatello and Xing, 1996 and references therein; Wang et al., 2017).

Besides simple one-step (e.g., Wang et al., 2017) or multi-step (e.g., Yuan et al., 2021) batch desorption experiments, several researchers have also utilized extraction techniques to study the remobilization of sorbed contaminants. Ahmad et al. (2012) used n-hexane extraction to assess desorption of TCE from different biochars and activated carbon. Liu et al. (2019b) utilized ultrasonic assisted solvent extraction with an acetonitrile/methanol mixture to evaluate the desorption resistance of pre-sorbed lincomycin from biochars.

In all cases, the researchers reported that the biochars' pore structure had a pronounced effect on the extent of hysteresis or irreversible sorption. Further, Wang et al. (2017) and Liu et al. (2019b) highlighted the importance of leachable compounds in irreversible sorption. This underscores that biochar properties are a key factor in understanding the remobilization behavior of sorbed contaminants and its driving mechanisms.
Although numerous studies have investigated desorption behavior and the phenomenon of irreversible sorption, the mechanistic understanding remains limited. In 2011, Pignatello highlighted this issue with the following comment:

"Sorption hysteresis and resistant desorption are the "elephants in the room" of sorption research - common problems with serious implications that nobody wants to tackle." (Pignatello, 2011)

This, for the most part, remains true until this day. Therefore, a series of sorption-extraction experiments was conducted, designed to gain further insights into the effect of sorbent properties on the extractability of organic compounds sorbed on carbonaceous sorbents. One hypothesis is that properties such as the amount of LOC and the sorbent pore structure, like micropore volume and pore size distribution, have a distinct influence on the remobilization of sorbed organic compounds.
To investigate this, three different biochars and one activated carbon, previously characterized (see section 3.2.1), were pre-loaded with defined amounts of TCE and PCE. Following, the sorbed compounds were sequentially extracted with different solvents to analyze their remobilization behavior.

5.1. Materials and methods

The three biochars (BC-CM, BC-GH, and BC-WC) and the activated carbon used in this chapter are described in section 3.1.2. The properties of the two chlorinated compounds TCE and PCE, again used as model compounds, are listed in Table 1.

5.1.1. Experimental set-up

The adsorption step of the experiments was carried out in a dialysis-batch system. In the following, this is also referred to as "pre-loading". Either 100 mL headspace vials with Teflon-lined crimp top caps or 500 mL glass bottles, fitted with screw caps and Teflon-lined septa, were used for the experiments. Pre-wetted dialysis tubes (ZelluTrans, MWCO 12,000-14,000, Carl Roth, Germany) were filled with about 0.2 g of sorbent (Ohaus Explorer Pro; precision ± 0.1 mg) and 4 mL of deionized water to suspend the sorbent. Both ends of the dialysis tube were closed with copper wire and tubes were placed into glass vessels filled with deionized water (Mili-Q, Merck Millipore, Germany). TCE or PCE was spiked into the batch-system at pre-defined concentrations, either as pure

liquid or dissolved in methanol. After spiking, all bottles were immediately closed, sealed with parafilm, and shaken on a horizontal shaker at ambient conditions (21°C ± 1) in the dark for 14 days to attain equilibrium.

The experimental set-up consisted of two series. The first series aimed to pre-load the sorbents to its maximum sorption capacity (C_{max}). To achieve this, the test compound was added into the batch system in excess as pure liquid. This ensured that the aqueous phase concentration of the target compound (C_W) remained at water solubility (S_W) for the entire equilibration period.

The second series aimed to pre-load the sorbents to two specific concentration points. Batch-dialysis systems were designed to yield a C_W after sorption of 1 % and 10 % of the compounds' S_W, being about 10.9 and 109 mg L^{-1} for TCE and 1.51 and 15.1 mg L^{-1} for PCE. In the following these pre-loading levels are referred to as 0.01 S_W and 0.1 S_W. The actual C_W in the batch-dialysis system after the two-week equilibration period was measured by withdrawing 300 µL of the bottle headspace and analyzing it with a GC-FID system as described in section 3.1.4. In the second series, all samples were prepared in triplicate.

5.1.2. Sequential extraction of pre-loaded sorbents

After the 14-day equilibration period, all pre-loaded sorbent samples were sequentially extracted in five consecutive extraction steps using an Accelerated Solvent Extractor (ASE 300, Dionex, Germany). Dialysis bags were removed from the bottles, cut open, and placed into 30 mL stainless steel extraction cells. The extraction cells were fitted with glass fiber filters at the top and bottom (Thermo Scientific, Germany) and filled-up with pre-cleaned quartz sand. In cases where dialysis tubes had leaked small amounts of sorbent into the bulk solution during equilibration, supernatants were vacuum-filtered through glass fiber filters. The filters with the retained sorbent material were added into the extraction cell alongside the dialysis tube.

A five-step extraction scheme was employed to quantify the fractions of contaminant available for desorption under different conditions. Extraction steps 1 and 2 using deionized water (ultra-pure Millipore) at 40°C and 80°C, were followed by extraction with three different organic solvents at 50°C: methanol (step 3), toluene (step 4), and n-hexane (step 5). All extractions were performed at a constant cell pressure of 100 bar under static conditions, with an extraction time of 10 minutes. Extracts were collected in 200 mL glass collection bottles, fitted with screw caps and rubber septa. The volume of all extracts was determined gravimetrically. For extraction steps 1 and 2, 4 mL of n-hexane was added into the collection bottle prior to extraction for immediate in bottle liquid-liquid partitioning of the target compound. Collection bottles were shaken for about 2 minutes and placed in the refrigerator for 30 minutes to facilitate phase separation. Afterwards, the n-hexane phase was withdrawn using a glass pipet and transferred into 2 mL glass vials with crimp-top caps. Extracts obtained from steps 3, 4, and 5 were transferred directly into 20 mL crimp-top vials. All samples were stored frozen until analysis.

5.1.3. Quantification of TCE and PCE in extracts

All extracts were analyzed using a gas chromatograph with mass spectrometric detection (Agilent 7890A/5975C GC-MS system) equipped with an automatic sampler and a DB-624 column (Agilent J&W 122-1364 DB-624, 60 m x 250 µm x 1.4 µm) for sample separation. The MS was run in selective ion mode (SIM) with mass fragments (m/z) 95, 130, and 132 for TCE, and 129 and 166 for PCE detection. All concentrations were quantified with external standards prepared in methanol, toluene, or n-hexane.

5.1.4. Data analysis

The sorbent loading C_S prior to extraction was calculated by mass balance:

$$C_S = \frac{(C_{spiked} - C_W)\, V_{water}}{m} \qquad \text{(Eq. 14)}$$

Where C_{spiked} is the initially spiked compound concentration, C_W the concentration in the aqueous phase after sorption, V_{water} the water volume, and m the sorbent mass in the batch system.

The mass desorbed (m_{desorb}) by the individual extraction steps was calculated utilizing the concentration of the target compound detected with GC-MS ($C_{W,\,desorb}$) and the solvent volume used for extraction ($V_{extract}$).

$$m_{desorb} = C_{W,desorb}\, V_{extract} \qquad \text{(Eq. 15)}$$

Based on the initial sorbent loading C_S and the mass desorbed m_{desorb}, the mass fractions extracted for each sequential extraction step and the non-extracted mass fractions were calculated. Further, based on the cumulative mass extracted, the share of each extraction step of the cumulative extracted mass was also calculated.

Statistical analysis was carried out using the software SigmaPlot 12.0 (Sysstat Software Inc., USA). For each solvent used, the differences in fractions extracted between the four sorbents were assessed by using a one-way analysis of variance (ANOVA) with the Student-Newman-Keuls (SNK) post-hoc test. For each sorbent, the differences between the fractions extracted by the four solvents were tested with a one-way ANOVA followed by the Tukey's post-hoc test. For differences between TCE and PCE, and between the 0.01 and 0.1 S_W pre-loading levels, a one-sided t-test was applied. Results of $p < 0.05$ were considered as statistically significant.

5.2. Results and discussion

Table 18 and Figure 19 display the fractions of TCE and PCE that are released by the five consecutive extraction steps at the three different tested concentration levels (0.01 S_W, 0.1 S_W, and S_W). Results are expressed as the percentage of the total contaminant mass extracted. This presentation was chosen over the actual mass desorbed (e.g., mg of TCE or PCE) because the absolute sorption capacity between the four sorbents varies significantly (see chapter 3). The absolute mass released in each extraction step is additionally presented in Appendix A3 (Table A 21 and Table A 22).

On the first glance, one can see that there are notable differences between the four sorbents, the three concentration levels, and the two compounds. Although not all differences are statistically significant or could be tested (no statistics for the concentration level S_W as no replicates were performed), some noteworthy trends are described in the following paragraphs.

5.2.1. Total mass extracted – contribution of the different solvents

The first two extraction steps were performed with water at 40°C and 80°C. For ease of interpretation, these two steps are summed up and interpretation is based on the cumulative water-released fraction (sum of extraction steps 1 and 2) in the following.

Table 18: TCE and PCE fractions released by each of the five consecutive extraction steps as percentage of the total extracted mass. Values represent the mean values of three replicates ± standard deviation. Note that no replicate samples were available for the S_W pre-loading level.

	TCE				**PCE**			
	BC-CM	**BC-GH**	**BC-WC**	**AC**	**BC-CM**	**BC-GH**	**BC-WC**	**AC**
				0.01 S_W				
Water-1 [%]	5.8 ± 2.8	1.5 ± 0.5	1.4 ± 0.2	0.9 ± 0.4	4.5 ± 0.3	1.7 ± 0.7	0.7 ± 0.2	0.6 ± 0.1
Water-2 [%]	4.4 ± 2.3	3.4 ± 1.4	2.7 ± 0.2	2.2 ± 0.4	6.0 ± 1.9	3.6 ± 0.5	2.4 ± 1.1	1.0 ± 0.1
Sum water [%]	*10 ± 3.6*	*4.9 ± 1.5*	*4.1 ± 0.3*	*3.1 ± 0.5*	*10 ± 2.0*	*5.3 ± 0.9*	*3.0 ± 1.1*	*1.6 ± 0.2*
Methanol [%]	48 ± 7.4	57 ± 5.8	62 ± 5.4	32 ± 4.1	55 ± 5.5	53 ± 3.7	48 ± 7.0	13 ± 4.0
Toluene [%]	27 ± 2.3	26 ± 2.9	16 ± 7.3	44 ± 3.4	26 ± 4.3	23 ± 3.9	32 ± 4.9	71 ± 0.1
n-hexane [%]	15 ± 0.5	12 ± 4.6	18 ± 12	20 ± 3.5	8.6 ± 1.0	19 ± 2.5	17 ± 2.9	15 ± 3.9
				0.1 S_W				
Water-1 [%]	26 ± 4.6	4.5 ± 1.1	4.5 ± 1.8	2.4 ± 0.2	11 ± 0.8	4.2 ± 2.0	2.1 ± 0.6	2.8 ± 0.5
Water-2 [%]	5.6 ± 1.4	4.4 ± 1.9	4.1 ± 0.4	1.8 ± 0.4	4.6 ± 0.7	3.3 ± 1.2	4.0 ± 2.1	3.4 ± 0.8
Sum water [%]	*31 ± 4.8*	*9.0 ± 2.2*	*8.6 ± 1.8*	*4.2 ± 0.5*	*16 ± 1.1*	*7.5 ± 2.4*	*6.1 ± 2.2*	*6.2 ± 1.0*
Methanol [%]	49 ± 5.7	64 ± 3.1	65 ± 6.5	39 ± 0.8	48 ± 5.2	55 ± 3.0	53 ± 1.6	42 ± 2.9
Toluene [%]	15 ± 1.5	20 ± 2.1	18 ± 2.9	37 ± 0.8	25 ± 1.8	24 ± 0.6	27 ± 1.2	30 ± 3.2
n-hexane [%]	5.0 ± 1.0	7.0 ± 1.1	8.9 ± 1.4	20 ± 1.1	11 ± 2.2	14 ± 2.0	14 ± 0.6	22 ± 3.5
				S_W				
Water-1 [%]	44	18	17	6.3	16	12	3.8	5.0
Water-2 [%]	12	9.0	7.3	5.4	7.0	9.5	4.9	1.8
Sum water [%]	*56*	*27*	*24*	*12*	*23*	*22*	*8.6*	*6.8*
Methanol [%]	24	36	37	36	57	46	55	30
Toluene [%]	17	26	27	38	18	25	25	45
n-hexane [%]	4.3	11	12	14	2.0	7.8	11	18

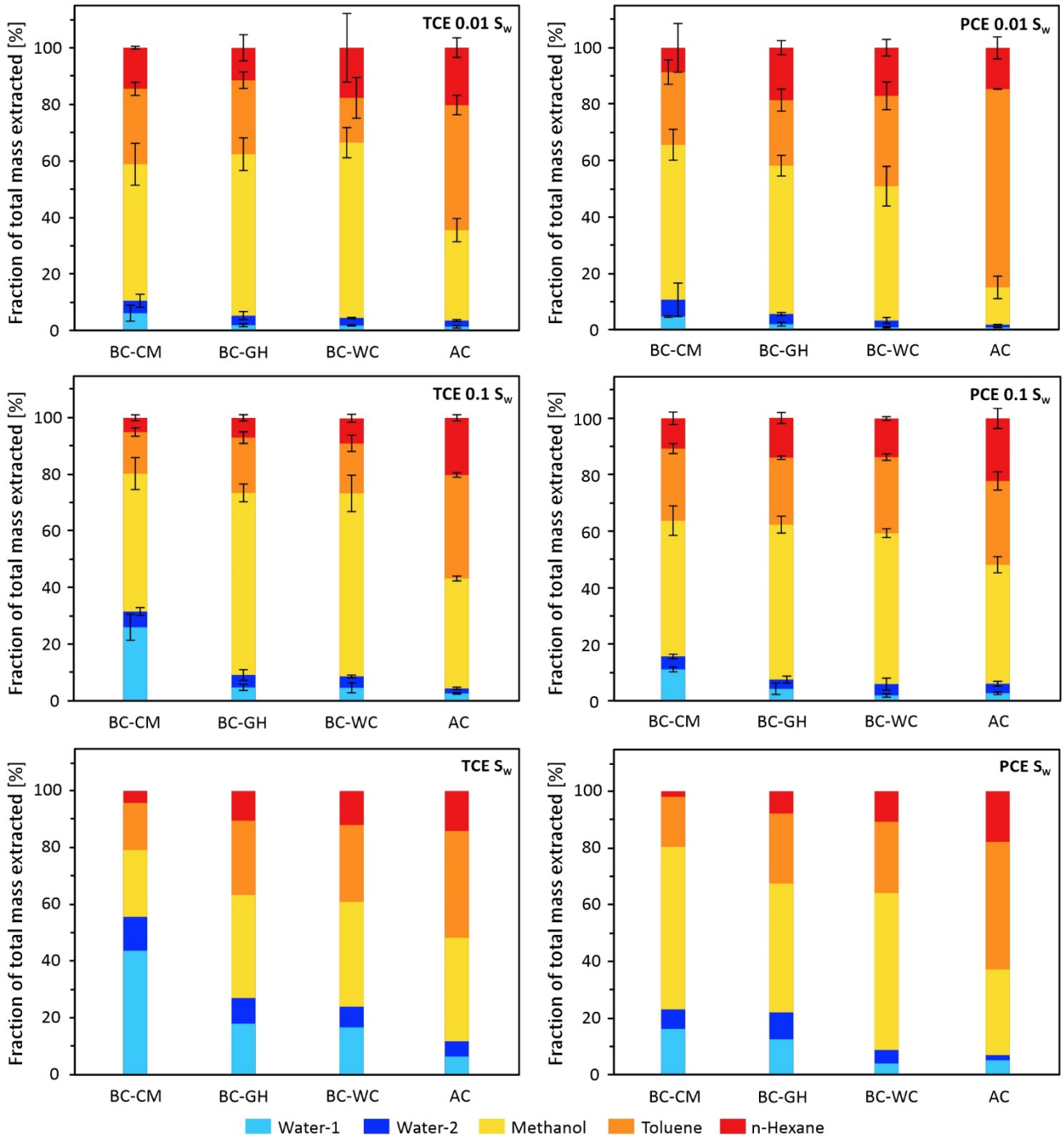

Figure 19: TCE and PCE extracted from the four sorbents (BC-CM, BC-GH, BC-WC, and AC) as percentage of the total mass extracted (= 100 %) at the three pre-loading levels 0.01 S_W, 0.1 S_W and S_W, by the five sequential extraction steps (water-1, water-2, methanol, toluene, and n-hexane). Data represent the mean values of three replicates ± standard deviation (error bars). Note that for the S_W pre-loading level no replicate samples were available.

Mobilization by water

At the lowest pre-loading level (0.01 S_W), water released the highest fraction of TCE and PCE from BC-CM (TCE: 10 ± 3.6 %; PCE: 10 ± 2.0 %). This is, in both cases, a significantly higher fraction than mobilized from the

other three sorbents ($p < 0.05$). These follow with mass fractions all clearly below 10 % (Table 18). Concerning PCE, the fraction released by water from BC-GH is significantly higher than the fraction released from BC-WC and AC ($p < 0.05$), which are not statistically different from each other ($p > 0.05$). For TCE, there is no statistical difference in the water-mobilized fraction between any of these three sorbents ($p > 0.05$).

The 0.1 S_W pre-loading level presents a similar picture. For both compounds, a significantly higher fraction was released from BC-CM compared to the other three sorbents ($p < 0.05$), which do not show a significant difference between each other ($p > 0.05$).

Although the results at the highest pre-loading level (S_W) could not be statistically examined, a similar trend is also apparent in these data. Especially the water-released TCE fraction from BC-CM is notably higher than the fractions released from any of the other three sorbents.

The differences between the three pre-loading levels are only significant in some cases. However, a general trend of increasing water-mobilized fraction from low to high pre-loading is evident (0.01 S_W < 0.01 S_W < S_W). This is especially prominent in BC-CM, where the water-released fraction of 0.01 S_W is significantly smaller than the share released at the 0.1 S_W level ($p < 0.05$). This is the case for TCE and PCE. For TCE, this difference is also significant for BC-WC ($p < 0.05$), however not for BC-GH.

Comparing the results of TCE and PCE, there is no statistical difference in the water-released fractions at the 0.01 S_W pre-loading level for any of the biochars ($p > 0.05$). However, at the 0.1 S_W level, the water-released TCE fraction is significantly higher for BC-CM ($p < 0.05$). This difference between TCE and PCE appears to further increase at the S_W level. For the three remaining sorbents, differences between TCE and PCE are small and do not follow a consistent trend.

Mobilization by organic solvents

Following the extraction with water, the samples were further sequentially extracted at 50°C with three different organic solvents: methanol, toluene, and n-hexane.

For all biochars, methanol contributed the highest share to the total extracted mass of all solvents at the 0.01 S_W and 0.1 S_W pre-loading level.

At the 0.01 S_W pre-loading level, methanol mobilized a higher mass fraction from all biochars compared to AC ($p < 0.05$). This is the case for both TCE and PCE. While for PCE there is no difference in the methanol fraction between any of the three biochars, for TCE there is a significant difference between BC-CM and BC-WC ($p < 0.05$).

At the 0.1 S_W level, the picture is less clear. For TCE, a significantly lower fraction was released from AC compared to all three biochars ($p < 0.05$). Additionally, the methanol fraction released from BC-CM is significantly lower than released from the other two biochars ($p < 0.05$ for both BC-GH and BC-WC), which do not show a significant difference between each other ($p > 0.05$). For PCE, no difference was detected between AC and BC-CM

($p > 0.05$). However, the fraction released from AC is significantly smaller compared to BC-WC and BC-GH ($p < 0.05$).

At the highest pre-loading (S_W), the trend for PCE is similar to the trends described for the lower concentration levels. The methanol fraction released from AC seems to be distinctly smaller than for the three biochars. However, for TCE the methanol-released fraction appears to be lowest for BC-CM, while there is no notable difference between BC-GH, BC-WC, and AC.

When the data for TCE and PCE are compared, there is no consistent pattern. Considering differences between the pre-loading concentrations, no differences are detectable for the three biochars. However, when looking at AC, the methanol fraction is significantly lower at the 0.01 S_W level for both compounds ($p < 0.05$).

When the first three extraction steps are summed up (water-1, water-2, and methanol), it is interesting to note that there is only little difference between the three biochars at the 0.01 S_W and 0.1 S_W pre-loading levels. For all three biochars, the majority of the extracted mass of TCE and PCE was mobilized in the first three extraction steps. Considering TCE, 59 to 66 % and 73 to 80 % of the extracted mass was mobilized at the 0.01 S_W and 0.1 S_W pre-loading level, respectively. For PCE, 51 to 66 % and 59 to 64 % of the extracted mass was mobilized in the first three steps for the 0.01 S_W and 0.1 S_W pre-loading level, respectively. For TCE, these values are not significantly different for the three biochars at both concentration levels ($p > 0.05$). For PCE, there is no significant difference between the three biochars at 0.01 S_W level. At the 0.1 S_W pre-loading level, the cumulative fraction released from BC-CM is statistically smaller than the BC-WC fraction ($p < 0.05$). However, BC-GH is not distinct compared to both BC-CM and BC-WC ($p > 0.05$). At the S_W pre-loading level, the cumulative extracted fraction seems to increase following the order BC-CM, BC-GH, BC-WC, and AC for both compounds.

In general, the cumulative released fraction tends to be smaller at the 0.01 S_W level, but only statistically significant for TCE released from BC-CM ($p < 0.05$). Differences between TCE and PCE are small at the 0.01 S_W level. At the 0.1 S_W level, significantly more TCE than PCE was cumulatively released in the first three extraction steps ($p < 0.05$).

In contrast, AC showed a significantly lower cumulative fraction extracted compared to all biochars ($p < 0.05$). This was the case for both compounds and at both pre-loading levels. Further, the cumulative fraction released is significantly smaller at the 0.01 S_W pre-loading level for both tested compounds (0.01 S_W < 0.1 S_W; $p < 0.05$ for TCE and PCE).

In the fourth extraction step with toluene, the most notable observation is that it contributed the highest share of the total extracted mass in the AC experiments at the 0.01 S_W level (TCE: 44 ± 3.4 %; PCE: 71 ± 0.1 %; $p < 0.05$). In the 0.01 S_W and 0.1 S_W experiments, the toluene-released fractions are smaller than the share released by methanol ($p < 0.05$). Although not statistically confirmed, a similar trend is also apparent in these data at the highest pre-loading level (S_W).

For the three biochars, the mass fractions extracted by toluene are comparably small at all pre-loading levels (Table 18), probably owing to the fact that the three previous extraction steps already contributed a big share to the total extractable mass. Differences between the biochars are generally small or not detectable.
The final extraction step with n-hexane only released a comparably low fraction for all sorbents (Table 18). Its share of the total extractable mass is the lowest for BC-CM. However, differences between the sorbents and concentration levels are small and do not show a consistent trend.

5.2.2. Unextractable fraction

For further evaluation, the data are now related to the actual mass that was pre-loaded onto the sorbents in the batch system. Biochar BC-CM was excluded from this evaluation, as due to very low sorption in the pre-loading step, it was not possible to determine the non-extractable mass fraction for this sorbent.
Further, the S_W pre-loading level is not included here, because the experimental set-up did not allow to quantify the total pre-loaded mass of these samples. All data are displayed in Table 19 and Figure 20.

Table 19: TCE and PCE fractions released for each extraction step as percentage of the total pre-loaded mass. Values represent the mean values of three replicates ± standard deviation.

	TCE			**PCE**		
	BC-GH	**BC-WC**	**AC**	**BC-GH**	**BC-WC**	**AC**
			0.01 S_W			
Water-1 [%]	1.8 ± 0.6	1.3 ± 0.3	0.7 ± 0.3	1.0 ± 0.4	0.3 ± 0.1	0.7 ± 0.1
Water-2 [%]	4.0 ± 1.7	2.4 ± 0.1	1.8 ± 0.2	2.1 ± 0.4	0.9 ± 0.5	1.1 ± 0.2
Sum water [%]	*5.8 ± 1.8*	*3.7 ± 0.4*	*2.6 ± 0.4*	*3.1 ± 0.6*	*1.2 ± 0.5*	*1.9 ± 0.2*
Methanol [%]	67 ± 4.6	56 ± 7.9	27 ± 3.4	31 ± 3.5	19 ± 5.0	16 ± 6.1
Toluene [%]	31 ± 4.4	15 ± 7.2	37 ± 7.8	14 ± 2.6	12 ± 0.7	84 ± 7.4
n-hexane [%]	14 ± 5.9	15 ± 9.4	17 ± 2.1	11 ± 0.8	6.5 ± 0.6	17 ± 3.2
Not extracted [%]	-18 ± 4.0	10 ± 5.8	17 ± 11	41 ± 4.2	61 ± 4.3	-19 ± 10
			0.1 S_W			
Water-1 [%]	5.5 ± 1.0	4.3 ± 1.2	2.5 ± 0.4	2.9 ± 1.4	0.9 ± 0.2	2.1 ± 0.4
Water-2 [%]	5.4 ± 2.1	4.0 ± 0.1	1.9 ± 0.5	2.2 ± 0.9	1.6 ± 0.7	2.4 ± 0.6
Sum water [%]	*11 ± 2.3*	*8.4 ± 1.2*	*4.4 ± 0.7*	*5.1 ± 1.7*	*2.5 ± 0.7*	*4.5 ± 0.7*
Methanol [%]	80 ± 12	66 ± 15	40 ± 2.4	37 ± 2.3	23 ± 2.9	31 ± 5.0
Toluene [%]	24 ± 2.2	17 ± 0.7	38 ± 3.3	16 ± 0.7	12 ± 1.4	22 ± 3.1
n-hexane [%]	8.7 ± 1.7	8.8 ± 0.3	21 ± 1.7	9.5 ± 1.1	5.9 ± 0.8	16 ± 1.7
Not extracted [%]	-24 ± 13	-0.6 ± 13	-3.2 ± 7.6	32 ± 1.7	57 ± 4.2	27 ± 6.6

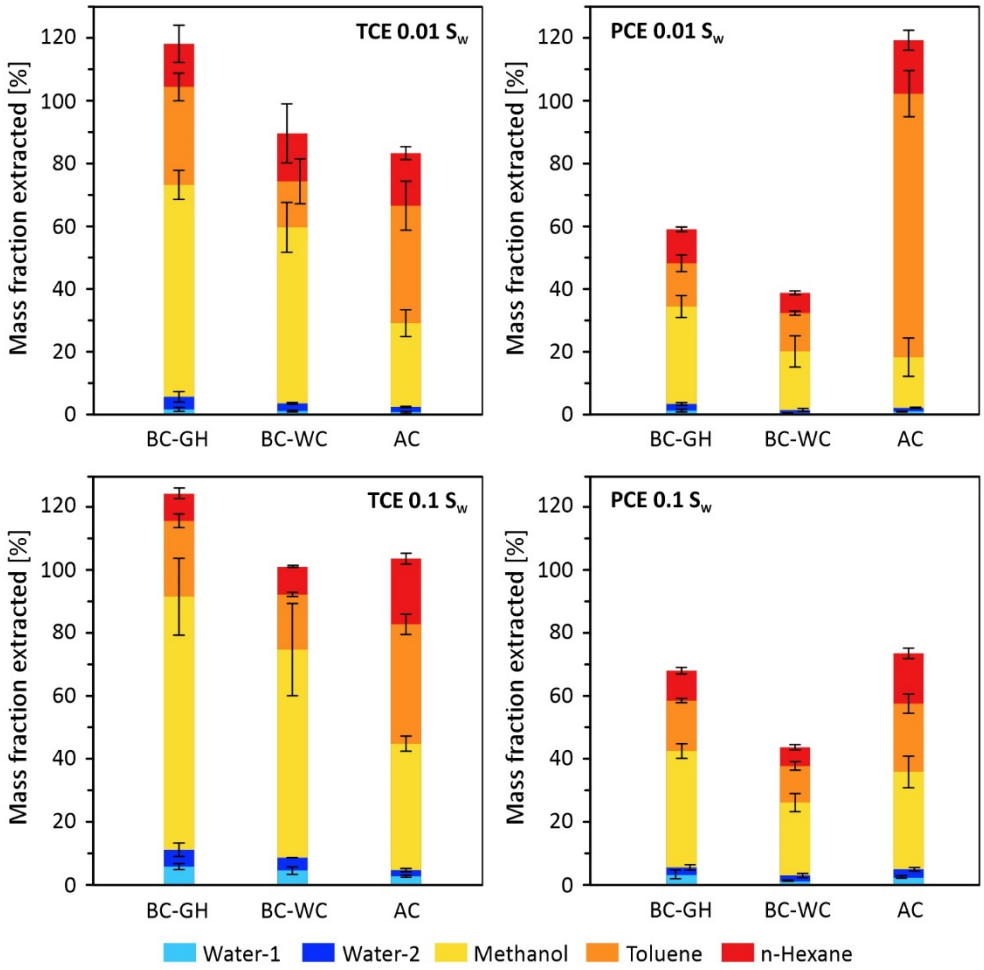

Figure 20: TCE and PCE fractions extracted from the three sorbents (BC-GH, BC-WC, and AC) as percentage of the total pre-loaded mass at the pre-loading levels 0.01 S_W and 0.1 S_W extracted by the five sequential extraction steps (water-1, water-2, methanol, toluene, and n-hexane). Data represent the mean values of three replicates ± standard deviation (error bars).

Figure 20 shows the cumulative and solvent-specific mass fractions of TCE and PCE that were extracted at the two investigated concentration levels (0.01 S_W and 0.1 S_W).

It is worth noting that the total TCE fraction that was extracted from BC-GH clearly exceeds 100 % at both pre-loading levels (118 ± 8.9 % and 124 ± 13 % for 0.01 and 0.1 S_W respectively). This is also the case for PCE extracted from AC at the 0.01 S_W level (119 ± 10 %). However, except for TCE extracted from BC-GH at the 0.1 S_W level, the results are not statistically different from 100 %. Two possible reasons for these high extraction results are either a ”contamination” of the sorbents prior to loading or a systematic error in the results due to the experimental or analytical set-up used. Although this can influence the absolute numbers presented here, it does not change the general trends that can be observed in the data set.

The mass fraction that was not extracted at the end of the experiment varies from around 0 % (several samples show negative values, all except TCE pre-loaded onto BC-GH at the 0.01 S_W level are not statistically different from 0 %; $p > 0.05$) to up to 61 ± 4.3 % (PCE pre-loaded onto BC-WC at the 0.01 S_W level).

On a first glance, the extraction patterns of TCE and PCE show some distinct features. The non-extractable TCE fraction is significantly lower for BC-GH at the 0.01 S_W pre-loading level ($p < 0.05$), while BC-WC and AC do not show a significant difference ($p > 0.05$). At the 0.1 S_W level, this trend is visible, but is not statistically significant. For PCE, the non-extractable fraction is highest for BC-WC at both pre-loading levels ($p < 0.05$), and tends to decrease over BC-GH to AC.

For both analyzed biochars, the fraction that remained un-extracted at the end of the experiment is higher for PCE compared to TCE ($p < 0.05$). This is the case at both pre-loading levels. Considering AC, at the 0.01 S_W concentration level the non-extractable fraction was higher for TCE, while at 0.1 S_W, PCE shows the higher non-extractable fraction (both $p < 0.05$).

Differences between the two pre-loading levels do not show any consistent pattern. The non-extractable fraction tends to be higher at the 0.01 S_W level, except for the case of PCE sorbed on AC, where it is clearly higher at the 0.1 S_W level. However, most of these differences are not statistically significant.

Water released between 1.2 ± 0.5 % (PCE BC-WC 0.01 S_W) and 11 ± 2.3 % (TCE BC-GH 0.1 S_W) of the total pre-loaded mass. At both pre-loading levels, BC-GH tends to release the highest fraction for sorbed TCE and PCE. As already observed for the total mass extracted, water tends to mobilize a higher fraction of TCE compared to PCE from the biochars. However, only at the 0.1 S_W pre-loading level this difference is actually statistically significant ($p < 0.05$; for BC-GH and BC-WC). This supports the trend of more pronounced differences at higher pre-loading levels, as already observed in the total mass data. This goes in line with the water-released fraction also being smaller at the 0.01 S_W level for all sorbents. This trend is more pronounced for TCE, where the data are actually statistically significant (TCE 0.01 S_W < TCE 0.1 S_W; $p < 0.05$). For PCE, the difference between the pre-loading levels is only statistically significant for AC ($p < 0.05$).

The fraction extracted by methanol varied notably between the different sorbents. For TCE, it tends to increase from AC over BC-WC to BC-GH. For PCE, the fraction released from BC-WC and AC are similar, but lower than what was released from BC-GH. These trends are apparent at both concentration levels. Further, for both biochars the methanol-extracted fraction is higher for TCE compared to PCE ($p < 0.05$). This is the case for both pre-loading levels. A similar trend is also evident for AC, however only significant at the 0.1 S_W level. Generally, differences are more pronounced in the experiments conducted with TCE.

Compared to methanol, the subsequent toluene extraction step released notably smaller fractions of TCE and PCE from both biochars. Thereby, the TCE fraction tends to be higher. This is statistically significant for BC-GH at the 0.01 S_W level and for both biochars at the 0.1 S_W level ($p < 0.05$). The toluene-released fraction increased from BC-WC over BC-GH to AC at both pre-loading levels and for both compounds. Although differences between sorbents are not statistically significant in all cases at the 0.01 S_W level, there is a significant difference between all three sorbents at the 0.1 S_W level ($p < 0.05$). This is the case for both compounds. Generally, the highest fraction was released from AC with 84 ± 7.4 % of sorbed PCE at the 0.01 S_W level. This is significantly higher than any other extracted fraction.

Considering the final extraction step with n-hexane, only small mass fractions were released compared to the preceding methanol and toluene steps. For TCE, there is no difference in the n-hexane extracted fraction between the three sorbents at the 0.01 S_W level. However, at the higher 0.1 S_W level, the fraction released from AC is significantly larger than for the two biochars ($p < 0.05$). Looking at PCE, there is a significant difference in the n-hexane-extracted fraction between all three sorbents at both concentration levels ($p < 0.05$). At both levels, it increases from BC-WC over BC-GH to AC. There are little to no differences between TCE and PCE, as well as between the two pre-loading levels.

5.2.3. Influence of sorbent properties on contaminant release

As described in the previous sections, there are distinct differences in the release behavior of the four investigated sorbents. Although not all described differences are statistically significant, there are noticeable trends that can be seen throughout the data set. As the four sorbents have distinct physical and chemical properties, their individual extraction behavior is likely a function of these characteristics.

BC-CM shows the highest water-extractable fraction for TCE and PCE at all three pre-loading levels. Compared to the other three sorbents, BC-CM only exhibits a rather small SSA, mostly comprising of external surface area (SSA_{ext}) in its mesopores. In contrast, BC-GH, BC-WC, and AC are microporous sorbents and contain a significantly higher specific surface area.

Several researchers reported that sorption irreversibility, sorbate extractability, and sorption hysteresis are strongly influenced by sorbent properties, especially by their pore structure. Wang et al. (2017) reported that irreversible sorption of different organic contaminants increased with decreasing biochar pore size. Yu et al. (2010) found that irreversible sorption of pyrimethanil was higher in a biochar with large surface area and high mircoporosity, and molecules sorbed in larger pores could “escape” more easily upon desorption. This could explain the comparably large fraction of TCE and PCE that was easily extracted from BC-CM in the first two extraction steps. Its relatively large pores allow water to access the sorbed molecules and release them into the bulk solution. In contrast, molecules sorbed in narrow micropores, as present in BC-GH, BC-WC, and AC, can become tightly trapped and are not easily accessible for desorption by water. These narrow pores are often considered “high-energy” sorption sites (e.g., Lastoskie et al., 1993; Yuan et al., 2021). Therefore, compounds sorbed via micropore-filling might be more resistant to immediate extraction and desorption.

This could not only explain the differences between the different sorbents but also the trend of increasing water-released fraction with increasing pre-loading level. As described in chapter 3, pore-filling dominates the sorption process at lower equilibrium concentrations. When the sorbent is approaching saturation at higher aqueous concentrations, TCE and PCE increasingly bind to less favorable sorption sites as high-energy sites become saturated (pores become filled). As the three pre-loading levels can be interpreted as increasing aqueous concentrations on an isotherm, the desorption from low-energy sites at higher concentration could explain the concentration-dependent release behavior of TCE and PCE. Similar findings were recently reported by Yuan et

al. (2021). They showed that sorption irreversibility of microcystin-LR from different biochars decreased with increasing aqueous equilibrium concentration.

This behavior should be more prominent in sorbents with lower porosity. Indeed, when locking at Figure 19 this trend is most pronounced in BC-CM, the sorbent with the lowest pore volume and smallest contribution of pore-filling to overall sorption (see chapter 3). The contribution of the water-released fraction to the total extracted mass notably increases from 0.01 S_W over 0.01 S_W to S_W.

Further, BC-CM is the sorbent with the highest polarity (see section 3.2.1). As water is a polar solvent, this could facilitate the accessibility of the sorbent surface and matrix for water molecules and alleviate the release of sorbed molecules. In contrast, the higher bulk hydrophobicity of BC-GH, BC-WC, and AC might hinder polar water molecules to approach the sorbent surface or penetrate the sorbent matrix. This could also be one reason for the lower water-extractable fraction of these three sorbents, compared to the less hydrophobic BC-CM. This is in line with findings by Jonker and Koelmans (2002), who hypothesized that low aqueous extraction recoveries of PAHs from soot was the result of the hydrophobic nature of soot that limited the ability of water molecules to penetrate the soot matrix.

The differences in the water-released fractions between TCE and PCE are small and likely a result of their difference in water solubility. TCE's water solubility is about one order of magnitude higher than PCE (see Table 1), which increases its tendency to be released into the bulk solution.

Another factor reported in the literature that can affect the desorption of organic contaminants are leachable compounds, like LOC. Wang et al. (2017) found that the presence of LOC in biochars significantly affected irreversible sorption. The hysteresis index of atrazine sorption decreased after the removal of LOC from the sorbent, indicating that the presence of LOC in biochars can hinder desorption.

On a first glance, this is contradicting to the findings where BC-CM with high amounts of LOC (see section 4.2) shows a rather high extractability of sorbed molecules. However, during the extraction process, LOC is also mobilized and released into the bulk solution. This could increase the overall desorption of compounds in two possible ways. First, when LOC is removed from pores in the initial extraction step, this could open up new pathways for solvents to enter the sorbent matrix in subsequent extraction cycles and facilitate further desorption. Further, LOC might initially act as a sorption site for organic compounds. Upon its release, it could simultaneously remove compounds from the sorbent matrix, which are subsequently released into the bulk solution.

As described previously, more than 50 % of the extracted TCE and PCE mass was released from the biochars in the first three extraction steps. In contrast, a much smaller cumulative fraction of both contaminants was released from AC in the initial three extractions. Especially at the lower pre-loading level 0.01 S_W, the majority of the total extractable TCE and PCE is only mobilized from AC by the more hydrophobic solvents toluene and n-hexane. Jonker and Koelmans (2002) hypothesized that besides the accessibility of the sorbed compound, also the displacement capacity of the used solvent plays an important role in extraction recoveries of PAHs from

soot. This might also play a role in the data set here presented. AC has a significantly higher bulk hydrophobicity compared to the three biochars. Therefore, desorption is mainly achieved by the less polar and more hydrophobic solvents toluene and n-hexane. Further, toluene, as an aromatic solvent, might be able to displace molecules, sorbed via interaction of attracting π-systems, more effectively. This could explain the high contribution of the toluene extract to the total extractable fraction from AC, as it is the sorbent with the highest aromaticity (see Table 2).

The overall extractability of the sorbed compounds from the different investigated sorbents (Figure 20), can be interpreted as a result of the interplay of these different sorbent- and compound-controlled mechanisms.

It should be noted that in experiments conducted with TCE at the 0.1 S_W level, the entire pre-loaded mass was recovered from both biochars and the AC sample. In the remaining three experiments (TCE at 0.01 S_W and PCE at both pre-loading levels), it is evident that a larger contaminant fraction remained un-extractable from BC-WC compared to BC-GH for both compounds. Also, for the two investigated biochars, the fraction of the pre-loaded mass recovered at the end of the experiments was clearly lower for PCE compared to TCE, at both studied pre-loading levels.

PCE is the more hydrophobic molecule (see Table 1), which should generally result in a higher affinity towards carbonaceous sorbents. However, as previously shown in the adsorption experiments (see chapter 3), this can be overridden by effects governed by sorbent properties, for example size exclusion. The interplay of these two effects is also evident in the biochar extraction data. Although the overall adsorption on both investigated biochars is higher for TCE (see chapter 3), PCE seems to be more resistant to desorption, likely because of its higher hydrophobicity. Additionally, desorption of both compounds is also influenced by the biochars' structural properties, i.e., pore size distribution and mircoporosity, especially at the lower pre-loading level. As the biochar with the highest micropore volume, BC-WC shows a larger un-extractable fraction compared to BC-GH in both experiments with PCE and in the 0.01 S_W experiments with TCE. This is in line with previous studies by Wang et al. (2017) who showed that irreversible sorption in biochars increased with increasing micropore volume. The un-extractable fraction tends to be higher at the 0.01 S_W level, which supports the hypothesis of micropore trapping in biochars being more pronounced at lower concentration levels (Yuan et al., 2021) and lower hysteresis at higher sorbate concentrations (Braida et al., 2003).

According to work done by Pignatello and co-workers (Lu and Pignatello, 2002; Braida et al., 2003; Sander et al., 2006), this trapping of sorbates upon desorption can be caused by pore deformation. It is the result of the swelling or structural expansion of the sorbent matrix caused by the incoming solute, which results in deformation of the pore structure and possibly the opening of previously closed sectors in the sorbent matrix (Braida et al., 2003). Upon desorption, solute molecules can be trapped in these sectors, figuratively described as "(…) the door shuts behind the adsorbate (…)" by Braida et al. (2003). Additionally, this structural expansion is often not fully reversible (Braida et al., 2003; Pignatello, 2011) and therefore can lead to a higher affinity of the sorbate towards the sorbent upon desorption. Braida et al. (2003) also suggested that softening and

resulting irreversible sorption/hysteresis depends on the sorbate structure, indicating that differences in desorption behavior of TCE and PCE might also be influenced by pore deformation. For example, TCE as the molecule with the lower molar volume and smaller dimensions (see Table 1) likely exerts lower pressure on the internal biochar pore structure, leading to lower matrix expansion and, in turn, lower irreversible sorption (Pignatello, 2011).

It is reasonable to expect that these mechanisms also govern the extractability of TCE and PCE from AC. Indeed, ElHaddad et al. (2013) detected a significant sorption hysteresis in experiments with both charcoal and AC. Thereby, the fraction considered as desorption-resistant was lower for AC compared to the tested charcoal sample for all four tested organic compounds, with no detectable concentration dependency (ElHaddad et al., 2013). The results obtained from AC experiments in the present study show a less coherent picture. Considering TCE, the un-extractable fraction at the 0.01 S_W level is similar to BC-WC and notably higher than determined for BC-GH. At the 0.1 S_W pre-loading level, the entire adsorbed TCE mass was recovered at the end of the experiment. In contrast, for PCE this was the case at the 0.01 S_W pre-loading level, whereby a significant fraction remained unextracted at the 0.1 S_W level. Generally, the PCE fraction remaining unextractable from AC at the end of the experiments tended to be lower than determined for the two biochars. These differences between TCE and PCE are especially surprising, because solubility-normalized adsorption isotherms of both compounds on AC did not show a significant difference (see section 3.2.2). Although TCE results are in line with the pore deformation hypothesis, it cannot explain the desorption pattern observed for PCE. This suggests that additional mechanisms also influence the remobilization behavior of organic compounds from AC.

5.3. Conclusions

The presented adsorption-extraction experiments illustrate that the properties of carbonaceous sorbents can have a pronounced influence on the remobilization behavior of sorbed organic contaminants. Generally, water was only able to mobilize a comparably low fraction of the actual extractable mass. Thereby, a significantly higher mobilized fraction of TCE and PCE was water-extractable from BC-CM, the polar, low surface area, mesoporous biochar compared to the three more hydrophobic sorbents (BC-GH, BC-WC, and AC) containing significant micropore volume. This is accompanied by a pronounced concentration effect where the water-extractable fraction of the overall mobilized mass notably increases with increasing pre-loading concentration. These results indicate that contaminant trapping in narrow micropores, especially at low concentrations, significantly influences the release behavior of sorbed compounds. Additionally, overall matrix and pore accessibility governed by sorbent bulk hydrophobicity also seem to play an important role. This is further supported by the high contribution of toluene to the extractable mass in AC experiment, due to its high hydrophobicity and aromaticity. In addition, the mobilization of LOC during extraction likely also contributes to organic contaminant release.

While no results could be obtained for the overall extractability from the manure-based biochar BC-CM, results from the two plant-based biochars (BC-GH and BC-WC) showed that PCE was more resistant to extraction compared to TCE. Despite its higher initial adsorption due to advantages in pore accessibility (see chapter 3), TCE tends to be mobilized more easily, as it would be expected from its lower $\log K_{OW}$. While the total sorbed TCE mass was recovered in the experiment at high pre-loading, significantly lower extractability was observed for TCE at low pre-loading and both PCE experiments. Together with the prominent influence of mircoporosity on contaminant extractability, this supports the hypothesis of contaminant trapping caused by swelling and deformation of the pore structure as a cause for irreversible sorption in the investigated biochars. Although results for the overall extractability from AC are less conclusive, pore deformation likely also plays a role for this sorbent.

6. Overall conclusions and outlook

The overall aim of this thesis was to get a better understanding of biochar-pollutant interaction and expand the knowledge on the underlying mechanisms that drive the sorption and remobilization of organic compounds on biochar. To this end, a number of overall conclusions can be drawn from the results described in the three core chapters of this thesis.

The single and bi-solute adsorption experiments presented in chapter 3 showed that all three biochars, produced from different feedstock materials, are effective sorbents for chlorinated hydrocarbons. Biochars' distinct properties, such as polarity, micropore volume, and pore size distribution, have a pronounced influence on the sorption mechanisms involved. Although their overall sorption capacity is lower compared to activated carbon, the biochars show some distinct advantages, especially in bi-solute systems. Sorption to activated carbon in mixed contaminant systems is affected by strong competition, significantly suppressing sorption of the compound with the lower hydrophobicity. Competitive effects were also evident for all biochars, but all three sorbents still sorbed significant amounts of both compounds. Thereby, the overall sorbed contaminant volume was higher than in single-solute experiments. Further, plant-based, microporous biochars show stronger competition with a pronounced concentration effect. In case of the manure-based biochar, competition is less pronounced and not concentration-dependent. These results indicate that biochars with a large partitioning domain facilitate non-competitive sorption, thereby offering the option for enhanced overall sorption in bi-solute systems.

This aspect is especially interesting for the application of biochars in water treatment, where usually a variety of different contaminants are present simultaneously. Activated carbon is a tried and tested material that can be used in water treatment as an additional filtration step. Its overall superior sorption capacity for most contaminants is the result of high surface area and microporosity (as shown in chapter 3). However, activated carbons are usually highly engineered materials, often customized for specific applications or contaminant groups. In contrast, biochar is a more heterogenous material containing a variety of different sorption sites, including micro- and mesopores, different functional groups, and partitioning domains. This offers the option to simultaneously sorb a wide range of compounds with different physical and chemical properties, especially if these are present in relatively low concentrations.

The applicability of biochar in sewage (e.g., Dalahmeh et al., 2018), stormwater (e.g., Lu and Chen, 2018), and wastewater (e.g., Perez-Mercado et al., 2018) treatment systems has been demonstrated in recent years in several bench scale column experiments. However, batch experiments still represent the majority of the literature body. Only very few studies investigating the performance of biochar under real-world conditions are available (e.g., Ashoori et al., 2019; Blum et al., 2019). Therefore, there is a clear research need for larger scale studies investigating the effectiveness of biochars in filtration systems, for instance in larger column experiments

or pilot water treatment plants. Thereby, especially engineering aspects (e.g., filter design and operation) as well as long-term studies should be considered.

With the leaching experiments presented in chapter 4, one aspect in long-term effectiveness of biochars was investigated. The results showed that the sorption behavior of biochars is not constant and can be significantly altered through the release of LOC and mineral elements. This highlights that when biochars are applied in remediation efforts, either in water or soil, it is important to consider that their sorption properties may change over time, depending on their initial characteristics and the feedstock material used. The experiments revealed that the release of soluble constituents during "aging" can enhance sorption of organic contaminants. However, "aging" encompasses a variety of mechanisms, including chemical, biological, and physical processes (Wang et al., 2020), which may result in a range of different effects. These can either enhance sorption, as revealed in the present study or in experiments by Ghaffar et al. (2015) and Feng et al. (2018), or attenuate sorption as shown by Luo et al. (2017) and Ren et al. (2018b). This is not only an effect of different aging mechanisms, but also the result of different sorption mechanisms, which greatly differ depending on the properties of the sorbing compound and the biochar.

Although great efforts have been made over the last decades to simulate biochar aging using different techniques, it remains difficult to predict the long-term effects of environmental exposure on biochar properties and their impact on contaminant sorption. Therefore, clearly more long-term studies especially under real-world conditions are warranted. The topic of biochar aging applied as filter material in water treatment has not received much attention. Thus, research into aspects such as filter clogging, or regeneration of used material should be considered in future studies.

Besides the long-term sorption performance, sorption reversibility is another crucial aspect in the overall applicability of biochars in remediation technologies. The experiments presented in chapter 5, showed that sorbent properties have a distinct influence on the remobilization of sorbed organic contaminants. Water was only able to mobilize a comparatively low contaminant fraction of the actually extractable mass, indicating that under environmental conditions pollutants might not be easily mobilized. Thereby, a significantly higher pollutant fraction was water-extractable from the polar, low surface area, mesoporous biochar compared to the three more hydrophobic sorbents (plant-based biochars and activated carbon) containing significant micropore volume. This aspect is especially interesting, as it suggests that contaminants trapped in small pores are likely more resistant to immediate and long-term remobilization. Thereby, the overall matrix and pore accessibility seems to play an important role.

These findings have immediate implications for the environmental fate of organic compounds in water and soil. Long-term immobilization in soil can reduce pollutant transport through the soil profile and leaching into groundwater. Further, it is likely that strong, resistant sorption reduces the bioavailability of pollutants to soil organisms and plants, which has been shown, for example, by Gomez-Eyles et al. (2011) for PAH-contaminated

soil. Decreased bioavailability often also leads to a decrease in toxicity to soil microorganisms (Bielská et al., 2017) and plants (Jośko et al., 2013).

However, immobilizing contaminants is usually not the ultimate goal of remediation efforts, as it is only an intermediate solution to reduce risks. Rather, biodegradation and following de-toxification of contaminants is often the preferred option. However, limiting the bioavailability of compounds to soil microorganisms could inhibit the potential for this process. This has been observed, for example, by Marchal et al. (2013) for phenanthrene in biochar- and activated carbon-amended soils, where they identified desorption as the rate-limiting step for pollutant degradation. Thereby, activated carbon had a more pronounced negative impact on biodegradation, because it reduced the bioavailability more effectively. This is in line with the findings that a lower contaminant fraction is easily mobilized from microporous sorbents. It suggests that these sorbents could be the preferred option for immobilization. However, if remediation efforts rely on biodegradation and finally mineralization of the pollutants, biochars with more easily "accessible" sorption sites that allow slow remobilization of sorbed compounds might be the better option. Further benefits of biochars are their potential to enhance biodegradation, for instance, by providing shelter to degrading microorganism, supplying nutrients, and by improving the overall soil properties (Zhu et al., 2017 and references therein).

Additionally to biochar's advantages as a sorbent from a mechanistic point of view, several researchers have suggested that it is a more environmentally friendly material compared to conventional activated carbon (e.g., Alhashimi and Aktas, 2017). In recent years, several researchers compared the environmental impact of biochar and activated carbon as an adsorbent material using life cycle assessments (e.g., Alhashimi and Aktas, 2017; Moreira et al., 2017). Thompson et al. (2016) specifically evaluated the viability of wood-derived biochars in wastewater treatment, compared to activated carbon, considering environmental and economic aspects. All three studies found that biochar usually has a lower environmental impact compared to activated carbon, showing that biochar can be a low-cost alternative in water treatment. However, Alhashimi and Aktas (2017) pointed out that there is still a lack of consistent data on the performance of biochars as a reliable adsorbent. To this end, the work presented in this thesis hopefully contributes to a better understanding of biochar-pollutant interaction, showing that biochar is a viable and safe alternative to conventional activated carbon.

While biochar has been proposed as a promising option for water filtration systems by many researchers, examples of commercial real-world applications are scarce. Researchers from the University of Idaho in the US developed and patented a biochar-based water treatment system called N-E-W Tech™, which "promises to remove organic and mineral contaminants in wastewater with high efficiency and generate energy while using the minerals it strips from water to produce fertilizer" (University of Idaho, 2021). Another example is the consortium "Aqueous Solutions", which promotes the use of small-scale biochar filter systems in Southeast Asia (Aqueous Solutions, 2021). Although these examples highlight that biochar is increasingly recognized in the commercial sector as a valuable adsorbent material, important knowledge on the long-term performance and large-scale applicability of such systems is still limited. Therefore, larger scale column experiments or

experiments in pilot plants alongside established sorbent materials (e.g., activated carbon) using actual pre-treated wastewater could be the next step towards real-world applications.

Commercial application of biochar in the remediation of soils contaminated with organic compounds has not yet attracted much attention. This is probably also caused by the lack of knowledge on long-term performance of biochar amendments on contaminated sites, as only a limited number of field studies have been conducted (see section 2.6). This highlights the urgent need for more large scale and long-term studies. Thereby, lysimeter trials might be a good alternative to full field trials as they allow to study all environmental compartments. In this way, the effect of biochar amendments on the fate of organic pollutants under real-world conditions could be investigated without the risk of triggering unintended consequences off site (e.g., leaching into the groundwater). A special focus should be placed on effects of different soil types and the influence of climatic conditions on the long-term stability and sorptive performance of biochars in soil. On the way towards a better understanding of biochar aging and stability in soil, the U.S. Department of Agriculture (USDA) has launched a citizen science project, in which they ask participants all over the world to burry small bags of biochar in their local soil for a set period of time. They hope to generate a data set that will help to better understand "the factors determining the fate and disintegration of the same biochar located at different locations" (USDA, 2021). Following such initiatives, the effect of biochar on the fate of organic compounds should be studied in a variety of different soils over longer time periods under controlled conditions to establish a better mechanistic understanding of the biological, chemical, and physical processes taking place. This will allow practitioners to make better informed decisions before starting to put biochar concepts into practice.

Besides the application of biochar alone, several researchers have been working on innovative concepts combining biochar with other smart materials for remediation. Recently, a pilot field study was conducted in China applying biochar-supported nano zero-valent iron (nZVI) for the remediation of groundwater contaminated with chlorinated hydrocarbons (Qian et al., 2020). The researchers were able to show that the addition of biochar increased degradation and helped to maintain the effectiveness of nZVI over a period of up to 42 days after its injection into the aquifer. However, several questions, e.g., concerning the behavior of biochar in the subsurface, its stability, and its potential transport off-site remained unanswered, and clearly more research is needed before biochar can be applied for groundwater remediation on a larger scale. Nevertheless, this example highlights that biochar is a material that can be applied in combination with already existing technologies to support or enhance remediation efforts.

Besides field experiments, also more targeted laboratory experiments could be helpful to answer specific open questions. The experimental set-up presented in chapter 5 quantified the amount of non-extractable contaminant by a calculated mass balance instead of direct measurements. However, it is difficult to quantify the uncertainty of this approach. A valuable tool to study the fate of organic compounds in sorption experiments more directly can be the use of radio-labelled materials as shown, for example, by Mendes et al. (2020) in a adsorption/desorption study of three different pesticides using ^{14}C-labelled compounds. This approach would

offer the possibility to quantify the amount of irreversibly sorbed target compound and obtain a fully closed mass balance by analyzing the radioactivity remaining in the extracted/desorbed biochar samples via combustion and subsequent quantification of the evolved and trapped $^{14}CO_2$ by liquid scintillation counting. Overall, the results from this thesis highlight that biochar is an excellent sorption material and has great potential for a variety of different applications in environmental remediation technologies.

7. Acknowledgements

First and foremost, I would like to thank Prof. Dr. Christoph Schüth for his supervision and continuous support throughout my work. When he offered me this doctoral position, even before I finished my master's thesis, it was the first time I truly realized that I could see myself doing research. Throughout the years, his open-minded and at eye-level discussion- and leadership-style created a relaxed, supportive, and encouraging work environment.

I also would like to thank Prof. Dr. Peter Grathwohl for readily accepting the invitation to be the co-referee for my thesis, as well as Prof. Dr. Matthias Hinderer and Prof. Dr. Wolfgang Ensinger for agreeing to be committee members for my defense.

I would like to express my deep gratitude to Dr. Wolfgang Schmidt from the Max-Planck-Institut für Kohlenforschung, who conducted the argon sorption measurements for the determination of surface area and porosity that became a cornerstone of this thesis. Without him jumping in and collaborating when other options failed, big parts of this work would not have been possible.

I also thank Dr. Ellen Graber and Dr. Abhay Kumar from the Volcani Center in Bet-Dagan (Israel) for their collaboration on the biochar project, for providing the biochar samples, and for hosting me during a short research stay.

A special thank-you goes to Dr. Thomas Schiedek for his help with the GC method development and for always having an open office door and ear when needed. His advice and support with big and small problems in the lab greatly contributed to the success of this thesis. Further, I would like to thank the entire lab team, especially Claudia Cosma, Stefanie Schmidt, and Zarah Neumann. Their knowledge and unreserved support made working in the lab really enjoyable.

Not to forget, I want to say a heartfelt thank-you to all colleagues from the Hydrogeology group, but also from other working groups, who shared this PhD experience with me. Thank you for the positive and supportive lab and office environment, the fun and discussion-filled coffee breaks, and the relaxing Ratskeller evenings. I will always keep fond memories of these fun times.

A special thank-you goes to my friends and family for their continuous encouragement and support, especially in rough and uncertain times. Knowing that you always have my back and that you believed in me and my decisions, no matter what, gave me the courage that was needed to complete this work. Thank you.

Lastly, I would like to thank Nils, not only for being a loving partner, but also for encouraging me in every step of the way. Without your support I am not sure if this thesis would have ever come to its completion. Thank you for always being there to listen, but also for continuously challenging my ideas and making me a better scientist. Thank you so much.

8. References

Abbas, Z., Ali, S., Rizwan, M., Zaheer, I.E., Malik, A., Riaz, M.A., Shahid, M.R., Rehman, M.Z.u., Al-Wabel, M.I., 2018. A critical review of mechanisms involved in the adsorption of organic and inorganic contaminants through biochar. Arabian Journal of Geosciences 11, p. 448.

Ahmad, M., Lee, S., Oh, S.-E., Mohan, D., Moon, D., Lee, Y., Ok, Y., 2013a. Modeling adsorption kinetics of trichloroethylene onto biochars derived from soybean stover and peanut shell wastes. Environmental Science and Pollution Research 20, pp. 8364-8373.

Ahmad, M., Lee, S.S., Dou, X., Mohan, D., Sung, J.-K., Yang, J.E., Ok, Y.S., 2012. Effects of pyrolysis temperature on soybean stover- and peanut shell-derived biochar properties and TCE adsorption in water. Bioresource Technology 118, pp. 536-544.

Ahmad, M., Lee, S.S., Rajapaksha, A.U., Vithanage, M., Zhang, M., Cho, J.S., Lee, S.-E., Ok, Y.S., 2013b. Trichloroethylene adsorption by pine needle biochars produced at various pyrolysis temperatures. Bioresource Technology 143, pp. 615-622.

Ahmad, M., Moon, D.H., Vithanage, M., Koutsospyros, A., Lee, S.S., Yang, J.E., Lee, S.E., Jeon, C., Ok, Y.S., 2014a. Production and use of biochar from buffalo-weed (Ambrosia trifida L.) for trichloroethylene removal from water. Journal of Chemical Technology & Biotechnology 89, pp. 150-157.

Ahmad, M., Rajapaksha, A.U., Lim, J.E., Zhang, M., Bolan, N., Mohan, D., Vithanage, M., Lee, S.S., Ok, Y.S., 2014b. Biochar as a sorbent for contaminant management in soil and water: A review. Chemosphere 99, pp. 19-33.

Al-Wabel, M.I., Hussain, Q., Usman, A.R.A., Ahmad, M., Abduljabbar, A., Sallam, A.S., Ok, Y.S., 2018. Impact of biochar properties on soil conditions and agricultural sustainability: A review. Land Degradation & Development 29, pp. 2124-2161.

Alhashimi, H.A., Aktas, C.B., 2017. Life cycle environmental and economic performance of biochar compared with activated carbon: A meta-analysis. Resources, Conservation and Recycling 118, pp. 13-26.

Allen-King, R.M., Grathwohl, P., Ball, W.P., 2002. New modeling paradigms for the sorption of hydrophobic organic chemicals to heterogeneous carbonaceous matter in soils, sediments, and rocks. Advances in Water Resources 25, pp. 985-1016.

Aller, M.F., 2016. Biochar properties: Transport, fate, and impact. Critical Reviews in Environmental Science and Technology 46, pp. 1183-1296.

Amonette, J.E.J., Stephen 2009. Characteristics of Biochar: Microchemical Properties. in: Lehmann, J., Joseph, S. (Eds.). Biochar for Environmental Management: Science and Technology. Earthscan, London, U.K., p. 416.

Angst, T.E., Sohi, S.P., 2013. Establishing release dynamics for plant nutrients from biochar. GCB Bioenergy 5, pp. 221-226.

Antal, M.J., Mochidzuki, K., Paredes, L.S., 2003. Flash Carbonization of Biomass. Industrial & Engineering Chemistry Research 42, pp. 3690-3699.

Antonangelo, J.A., Zhang, H., Sun, X., Kumar, A., 2019. Physicochemical properties and morphology of biochars as affected by feedstock sources and pyrolysis temperatures. Biochar 1, pp. 325-336.

Anyika, C., Abdul Majid, Z., Ibrahim, Z., Zakaria, M., Yahya, A., 2015. The impact of biochars on sorption and biodegradation of polycyclic aromatic hydrocarbons in soils—a review. Environmental Science and Pollution Research 22, pp. 3314-3341.

Aqueous Solutions, 2021. Charcoal / Biochar Water Treatment, accessed on the 24th of May, 2021, https://www.aqsolutions.org/charcoal-biochar-water-treatment/.

Ashoori, N., Teixido, M., Spahr, S., LeFevre, G.H., Sedlak, D.L., Luthy, R.G., 2019. Evaluation of Pilot-Scale Biochar-Amended Woodchip Bioreactors to Remove Nitrate, Metals, and Trace Organic Contaminants from Urban Stormwater Runoff. Water Research.

ASTM D 1762-84, 2013. Standard Test Method for Chemical Analysis of Wood Charcoal. ASTM International, West Conshohocken, PA.

ATSDR, 2014. Public health statement tetrachloroethylene. Department of Health and Human Services, Public Health Service, Atlanta, GA.

ATSDR, 2016. Public health statement trichloroethylene. Department of Health and Human Services, Public Health Service, Atlanta, GA.

Bansal, R.C., Goyal, M., 2005. Activated carbon adsorption. CRC press.

Bapat, H., Manahan, S., 1998. Chemchar gasification of hazardous wastes and mixed wastes on a biochar matrix. Abstracts of papers of the American Chemical Society. American Chemical Society, pp. U571-U571.

Bastos, A.C., Prodana, M., Abrantes, N., Keizer, J.J., Soares, A.M.V.M., Loureiro, S., 2014. Potential risk of biochar-amended soil to aquatic systems: an evaluation based on aquatic bioassays. Ecotoxicology 23, pp. 1784-1793.

Beesley, L., Moreno-Jiménez, E., Gomez-Eyles, J.L., 2010. Effects of biochar and greenwaste compost amendments on mobility, bioavailability and toxicity of inorganic and organic contaminants in a multi-element polluted soil. Environmental Pollution 158, pp. 2282-2287.

Beesley, L., Moreno-Jiménez, E., Gomez-Eyles, J.L., Harris, E., Robinson, B., Sizmur, T., 2011. A review of biochars' potential role in the remediation, revegetation and restoration of contaminated soils. Environmental Pollution 159, pp. 3269-3282.

Bembnowska, A., Pełech, R., Milchert, E., 2003. Adsorption from aqueous solutions of chlorinated organic compounds onto activated carbons. Journal of Colloid and Interface Science 265, pp. 276-282.

Biederman, L.A., Harpole, W.S., 2013. Biochar and its effects on plant productivity and nutrient cycling: a meta-analysis. GCB Bioenergy 5, pp. 202-214.

Bielská, L., Kah, M., Sigmund, G., Hofmann, T., Höss, S., 2017. Bioavailability and toxicity of pyrene in soils upon biochar and compost addition. Science of the Total Environment 595, pp. 132-140.

Blum, K.M., Gallampois, C., Andersson, P.L., Renman, G., Renman, A., Haglund, P., 2019. Comprehensive assessment of organic contaminant removal from on-site sewage treatment facility effluent by char-fortified filter beds. Journal of Hazardous materials 361, pp. 111-122.

Boehm, H.-P., Diehl, E., Heck, W., Sappok, R., 1964. Surface Oxides of Carbon. Angewandte Chemie International Edition in English 3, pp. 669-677.

Borisover, M.D., Graber, E.R., 1997. Specific interactions of organic compounds with soil organic carbon. Chemosphere 34, pp. 1761-1776.

Braida, W.J., Pignatello, J.J., Lu, Y., Ravikovitch, P.I., Neimark, A.V., Xing, B., 2003. Sorption Hysteresis of Benzene in Charcoal Particles. Environmental Science & Technology 37, pp. 409-417.

Břendová, K., Tlustoš, P., Száková, J., 2015. Biochar immobilizes cadmium and zinc and improves phytoextraction potential of willow plants on extremely contaminated soil. Plant, Soil and Environment 61, pp. 303-308.

Brown, R., 2009. Biochar Production Technology. in: Lehmann, J., Joseph, S. (Eds.). Biochar for Environmental Management: Science and Technology. Earthscan, London, U.K., p. 416.

Brown, R.A., Kercher, A.K., Nguyen, T.H., Nagle, D.C., Ball, W.P., 2006. Production and characterization of synthetic wood chars for use as surrogates for natural sorbents. Organic Geochemistry 37, pp. 321-333.

Brunauer, S., Emmett, P.H., Teller, E., 1938. Adsorption of Gases in Multimolecular Layers. Journal of the American Chemical Society 60, pp. 309-319.

Brusseau, M.L., Jessup, R.E., Rao, P.S.C., 1991. Nonequilibrium sorption of organic chemicals: elucidation of rate-limiting processes. Environmental Science & Technology 25, pp. 134-142.

Brusseau, M.L., Rao, P.S.C., Gillham, R.W., 1989. Sorption nonideality during organic contaminant transport in porous media. Critical Reviews in Environmental Control 19, pp. 33-99.

Cao, X., Harris, W., 2010. Properties of dairy-manure-derived biochar pertinent to its potential use in remediation. Bioresource Technology 101, pp. 5222-5228.

Cao, X., Ma, L., Liang, Y., Gao, B., Harris, W., 2011. Simultaneous Immobilization of Lead and Atrazine in Contaminated Soils Using Dairy-Manure Biochar. Environmental Science & Technology 45, pp. 4884-4889.

Carmo, A.M., Hundal, L.S., Thompson, M.L., 2000. Sorption of Hydrophobic Organic Compounds by Soil Materials: Application of Unit Equivalent Freundlich Coefficients. Environmental Science & Technology 34, pp. 4363-4369.

Cayuela, M.L., van Zwieten, L., Singh, B.P., Jeffery, S., Roig, A., Sánchez-Monedero, M.A., 2014. Biochar's role in mitigating soil nitrous oxide emissions: A review and meta-analysis. Agriculture, Ecosystems & Environment 191, pp. 5-16.

Çeçen, F., Aktas, Ö., 2011. Activated carbon for water and wastewater treatment: Integration of adsorption and biological treatment. John Wiley & Sons.

Cha, J.S., Park, S.H., Jung, S.-C., Ryu, C., Jeon, J.-K., Shin, M.-C., Park, Y.-K., 2016. Production and utilization of biochar: A review. Journal of Industrial and Engineering Chemistry 40, pp. 1-15.

Chefetz, B., Xing, B., 2009. Relative Role of Aliphatic and Aromatic Moieties as Sorption Domains for Organic Compounds: A Review. Environmental Science & Technology 43, pp. 1680-1688.

Chen, B., Chen, Z., 2009. Sorption of naphthalene and 1-naphthol by biochars of orange peels with different pyrolytic temperatures. Chemosphere 76, pp. 127-133.

Chen, B., Zhou, D., Zhu, L., 2008. Transitional adsorption and partition of nonpolar and polar aromatic contaminants by biochars of pine needles with different pyrolytic temperatures. Environmental Science & Technology 42, pp. 5137-5143.

Chen, J., Zhang, D., Zhang, H., Ghosh, S., Pan, B., 2017. Fast and slow adsorption of carbamazepine on biochar as affected by carbon structure and mineral composition. Science of the Total Environment 579, pp. 598-605.

Chen, W.-H., Peng, J., Bi, X.T., 2015. A state-of-the-art review of biomass torrefaction, densification and applications. Renewable and Sustainable Energy Reviews 44, pp. 847-866.

Chen, Y., Zhu, Y., Wang, Z., Li, Y., Wang, L., Ding, L., Gao, X., Ma, Y., Guo, Y., 2011. Application studies of activated carbon derived from rice husks produced by chemical-thermal process—A review. Advances in Colloid and Interface Science 163, pp. 39-52.

Chen, Z., Chen, B., Chiou, C.T., 2012a. Fast and Slow Rates of Naphthalene Sorption to Biochars Produced at Different Temperatures. Environmental Science & Technology 46, pp. 11104-11111.

Chen, Z., Chen, B., Zhou, D., Chen, W., 2012b. Bisolute Sorption and Thermodynamic Behavior of Organic Pollutants to Biomass-derived Biochars at Two Pyrolytic Temperatures. Environmental Science & Technology 46, pp. 12476-12483.

Chia, C.H., Downie, A., Munroe, P., 2015. Characteristics of biochar: physical and structural properties. in: Lehmann, J., Joseph, S. (Eds.). Biochar for Environmental Management: Science, Technology and Implementation. Routledge, London, U.K., pp. 121-142.

Chiou, C.T., Cheng, J., Hung, W.-N., Chen, B., Lin, T.-F., 2015. Resolution of Adsorption and Partition Components of Organic Compounds on Black Carbons. Environmental Science & Technology 49, pp. 9116-9123.

Chiou, C.T., Peters, L.J., Freed, V.H., 1979. A Physical Concept of Soil-Water Equilibria for Nonionic Organic Compounds. Science 206, pp. 831-832.

Chiou, C.T., Porter, P.E., Schmedding, D.W., 1983. Partition equilibriums of nonionic organic compounds between soil organic matter and water. Environmental Science & Technology 17, pp. 227-231.

Chiou, C.T., Schmedding, D.W., Manes, M., 1982. Partitioning of organic compounds in octanol-water systems. Environmental Science & Technology 16, pp. 4-10.

Cho, J., Chu, S., Dauenhauer, P.J., Huber, G.W., 2012. Kinetics and reaction chemistry for slow pyrolysis of enzymatic hydrolysis lignin and organosolv extracted lignin derived from maplewood. Green Chemistry 14, pp. 428-439.

Christophe, N., Cyril, G., Romain, L., Alessandro, P., Robert, M., Arne, S., Cornelia, R., 2015. Effect of physical weathering on the carbon sequestration potential of biochars and hydrochars in soil. GCB Bioenergy 7, pp. 488-496.

Chu, S., Subrahmanyam, A.V., Huber, G.W., 2013. The pyrolysis chemistry of a β-O-4 type oligomeric lignin model compound. Green Chemistry 15, pp. 125-136.

Chun, Y., Sheng, G., Chiou, C.T., Xing, B., 2004. Compositions and Sorptive Properties of Crop Residue-Derived Chars. Environmental Science & Technology 38, pp. 4649-4655.

Cumming, G., 2009. Inference by eye: Reading the overlap of independent confidence intervals. Statistics in Medicine 28, pp. 205-220.

Dai, Z., Zhang, X., Tang, C., Muhammad, N., Wu, J., Brookes, P.C., Xu, J., 2017. Potential role of biochars in decreasing soil acidification - A critical review. Science of the Total Environment 581-582, pp. 601-611.

Dalahmeh, S., Ahrens, L., Gros, M., Wiberg, K., Pell, M., 2018. Potential of biochar filters for onsite sewage treatment: Adsorption and biological degradation of pharmaceuticals in laboratory filters with active, inactive and no biofilm. Science of the Total Environment 612, pp. 192-201.

Dalahmeh, S.S., Alziq, N., Ahrens, L., 2019. Potential of biochar filters for onsite wastewater treatment: Effects of active and inactive biofilms on adsorption of per- and polyfluoroalkyl substances in laboratory column experiments. Environmental Pollution 247, pp. 155-164.

Damgaard, I., Bjerg, P.L., Bælum, J., Scheutz, C., Hunkeler, D., Jacobsen, C.S., Tuxen, N., Broholm, M.M., 2013. Identification of chlorinated solvents degradation zones in clay till by high resolution chemical, microbial and compound specific isotope analysis. Journal of Contaminant Hydrology 146, pp. 37-50.

de Figueredo, N.A., da Costa, L.M., Melo, L.C.A., Siebeneichlerd, E.A., Tronto, J., 2017. Characterization of biochars from different sources and evaluation of release of nutrients and contaminants. Revista Ciencia Agronomica 48, pp. 395-403.

Denyes, M.J., Langlois, V.S., Rutter, A., Zeeb, B.A., 2012. The use of biochar to reduce soil PCB bioavailability to Cucurbita pepo and Eisenia fetida. Science of the Total Environment 437, pp. 76-82.

Denyes, M.J., Rutter, A., Zeeb, B.A., 2013. In situ application of activated carbon and biochar to PCB-contaminated soil and the effects of mixing regime. Environmental Pollution 182, pp. 201-208.

Denyes, M.J., Rutter, A., Zeeb, B.A., 2016. Bioavailability assessments following biochar and activated carbon amendment in DDT-contaminated soil. Chemosphere 144, pp. 1428-1434.

ElHaddad, E., Ensinger, W., Schüth, C., 2013. Untersuchungen zur Sorptionsreversibilität von organischen Schadstoffen in Aktivkohle, Holzkohle und Zeolith Y-200. Grundwasser 18, pp. 197-202.

Erto, A., Lancia, A., Musmarra, D., 2011. A modelling analysis of PCE/TCE mixture adsorption based on Ideal Adsorbed Solution Theory. Separation and Purification Technology 80, pp. 140-147.

European Comission, 2000. Directive 2000/60/EC of the European Parliament and of the Council establishing a framework for the Community action in the field of water policy. Official Journal L 327.

Faria, W.M., Figueiredo, C.C.d., Coser, T.R., Vale, A.T., Schneider, B.G., 2018. Is sewage sludge biochar capable of replacing inorganic fertilizers for corn production? Evidence from a two-year field experiment. Archives of Agronomy and Soil Science 64, pp. 505-519.

Feng, M., Zhang, W., Wu, X., Jia, Y., Jiang, C., Wei, H., Qiu, R., Tsang, D.C.W., 2018. Continuous leaching modifies the surface properties and metal(loid) sorption of sludge-derived biochar. Science of the Total Environment 625, pp. 731-737.

Fetter, C.W., Boving, T., Kreamer, D., 2017. Contaminant hydrogeology. Waveland Press.

Fidel, R.B., Laird, D.A., Thompson, M.L., 2013. Evaluation of Modified Boehm Titration Methods for Use with Biochars. Journal of Environmental Quality 42, pp. 1771-1778.

Foo, K.Y., Hameed, B.H., 2010. Insights into the modeling of adsorption isotherm systems. Chemical Engineering Journal 156, pp. 2-10.

Freundlich, H., 1907. Über die Adsorption in Lösungen. Zeitschrift fur Physikalische Chemie 57U, p. 385.

Freundlich, H., 1909. Kappilarchemie. Akademische Verlagsgesellschaft, Leipzig.

Fu, H., Wei, C., Qu, X., Li, H., Zhu, D., 2018. Strong binding of apolar hydrophobic organic contaminants by dissolved black carbon released from biochar: A mechanism of pseudomicelle partition and environmental implications. Environmental Pollution 232, pp. 402-410.

Fu, P., Hu, S., Xiang, J., Sun, L., Su, S., Wang, J., 2012. Evaluation of the porous structure development of chars from pyrolysis of rice straw: Effects of pyrolysis temperature and heating rate. Journal of Analytical and Applied Pyrolysis 98, pp. 177-183.

Gai, X., Wang, H., Liu, J., Zhai, L., Liu, S., Ren, T., Liu, H., 2014. Effects of Feedstock and Pyrolysis Temperature on Biochar Adsorption of Ammonium and Nitrate. PLOS ONE 9, p. e113888.

Gámiz, B., López-Cabeza, R., Facenda, G., Velarde, P., Hermosín, M.C., Cox, L., Celis, R., 2016. Effect of synthetic clay and biochar addition on dissipation and enantioselectivity of tebuconazole and metalaxyl in an agricultural soil: Laboratory and field experiments. Agriculture, Ecosystems & Environment 230, pp. 32-41.

Gao, F., Xue, Y., Deng, P., Cheng, X., Yang, K., 2015. Removal of aqueous ammonium by biochars derived from agricultural residuals at different pyrolysis temperatures. Chemical Speciation & Bioavailability 27, pp. 92-97.

Gascó, G., Álvarez, M.L., Paz-Ferreiro, J., Méndez, A., 2019. Combining phytoextraction by Brassica napus and biochar amendment for the remediation of a mining soil in Riotinto (Spain). Chemosphere 231, pp. 562-570.

Ghaffar, A., Ghosh, S., Li, F., Dong, X., Zhang, D., Wu, M., Li, H., Pan, B., 2015. Effect of biochar aging on surface characteristics and adsorption behavior of dialkyl phthalates. Environmental Pollution 206, pp. 502-509.

Glaser, B., 2006. Prehistorically modified soils of central Amazonia: a model for sustainable agriculture in the twenty-first century. Philosophical Transactions of the Royal Society B: Biological Sciences 362, pp. 187-196.

Glaser, B., Haumaier, L., Guggenberger, G., Zech, W., 2001. The 'Terra Preta' phenomenon: a model for sustainable agriculture in the humid tropics. Naturwissenschaften 88, pp. 37-41.

Glaser, B., Lehmann, J., Zech, W., 2002. Ameliorating physical and chemical properties of highly weathered soils in the tropics with charcoal – a review. Biology and Fertility of Soils 35, pp. 219-230.

Gomez-Eyles, J.L., Sizmur, T., Collins, C.D., Hodson, M.E., 2011. Effects of biochar and the earthworm Eisenia fetida on the bioavailability of polycyclic aromatic hydrocarbons and potentially toxic elements. Environmental Pollution 159, pp. 616-622.

Gomez-Eyles, J.L., Yupanqui, C., Beckingham, B., Riedel, G., Gilmour, C., Ghosh, U., 2013. Evaluation of Biochars and Activated Carbons for In Situ Remediation Of Sediments Impacted With Organics, Mercury, And Methylmercury. Environmental Science & Technology 47, pp. 13721-13729.

Graber, E.R., Meller Harel, Y., Kolton, M., Cytryn, E., Silber, A., Rav David, D., Tsechansky, L., Borenshtein, M., Elad, Y., 2010. Biochar impact on development and productivity of pepper and tomato grown in fertigated soilless media. Plant and Soil 337, pp. 481-496.

Graber, E.R., Tsechansky, L., Gerstl, Z., Lew, B., 2012. High surface area biochar negatively impacts herbicide efficacy. Plant and Soil 353, pp. 95-106.

Gul, S., Whalen, J.K., Thomas, B.W., Sachdeva, V., Deng, H., 2015. Physico-chemical properties and microbial responses in biochar-amended soils: Mechanisms and future directions. Agriculture, Ecosystems & Environment 206, pp. 46-59.

Gupta, S., Kua, H.W., 2017. Factors Determining the Potential of Biochar As a Carbon Capturing and Sequestering Construction Material: Critical Review. Journal of Materials in Civil Engineering 29, p. 04017086.

Gwenzi, W., Chaukura, N., Noubactep, C., Mukome, F.N.D., 2017. Biochar-based water treatment systems as a potential low-cost and sustainable technology for clean water provision. Journal of Environmental Management 197, pp. 732-749.

Hagemann, N., Spokas, K., Schmidt, H.-P., Kägi, R., Böhler, M., Bucheli, T., 2018. Activated Carbon, Biochar and Charcoal: Linkages and Synergies across Pyrogenic Carbon's ABCs. Water 10, p. 182.

Hale, S.E., Arp, H.P.H., Kupryianchyk, D., Cornelissen, G., 2016. A synthesis of parameters related to the binding of neutral organic compounds to charcoal. Chemosphere 144, pp. 65-74.

Han, L., Qian, L., Yan, J., Chen, M., 2016. Contributions of different biomass components to the sorption of 1,2,4-trichlorobenzene under a series of pyrolytic temperatures. Chemosphere 156, pp. 262-271.

Han, L., Qian, L., Yan, J., Chen, M., 2017. Effects of the biochar aromaticity and molecular structures of the chlorinated organic compounds on the adsorption characteristics. Environmental Science and Pollution Research 24, pp. 5554-5565.

Hassan, M., Liu, Y., Naidu, R., Parikh, S.J., Du, J., Qi, F., Willett, I.R., 2020. Influences of feedstock sources and pyrolysis temperature on the properties of biochar and functionality as adsorbents: A meta-analysis. Science of the Total Environment 744, p. 140714.

Heidarinejad, Z., Dehghani, M.H., Heidari, M., Javedan, G., Ali, I., Sillanpää, M., 2020. Methods for preparation and activation of activated carbon: a review. Environmental Chemistry Letters 18, pp. 393-415.

Herath, I., Kumarathilaka, P., Navaratne, A., Rajakaruna, N., Vithanage, M., 2015. Immobilization and phytotoxicity reduction of heavy metals in serpentine soil using biochar. Journal of Soils and Sediments 15, pp. 126-138.

Ho, Y.S., McKay, G., 1998. A Comparison of Chemisorption Kinetic Models Applied to Pollutant Removal on Various Sorbents. Process Safety and Environmental Protection 76, pp. 332-340.

Hollister, C.C., Bisogni, J.J., Lehmann, J., 2013. Ammonium, Nitrate, and Phosphate Sorption to and Solute Leaching from Biochars Prepared from Corn Stover (Zea mays L.) and Oak Wood (Quercus spp.). Journal of Environmental Quality 42, pp. 137-144.

Hu, S., Jiang, L., Wang, Y., Su, S., Sun, L., Xu, B., He, L., Xiang, J., 2015. Effects of inherent alkali and alkaline earth metallic species on biomass pyrolysis at different temperatures. Bioresource Technology 192, pp. 23-30.

Huang, B., Lei, C., Wei, C., Zeng, G., 2014. Chlorinated volatile organic compounds (Cl-VOCs) in environment — sources, potential human health impacts, and current remediation technologies. Environment International 71, pp. 118-138.

Huang, Q., Song, S., Chen, Z., Hu, B., Chen, J., Wang, X., 2019. Biochar-based materials and their applications in removal of organic contaminants from wastewater: state-of-the-art review. Biochar 1.

Huggins, T.M., Haeger, A., Biffinger, J.C., Ren, Z.J., 2016. Granular biochar compared with activated carbon for wastewater treatment and resource recovery. Water Research 94, pp. 225-232.

IBI, 2015. Standardized product definition and product testing guidelines for biochar that is used in soil, Version 2.1. International Biochar Initiative, https://biochar-international.org/characterizationstandard/.

Igalavithana, A.D., Mandal, S., Niazi, N.K., Vithanage, M., Parikh, S.J., Mukome, F.N.D., Rizwan, M., Oleszczuk, P., Al-Wabel, M., Bolan, N., Tsang, D.C.W., Kim, K.-H., Ok, Y.S., 2018. Advances and future directions of biochar characterization methods and applications. Critical Reviews in Environmental Science and Technology, pp. 1-56.

Inyang, M., Dickenson, E., 2015. The potential role of biochar in the removal of organic and microbial contaminants from potable and reuse water: A review. Chemosphere 134, pp. 232-240.

Inyang, M.I., Gao, B., Yao, Y., Xue, Y., Zimmerman, A., Mosa, A., Pullammanappallil, P., Ok, Y.S., Cao, X., 2016. A review of biochar as a low-cost adsorbent for aqueous heavy metal removal. Critical Reviews in Environmental Science and Technology 46, pp. 406-433.

Ippolito, J.A., Cui, L., Kammann, C., Wrage-Mönnig, N., Estavillo, J.M., Fuertes-Mendizabal, T., Cayuela, M.L., Sigua, G., Novak, J., Spokas, K., Borchard, N., 2020. Feedstock choice, pyrolysis temperature and type influence biochar characteristics: a comprehensive meta-data analysis review. Biochar.

Jamieson, T., Sager, E., Guéguen, C., 2014. Characterization of biochar-derived dissolved organic matter using UV–visible absorption and excitation–emission fluorescence spectroscopies. Chemosphere 103, pp. 197-204.

Jeffery, S., Verheijen, F.G.A., Kammann, C., Abalos, D., 2016. Biochar effects on methane emissions from soils: A meta-analysis. Soil Biology and Biochemistry 101, pp. 251-258.

Jing, F., Pan, M., Chen, J., 2018. Kinetic and isothermal adsorption-desorption of PAEs on biochars: effect of biomass feedstock, pyrolysis temperature, and mechanism implication of desorption hysteresis. Environmental Science and Pollution Research 25, pp. 11493-11504.

Jones, D.L., Edwards-Jones, G., Murphy, D.V., 2011. Biochar mediated alterations in herbicide breakdown and leaching in soil. Soil Biology and Biochemistry 43, pp. 804-813.

Jonker, M.T.O., Koelmans, A.A., 2002. Extraction of Polycyclic Aromatic Hydrocarbons from Soot and Sediment: Solvent Evaluation and Implications for Sorption Mechanism. Environmental Science & Technology 36, pp. 4107-4113.

Jośko, I., Oleszczuk, P., Pranagal, J., Lehmann, J., Xing, B., Cornelissen, G., 2013. Effect of biochars, activated carbon and multiwalled carbon nanotubes on phytotoxicity of sediment contaminated by inorganic and organic pollutants. Ecological Engineering 60, pp. 50-59.

Jung, C., Boateng, L.K., Flora, J.R.V., Oh, J., Braswell, M.C., Son, A., Yoon, Y., 2015. Competitive adsorption of selected non-steroidal anti-inflammatory drugs on activated biochars: Experimental and molecular modeling study. Chemical Engineering Journal 264, pp. 1-9.

Kah, M., Sigmund, G., Xiao, F., Hofmann, T., 2017. Sorption of ionizable and ionic organic compounds to biochar, activated carbon and other carbonaceous materials. Water Research 124, pp. 673-692.

Kah, M., Sun, H., Sigmund, G., Hüffer, T., Hofmann, T., 2016. Pyrolysis of waste materials: Characterization and prediction of sorption potential across a wide range of mineral contents and pyrolysis temperatures. Bioresource Technology 214, pp. 225-233.

Kambo, H.S., Dutta, A., 2015. A comparative review of biochar and hydrochar in terms of production, physico-chemical properties and applications. Renewable and Sustainable Energy Reviews 45, pp. 359-378.

Karami, N., Clemente, R., Moreno-Jiménez, E., Lepp, N.W., Beesley, L., 2011. Efficiency of green waste compost and biochar soil amendments for reducing lead and copper mobility and uptake to ryegrass. Journal of Hazardous materials 191, pp. 41-48.

Karanfil, T., Dastgheib, S.A., 2004. Trichloroethylene Adsorption by Fibrous and Granular Activated Carbons: Aqueous Phase, Gas Phase, and Water Vapor Adsorption Studies. Environmental Science & Technology 38, pp. 5834-5841.

Karickhoff, S.W., Brown, D.S., Scott, T.A., 1979. Sorption of hydrophobic pollutants on natural sediments. Water Research 13, pp. 241-248.

Kasaoka, S., Sakata, Y., Tanaka, E., Naitoh, R., 1989. Design of molecular-sieving carbon. Studies on adsorption of various dyes in liquid phase. International Chemical Engineering 29, pp. 734-742.

Kavitha, B., Reddy, P.V.L., Kim, B., Lee, S.S., Pandey, S.K., Kim, K.-H., 2018. Benefits and limitations of biochar amendment in agricultural soils: A review. Journal of Environmental Management 227, pp. 146-154.

Keiluweit, M., Kleber, M., 2009. Molecular-Level Interactions in Soils and Sediments: The Role of Aromatic π-Systems. Environmental Science & Technology 43, pp. 3421-3429.

Keiluweit, M., Nico, P.S., Johnson, M.G., Kleber, M., 2010. Dynamic Molecular Structure of Plant Biomass-Derived Black Carbon (Biochar). Environmental Science & Technology 44, pp. 1247-1253.

Klasson, K.T., Ledbetter, C.A., Uchimiya, M., Lima, I.M., 2013. Activated biochar removes 100 % dibromochloropropane from field well water. Environmental Chemistry Letters 11, pp. 271-275.

Klasson, K.T., Uchimiya, M., Lima, I.M., 2014. Uncovering surface area and micropores in almond shell biochars by rainwater wash. Chemosphere 111, pp. 129-134.

Kleber, M., Hockaday, W., Nico, P.S., 2015. Characteristics of biochar: macro-molecular properties. in: Lehmann, J., Joseph, S. (Eds.). Biochar for Environmental Management: Science, Technology and Implementation. Routledge, London, U.K.

Kleineidam, S., Schüth, C., Grathwohl, P., 2002. Solubility-Normalized Combined Adsorption-Partitioning Sorption Isotherms for Organic Pollutants. Environmental Science & Technology 36, pp. 4689-4697.

Kloss, S., Zehetner, F., Dellantonio, A., Hamid, R., Ottner, F., Liedtke, V., Schwanninger, M., Gerzabek, M.H., Soja, G., 2012. Characterization of Slow Pyrolysis Biochars: Effects of Feedstocks and Pyrolysis Temperature on Biochar Properties. Journal of Environmental Quality 41, pp. 990-1000.

Kong, Z., Liaw, S.B., Gao, X., Yu, Y., Wu, H., 2014. Leaching characteristics of inherent inorganic nutrients in biochars from the slow and fast pyrolysis of mallee biomass. Fuel 128, pp. 433-441.

Kosa, M., Ben, H., Theliander, H., Ragauskas, A.J., 2011. Pyrolysis oils from CO2 precipitated Kraft lignin. Green Chemistry 13, pp. 3196-3202.

Kronberg, B., 2016. The hydrophobic effect. Current Opinion in Colloid & Interface Science 22, pp. 14-22.

Kumar, A., Elad, Y., Tsechansky, L., Abrol, V., Lew, B., Offenbach, R., Graber, E.R., 2018. Biochar potential in intensive cultivation of Capsicum annuum L. (sweet pepper): crop yield and plant protection. Journal of the Science of Food and Agriculture 98, pp. 495-503.

Kuoppamäki, K., Hagner, M., Valtanen, M., Setälä, H., 2019. Using biochar to purify runoff in road verges of urbanised watersheds: A large-scale field lysimeter study. Watershed Ecology and the Environment.

Kuppusamy, S., Palanisami, T., Megharaj, M., Venkateswarlu, K., Naidu, R., 2016a. Ex-Situ Remediation Technologies for Environmental Pollutants: A Critical Perspective. in: de Voogt, P. (Ed.). Reviews of Environmental Contamination and Toxicology Volume 236. Springer International Publishing, Cham, pp. 117-192.

Kuppusamy, S., Palanisami, T., Megharaj, M., Venkateswarlu, K., Naidu, R., 2016b. In-Situ Remediation Approaches for the Management of Contaminated Sites: A Comprehensive Overview. in: de Voogt, P. (Ed.). Reviews of Environmental Contamination and Toxicology Volume 236. Springer International Publishing, Cham, pp. 1-115.

Kupryianchyk, D., Hale, S., Zimmerman, A.R., Harvey, O., Rutherford, D., Abiven, S., Knicker, H., Schmidt, H.-P., Rumpel, C., Cornelissen, G., 2016. Sorption of hydrophobic organic compounds to a diverse suite of carbonaceous materials with emphasis on biochar. Chemosphere 144, pp. 879-887.

Kwon, S., Pignatello, J.J., 2005. Effect of Natural Organic Substances on the Surface and Adsorptive Properties of Environmental Black Carbon (Char): Pseudo Pore Blockage by Model Lipid Components and Its Implications for N2-Probed Surface Properties of Natural Sorbents. Environmental Science & Technology 39, pp. 7932-7939.

Langmuir, I., 1918. The adsorption of gases on plane surfaces of glass, mica and platinum. Journal of the American Chemical Society 40, pp. 1361-1403.

Lastoskie, C., Gubbins, K.E., Quirke, N., 1993. Pore size distribution analysis of microporous carbons: a density functional theory approach. The Journal of Physical Chemistry 97, pp. 4786-4796.

Lattao, C., Cao, X., Mao, J., Schmidt-Rohr, K., Pignatello, J.J., 2014. Influence of molecular structure and adsorbent properties on sorption of organic compounds to a temperature series of wood chars. Environmental Science & Technology 48, pp. 4790-4798.

Lehmann, J., Gaunt, J., Rondon, M., 2006. Bio-char Sequestration in Terrestrial Ecosystems – A Review. Mitigation and Adaptation Strategies for Global Change 11, pp. 403-427.

Lehmann, J., Joseph, S., 2009. Biochar for Environmental Management: An Introduction. in: Lehmann, J., Joseph, S. (Eds.). Biochar for Environmental Management: Science and Technology. Earthscan, London, U.K., p. 416.

Leng, L., Huang, H., Li, H., Li, J., Zhou, W., 2019. Biochar stability assessment methods: A review. Science of the Total Environment 647, pp. 210-222.

Leng, L., Xu, S., Liu, R., Yu, T., Zhuo, X., Leng, S., Xiong, Q., Huang, H., 2020. Nitrogen containing functional groups of biochar: An overview. Bioresource Technology 298, p. 122286.

Li, D.-C., Jiang, H., 2017. The thermochemical conversion of non-lignocellulosic biomass to form biochar: a review on characterizations and mechanism elucidation. Bioresource Technology.

Li, H., Dong, X., da Silva, E.B., de Oliveira, L.M., Chen, Y., Ma, L.Q., 2017. Mechanisms of metal sorption by biochars: Biochar characteristics and modifications. Chemosphere 178, pp. 466-478.

Li, J., Chen, Y., He, L., Liang, N., Wang, L., Zhao, J., Pan, B., 2020. Sorption of sulfamethoxazole on biochars of varying mineral content. Environmental Science: Processes & Impacts 22, pp. 1287-1294.

Li, J., Werth, C.J., 2001. Evaluating Competitive Sorption Mechanisms of Volatile Organic Compounds in Soils and Sediments Using Polymers and Zeolites. Environmental Science & Technology 35, pp. 568-574.

Li, L., Quinlivan, P.A., Knappe, D.R.U., 2002. Effects of activated carbon surface chemistry and pore structure on the adsorption of organic contaminants from aqueous solution. Carbon 40, pp. 2085-2100.

Lian, F., Chang, C., Du, Y., Zhu, L., Xing, B., Liu, C., 2012. Adsorptive removal of hydrophobic organic compounds by carbonaceous adsorbents: A comparative study of waste-polymer-based, coal-based activated carbon, and carbon nanotubes. Journal of Environmental Sciences 24, pp. 1549-1558.

Lian, F., Xing, B., 2017. Black Carbon (Biochar) In Water/Soil Environments: Molecular Structure, Sorption, Stability, and Potential Risk. Environmental Science & Technology.

Libra, J.A., Ro, K.S., Kammann, C., Funke, A., Berge, N.D., Neubauer, Y., Titirici, M.-M., Fühner, C., Bens, O., Kern, J., Emmerich, K.-H., 2011. Hydrothermal carbonization of biomass residuals: a comparative review of the chemistry, processes and applications of wet and dry pyrolysis. Biofuels 2, pp. 71-106.

Lima, I.M., Boateng, A.A., Klasson, K.T., 2010. Physicochemical and adsorptive properties of fast-pyrolysis bio-chars and their steam activated counterparts. Journal of Chemical Technology & Biotechnology 85, pp. 1515-1521.

Limousin, G., Gaudet, J.P., Charlet, L., Szenknect, S., Barthès, V., Krimissa, M., 2007. Sorption isotherms: A review on physical bases, modeling and measurement. Applied Geochemistry 22, pp. 249-275.

Lin, Y., Munroe, P., Joseph, S., Henderson, R., Ziolkowski, A., 2012a. Water extractable organic carbon in untreated and chemical treated biochars. Chemosphere 87, pp. 151-157.

Lin, Y., Munroe, P., Joseph, S., Kimber, S., Van Zwieten, L., 2012b. Nanoscale organo-mineral reactions of biochars in ferrosol: an investigation using microscopy. Plant and Soil 357, pp. 369-380.

Liu, C.-H., Chu, W., Li, H., Boyd, S.A., Teppen, B.J., Mao, J., Lehmann, J., Zhang, W., 2019a. Quantification and characterization of dissolved organic carbon from biochars. Geoderma 335, pp. 161-169.

Liu, C.-H., Chuang, Y.-H., Li, H., Boyd, S.A., Teppen, B.J., Gonzalez, J.M., Johnston, C.T., Lehmann, J., Zhang, W., 2019b. Long-term sorption of lincomycin to biochars: The intertwined roles of pore diffusion and dissolved organic carbon. Water Research 161, pp. 108-118.

Liu, G., Zheng, H., Jiang, Z., Zhao, J., Wang, Z., Pan, B., Xing, B., 2018. Formation and Physicochemical Characteristics of Nano Biochar: Insight into Chemical and Colloidal Stability. Environmental Science & Technology 52, pp. 10369-10379.

Liu, W.-J., Jiang, H., Yu, H.-Q., 2015. Development of Biochar-Based Functional Materials: Toward a Sustainable Platform Carbon Material. Chemical Reviews 115, pp. 12251-12285.

Liu, X., Ji, R., Shi, Y., Wang, F., Chen, W., 2019c. Release of polycyclic aromatic hydrocarbons from biochar fine particles in simulated lung fluids: Implications for bioavailability and risks of airborne aromatics. Science of the Total Environment 655, pp. 1159-1168.

Liu, Y., Zhao, X., Li, J., Ma, D., Han, R., 2012. Characterization of bio-char from pyrolysis of wheat straw and its evaluation on methylene blue adsorption. Desalination and Water Treatment 46, pp. 115-123.

Lonappan, L., Rouissi, T., Kaur Brar, S., Verma, M., Surampalli, R.Y., 2018. An insight into the adsorption of diclofenac on different biochars: Mechanisms, surface chemistry, and thermodynamics. Bioresource Technology 249, pp. 386-394.

Lu, H., Zhang, W., Wang, S., Zhuang, L., Yang, Y., Qiu, R., 2013. Characterization of sewage sludge-derived biochars from different feedstocks and pyrolysis temperatures. Journal of Analytical and Applied Pyrolysis 102, pp. 137-143.

Lu, L., Chen, B., 2018. Enhanced bisphenol A removal from stormwater in biochar-amended biofilters: Combined with batch sorption and fixed-bed column studies. Environmental Pollution 243, pp. 1539-1549.

Lu, L., Yu, W., Wang, Y., Zhang, K., Zhu, X., Zhang, Y., Wu, Y., Ullah, H., Xiao, X., Chen, B., 2020. Application of biochar-based materials in environmental remediation: from multi-level structures to specific devices. Biochar.

Lu, Y., Pignatello, J.J., 2002. Demonstration of the “Conditioning Effect” in Soil Organic Matter in Support of a Pore Deformation Mechanism for Sorption Hysteresis. Environmental Science & Technology 36, pp. 4553-4561.

Luo, L., Lv, J., Chen, Z., Huang, R., Zhang, S., 2017. Insights into the attenuated sorption of organic compounds on black carbon aged in soil. Environmental Pollution 231, pp. 1469-1476.

Lyu, H., Zhang, Q., Shen, B., 2020. Application of biochar and its composites in catalysis. Chemosphere 240, p. 124842.

Ma, X., Anand, D., Zhang, X., Talapatra, S., 2011. Adsorption and Desorption of Chlorinated Compounds from Pristine and Thermally Treated Multiwalled Carbon Nanotubes. Journal of Physical Chemistry C 115, pp. 4552-4557.

Mandal, A., Singh, N., Purakayastha, T.J., 2017. Characterization of pesticide sorption behaviour of slow pyrolysis biochars as low cost adsorbent for atrazine and imidacloprid removal. Science of the Total Environment 577, pp. 376-385.

Manyà, J.J., 2012. Pyrolysis for Biochar Purposes: A Review to Establish Current Knowledge Gaps and Research Needs. Environmental Science & Technology 46, pp. 7939-7954.

Marchal, G., Smith, K.E.C., Rein, A., Winding, A., Wollensen de Jonge, L., Trapp, S., Karlson, U.G., 2013. Impact of activated carbon, biochar and compost on the desorption and mineralization of phenanthrene in soil. Environmental Pollution 181, pp. 200-210.

Matteucci, F., Ercole, C., del Gallo, M., 2015. A study of chlorinated solvent contamination of the aquifers of an industrial area in central Italy: a possibility of bioremediation. Frontiers in Microbiology 6, p. 924.

Mendes, K.F., de Sousa, R.N., Goulart, M.O., Tornisielo, V.L., 2020. Role of raw feedstock and biochar amendments on sorption-desorption and leaching potential of three 3H- and 14C-labelled pesticides in soils. Journal of Radioanalytical and Nuclear Chemistry 324, pp. 1373-1386.

Mohan, D., Rajput, S., Singh, V.K., Steele, P.H., Pittman Jr, C.U., 2011. Modeling and evaluation of chromium remediation from water using low cost bio-char, a green adsorbent. Journal of Hazardous materials 188, pp. 319-333.

Mohan, D., Sarswat, A., Ok, Y.S., Pittman Jr, C.U., 2014. Organic and inorganic contaminants removal from water with biochar, a renewable, low cost and sustainable adsorbent – A critical review. Bioresource Technology 160, pp. 191-202.

Mohan, D., Sharma, R., Singh, V.K., Steele, P., Pittman, C.U., 2012. Fluoride Removal from Water using Bio-Char, a Green Waste, Low-Cost Adsorbent: Equilibrium Uptake and Sorption Dynamics Modeling. Industrial & Engineering Chemistry Research 51, pp. 900-914.

Mohanty, S.K., Valenca, R., Berger, A.W., Yu, I.K.M., Xiong, X., Saunders, T.M., Tsang, D.C.W., 2018. Plenty of room for carbon on the ground: Potential applications of biochar for stormwater treatment. Science of the Total Environment 625, pp. 1644-1658.

Moreira, M.T., Noya, I., Feijoo, G., 2017. The prospective use of biochar as adsorption matrix – A review from a lifecycle perspective. Bioresource Technology 246, pp. 135-141.

Mukome, F.N.D., Zhang, X., Silva, L.C.R., Six, J., Parikh, S.J., 2013. Use of Chemical and Physical Characteristics To Investigate Trends in Biochar Feedstocks. Journal of Agricultural and Food Chemistry 61, pp. 2196-2204.

Nag, S.K., Kookana, R., Smith, L., Krull, E., Macdonald, L.M., Gill, G., 2011. Poor efficacy of herbicides in biochar-amended soils as affected by their chemistry and mode of action. Chemosphere 84, pp. 1572-1577.

Nguyen, T.H., Cho, H.-H., Poster, D.L., Ball, W.P., 2007. Evidence for a Pore-Filling Mechanism in the Adsorption of Aromatic Hydrocarbons to a Natural Wood Char. Environmental Science & Technology 41, pp. 1212-1217.

Nguyen, X.C., Tran, T.C.P., Hoang, V.H., Nguyen, T.P., Chang, S.W., Nguyen, D.D., Guo, W., Kumar, A., La, D.D., Bach, Q.-V., 2020. Combined biochar vertical flow and free-water surface constructed wetland system for dormitory sewage treatment and reuse. Science of the Total Environment 713, p. 136404.

Ni, J., Pignatello, J.J., Xing, B., 2011. Adsorption of aromatic carboxylate ions to black carbon (biochar) is accompanied by proton exchange with water. Environmental Science & Technology 45, pp. 9240-9248.

Nkedi-Kizza, P., Rao, P.S.C., Hornsby, A.G., 1987. Influence of organic cosolvents on leaching of hydrophobic organic chemicals through soils. Environmental Science & Technology 21, pp. 1107-1111.

Norwood, M.J., Louchouarn, P., Kuo, L.-J., Harvey, O.R., 2013. Characterization and biodegradation of water-soluble biomarkers and organic carbon extracted from low temperature chars. Organic Geochemistry 56, pp. 111-119.

O'Connor, D., Peng, T., Zhang, J., Tsang, D.C.W., Alessi, D.S., Shen, Z., Bolan, N.S., Hou, D., 2018. Biochar application for the remediation of heavy metal polluted land: A review of in situ field trials. Science of the Total Environment 619-620, pp. 815-826.

Ok, Y.S., Tsang, D.C., Bolan, N., Novak, J.M., 2018. Biochar from Biomass and Waste: Fundamentals and Applications. Elsevier.

Ok, Y.S., Uchimiya, S.M., Chang, S.X., Bolan, N., 2015. Biochar: Production, characterization, and applications. CRC press.

Oleszczuk, P., Godlewska, P., Reible, D.D., Kraska, P., 2017. Bioaccessibility of polycyclic aromatic hydrocarbons in activated carbon or biochar amended vegetated (Salix viminalis) soil. Environmental Pollution 227, pp. 406-413.

Olivier, J.P., 1995. Modeling physical adsorption on porous and nonporous solids using density functional theory. Journal of Porous Materials 2, pp. 9-17.

Olsen, R.L., Davis, A., 1990. Predicting the fate and transport of organic compounds in groundwater: Part 1. Hazardous Materials Control 3, pp. 38-64.

Palansooriya, K.N., Wong, J.T.F., Hashimoto, Y., Huang, L., Rinklebe, J., Chang, S.X., Bolan, N., Wang, H., Ok, Y.S., 2019a. Response of microbial communities to biochar-amended soils: a critical review. Biochar 1, pp. 3-22.

Palansooriya, K.N., Yang, Y., Tsang, Y.F., Sarkar, B., Hou, D., Cao, X., Meers, E., Rinklebe, J., Kim, K.-H., Ok, Y.S., 2019b. Occurrence of contaminants in drinking water sources and the potential of biochar for water quality improvement: A review. Critical Reviews in Environmental Science and Technology, pp. 1-63.

Pan, B., Xing, B., 2010. Competitive and Complementary Adsorption of Bisphenol A and 17α-Ethinyl Estradiol on Carbon Nanomaterials. Journal of Agricultural and Food Chemistry 58, pp. 8338-8343.

Park, J., Choppala, G., Bolan, N., Chung, J., Chuasavathi, T., 2011. Biochar reduces the bioavailability and phytotoxicity of heavy metals. Plant and Soil 348, pp. 439-451.

Paz-Ferreiro, J., Lu, H., Fu, S., Méndez, A., Gascó, G., 2014. Use of phytoremediation and biochar to remediate heavy metal polluted soils: a review. Solid Earth 5, pp. 65-75.

Pelekani, C., Snoeyink, V.L., 1999. Competitive adsorption in natural water: role of activated carbon pore size. Water Research 33, pp. 1209-1219.

Perez-Mercado, L.F., Lalander, C., Berger, C., Dalahmeh, S.S., 2018. Potential of Biochar Filters for Onsite Wastewater Treatment: Effects of Biochar Type, Physical Properties and Operating Conditions. Water 10, p. 1835.

Pignatello, J.J., 1989. Sorption Dynamics of Organic Compounds in Soils and Sediments. in: Sawhney, B.L., Brown, K. (Eds.). Reactions and Movement of Organic Chemicals in Soils. Soil Science Society of America and American Society of Agronomy, pp. 45-80.

Pignatello, J.J., 2011. Interactions of Anthropogenic Organic Chemicals with Natural Organic Matter and Black Carbon in Environmental Particles. Biophysico-Chemical Processes of Anthropogenic Organic Compounds in Environmental Systems, pp. 1-50.

Pignatello, J.J., 2013. Adsorption of dissolved organic compounds by black carbon. in: Xu, J.S., Donald L. (Ed.). Molecular Environmental Soil Science. Springer, New York, pp. 359-385.

Pignatello, J.J., Mitch, W.A., Xu, W., 2017. Activity and Reactivity of Pyrogenic Carbonaceous Matter toward Organic Compounds. Environmental Science & Technology.

Pignatello, J.J., Xing, B., 1996. Mechanisms of Slow Sorption of Organic Chemicals to Natural Particles. Environmental Science & Technology 30, pp. 1-11.

Pituello, C., Francioso, O., Simonetti, G., Pisi, A., Torreggiani, A., Berti, A., Morari, F., 2015. Characterization of chemical–physical, structural and morphological properties of biochars from biowastes produced at different temperatures. Journal of Soils and Sediments 15, pp. 792-804.

Polanyi, M., 1916. Adsorption von Gasen (Dämpfen) durch ein festes nichtfluchtiges Adsorbens. Verhandlungen der Deutschen Physekalischen Gesellschaft 18, pp. 55-80.

Prakongkep, N., Gilkes, R.J., Wiriyakitnateekul, W., 2015. Forms and solubility of plant nutrient elements in tropical plant waste biochars. Journal of Plant Nutrition and Soil Science 178, pp. 732-740.

Premarathna, K.S.D., Upamali Rajapaksha, A., Sarkar, B., Kwon, E.E., Bhatnagar, A., Sik Ok, Y., Vithanage, M., 2019. Biochar-Based Engineered Composites for Sorptive Decontamination of Water: A Review. Chemical Engineering Journal.

Qian, L., Chen, Y., Ouyang, D., Zhang, W., Han, L., Yan, J., Kvapil, P., Chen, M., 2020. Field demonstration of enhanced removal of chlorinated solvents in groundwater using biochar-supported nanoscale zero-valent iron. Science of the Total Environment 698, p. 134215.

Qin, G., Gong, D., Fan, M.-Y., 2013. Bioremediation of petroleum-contaminated soil by biostimulation amended with biochar. International Biodeterioration & Biodegradation 85, pp. 150-155.

Qiu, M., Sun, K., Jin, J., Gao, B., Yan, Y., Han, L., Wu, F., Xing, B., 2014. Properties of the plant-and manure-derived biochars and their sorption of dibutyl phthalate and phenanthrene. Scientific Reports 4, p. 5295.

Qu, X., Fu, H., Mao, J., Ran, Y., Zhang, D., Zhu, D., 2016. Chemical and structural properties of dissolved black carbon released from biochars. Carbon 96, pp. 759-767.

Rajapaksha, A.U., Vithanage, M., Lim, J.E., Ahmed, M.B.M., Zhang, M., Lee, S.S., Ok, Y.S., 2014. Invasive plant-derived biochar inhibits sulfamethazine uptake by lettuce in soil. Chemosphere 111, pp. 500-504.

Reddy, K.R., Xie, T., Dastgheibi, S., 2014. Evaluation of Biochar as a Potential Filter Media for the Removal of Mixed Contaminants from Urban Storm Water Runoff. Journal of Environmental Engineering 140, p. 04014043.

Ren, X., Sun, H., Wang, F., Zhang, P., Zhu, H., 2018a. Effect of aging in field soil on biochar's properties and its sorption capacity. Environmental Pollution.

Ren, X., Wang, F., Zhang, P., Guo, J., Sun, H., 2018b. Aging effect of minerals on biochar properties and sorption capacities for atrazine and phenanthrene. Chemosphere 206, pp. 51-58.

Ronsse, F., van Hecke, S., Dickinson, D., Prins, W., 2013. Production and characterization of slow pyrolysis biochar: influence of feedstock type and pyrolysis conditions. GCB Bioenergy 5, pp. 104-115.

Roque-Malherbe, R., 2000. Complementary approach to the volume filling theory of adsorption in zeolites. Microporous and Mesoporous Materials 41, pp. 227-240.

Rouquerol, J., Llewellyn, P., Rouquerol, F., 2007. Is the BET equation applicable to microporous adsorbents? in: Llewellyn, P.L., Rodriquez-Reinoso, F., Rouqerol, J., Seaton, N. (Eds.). Studies in Surface Science and Catalysis. Elsevier, pp. 49-56.

Sander, M., Lu, Y., Pignatello, J.J., 2006. Conditioning-Annealing Studies of Natural Organic Matter Solids Linking Irreversible Sorption to Irreversible Structural Expansion. Environmental Science & Technology 40, pp. 170-178.

Sander, M., Pignatello, J.J., 2005a. Characterization of Charcoal Adsorption Sites for Aromatic Compounds: Insights Drawn from Single-Solute and Bi-Solute Competitive Experiments. Environmental Science & Technology 39, pp. 1606-1615.

Sander, M., Pignatello, J.J., 2005b. An Isotope Exchange Technique to Assess Mechanisms of Sorption Hysteresis Applied to Naphthalene in Kerogenous Organic Matter. Environmental Science & Technology 39, pp. 7476-7484.

Sander, M., Pignatello, J.J., 2009. Sorption irreversibility of 1,4-dichlorobenzene in two natural organic matter–rich geosorbents. Environmental Toxicology and Chemistry 28, pp. 447-457.

Schaefer, C.E., Schüth, C., Werth, C.J., Reinhard, M., 2000. Binary Desorption Isotherms of TCE and PCE from Silica Gel and Natural Solids. Environmental Science & Technology 34, pp. 4341-4347.

Schimmelpfennig, S., Glaser, B., 2012. One Step Forward toward Characterization: Some Important Material Properties to Distinguish Biochars. Journal of Environmental Quality 41, pp. 1001-1013.

Schwarzenbach, R.P., Gschwend, P.M., Imboden, D.M., 2003. Environmental Organic Chemistry, 2nd ed. John Wiley & Sons, Inc., Hoboken, New Jersey, USA.

Seth, R., Mackay, D., Muncke, J., 1999. Estimating the Organic Carbon Partition Coefficient and Its Variability for Hydrophobic Chemicals. Environmental Science & Technology 33, pp. 2390-2394.

Sigmund, G., Sun, H., Hofmann, T., Kah, M., 2016. Predicting the sorption of aromatic acids to noncarbonized and carbonized sorbents. Environmental Science & Technology 50, pp. 3641-3648.

Sing, K.S.W., Everett, D.H., Haul, R.A.W., Moscou, R.A., Pieroti, R.A., Rouqerol, J., Siemieniewska, T., 1985. Reporting physisorption data for gas/solid systems with special reference to the determination of surface area and porosity (Recommendations 1984). Pure and Applied Chemistry 57, pp. 603-619.

Smith, C.R., Hatcher, P.G., Kumar, S., Lee, J.W., 2016. Investigation into the Sources of Biochar Water-Soluble Organic Compounds and Their Potential Toxicity on Aquatic Microorganisms. ACS Sustainable Chemistry and Engineering 4, pp. 2550-2558.

Smith, C.R., Sleighter, R.L., Hatcher, P.G., Lee, J.W., 2013. Molecular characterization of inhibiting biochar water-extractable substances using electrospray ionization fourier transform ion cyclotron resonance mass spectrometry. Environmental Science & Technology 47, pp. 13294-13302.

Sombroek, W.G., Nachtergaele, F.O., Hebel, A., 1993. Amounts, dynamics and sequestering of carbon in tropical and subtropical soils. Ambio. Stockholm 22, pp. 417-426.

Song, Y., Wang, F., Bian, Y., Kengara, F.O., Jia, M., Xie, Z., Jiang, X., 2012. Bioavailability assessment of hexachlorobenzene in soil as affected by wheat straw biochar. Journal of Hazardous materials 217–218, pp. 391-397.

Song, Y., Wang, F., Kengara, F.O., Yang, X., Gu, C., Jiang, X., 2013. Immobilization of Chlorobenzenes in Soil Using Wheat Straw Biochar. Journal of Agricultural and Food Chemistry 61, pp. 4210-4217.

Spokas, K.A., Novak, J.M., Masiello, C.A., Johnson, M.G., Colosky, E.C., Ippolito, J.A., Trigo, C., 2014. Physical Disintegration of Biochar: An Overlooked Process. Environmental Science & Technology Letters 1, pp. 326-332.

Srinivasan, P., Sarmah, A.K., 2015. Characterisation of agricultural waste-derived biochars and their sorption potential for sulfamethoxazole in pasture soil: A spectroscopic investigation. Science of the Total Environment 502, pp. 471-480.

Stefaniuk, M., Oleszczuk, P., 2016. Addition of biochar to sewage sludge decreases freely dissolved PAHs content and toxicity of sewage sludge-amended soil. Environmental Pollution 218, pp. 242-251.

Stefaniuk, M., Oleszczuk, P., Różyło, K., 2017. Co-application of sewage sludge with biochar increases disappearance of polycyclic aromatic hydrocarbons from fertilized soil in long term field experiment. Science of the Total Environment 599-600, pp. 854-862.

Stefaniuk, M., Tsang, D.C.W., Ok, Y.S., Oleszczuk, P., 2018. A field study of bioavailable polycyclic aromatic hydrocarbons (PAHs) in sewage sludge and biochar amended soils. Journal of Hazardous materials 349, pp. 27-34.

Suliman, W., Harsh, J.B., Abu-Lail, N.I., Fortuna, A.-M., Dallmeyer, I., Garcia-Perez, M., 2016. Influence of feedstock source and pyrolysis temperature on biochar bulk and surface properties. Biomass and Bioenergy 84, pp. 37-48.

Sun, K., Kang, M., Ro, K.S., Libra, J.A., Zhao, Y., Xing, B., 2016. Variation in sorption of propiconazole with biochars: The effect of temperature, mineral, molecular structure, and nano-porosity. Chemosphere 142, pp. 56-63.

Tan, X.-f., Liu, S.-b., Liu, Y.-g., Gu, Y.-l., Zeng, G.-m., Hu, X.-j., Wang, X., Liu, S.-h., Jiang, L.-h., 2017. Biochar as potential sustainable precursors for activated carbon production: Multiple applications in environmental protection and energy storage. Bioresource Technology 227, pp. 359-372.

Tang, J., Li, X., Luo, Y., Li, G., Khan, S., 2016. Spectroscopic characterization of dissolved organic matter derived from different biochars and their polycylic aromatic hydrocarbons (PAHs) binding affinity. Chemosphere 152, pp. 399-406.

Tanthapanichakoon, W., Ariyadejwanich, P., Japthong, P., Nakagawa, K., Mukai, S.R., Tamon, H., 2005. Adsorption–desorption characteristics of phenol and reactive dyes from aqueous solution on mesoporous activated carbon prepared from waste tires. Water Research 39, pp. 1347-1353.

Taskin, E., de Castro Bueno, C., Allegretta, I., Terzano, R., Rosa, A.H., Loffredo, E., 2019. Multianalytical characterization of biochar and hydrochar produced from waste biomasses for environmental and agricultural applications. Chemosphere 233, pp. 422-430.

Teixidó, M., Pignatello, J.J., Beltrán, J.L., Granados, M., Peccia, J., 2011. Speciation of the Ionizable Antibiotic Sulfamethazine on Black Carbon (Biochar). Environmental Science & Technology 45, pp. 10020-10027.

Thomas, E., Borchard, N., Sarmiento, C., Atkinson, R., Ladd, B., 2020. Key factors determining biochar sorption capacity for metal contaminants: a literature synthesis. Biochar 2, pp. 151-163.

Thommes, M., Cychosz, K.A., 2014. Physical adsorption characterization of nanoporous materials: progress and challenges. Adsorption 20, pp. 233-250.

Thommes, M., Kaneko, K., Neimark Alexander, V., Olivier James, P., Rodriguez-Reinoso, F., Rouquerol, J., Sing Kenneth, S.W., 2015. Physisorption of gases, with special reference to the evaluation of surface area and pore size distribution (IUPAC Technical Report). Pure and Applied Chemistry 87, p. 1051.

Thompson, K.A., Shimabuku, K.K., Kearns, J.P., Knappe, D.R.U., Summers, R.S., Cook, S.M., 2016. Environmental Comparison of Biochar and Activated Carbon for Tertiary Wastewater Treatment. Environmental Science & Technology 50, pp. 11253-11262.

Tomczyk, A., Sokołowska, Z., Boguta, P., 2020. Biochar physicochemical properties: pyrolysis temperature and feedstock kind effects. Reviews in Environmental Science and Bio/Technology.

Tong, Y., McNamara, P.J., Mayer, B.K., 2019. Adsorption of organic micropollutants onto biochar: a review of relevant kinetics, mechanisms and equilibrium. Environmental Science: Water Research & Technology.

Tran, H.N., You, S.-J., Hosseini-Bandegharaei, A., Chao, H.-P., 2017. Mistakes and inconsistencies regarding adsorption of contaminants from aqueous solutions: A critical review. Water Research 120, pp. 88-116.

Trigo, C., Spokas, K.A., Cox, L., Koskinen, W.C., 2014. Influence of Soil Biochar Aging on Sorption of the Herbicides MCPA, Nicosulfuron, Terbuthylazine, Indaziflam, and Fluoroethyldiaminotriazine. Journal of Agricultural and Food Chemistry 62, pp. 10855-10860.

Tsechansky, L., Graber, E.R., 2014. Methodological limitations to determining acidic groups at biochar surfaces via the Boehm titration. Carbon 66, pp. 730-733.

Uchimiya, M., Wartelle, L.H., Klasson, K.T., Fortier, C.A., Lima, I.M., 2011. Influence of Pyrolysis Temperature on Biochar Property and Function as a Heavy Metal Sorbent in Soil. Journal of Agricultural and Food Chemistry 59, pp. 2501-2510.

UN Environment, 2019. Global Environment Outlook – GEO-6: Healthy Planet, Healthy People. U. N. Environment, Nairobi, doi: 10.1017/9781108627146.

University of Idaho, 2021. Reimagining Wastewater, accessed on the 24th of May, 2021, https://www.uidaho.edu/research/news/research-reports/2016/environment/wastewater.

US EPA, 2021. Learn about superfund. United States Environmental Protection Agency, accessed on the 9th of April, 2021, https://www.epa.gov/superfund.

USDA, 2021. Biochar Soil Aging, accessed on the 24th of May, 2021, https://scistarter.org/biochar-soil-aging.

Vijayaraghavan, K., 2021. The importance of mineral ingredients in biochar production, properties and applications. Critical Reviews in Environmental Science and Technology 51, pp. 113-139.

Vithanage, M., Rajapaksha, A.U., Tang, X., Thiele-Bruhn, S., Kim, K.H., Lee, S.-E., Ok, Y.S., 2014. Sorption and transport of sulfamethazine in agricultural soils amended with invasive-plant-derived biochar. Journal of Environmental Management 141, pp. 95-103.

Wan, Q., Yuan, J.-H., Xu, R.-K., Li, X.-H., 2014. Pyrolysis temperature influences ameliorating effects of biochars on acidic soil. Environmental Science and Pollution Research 21, pp. 2486-2495.

Wang, B., Zhang, W., Li, H., Fu, H., Qu, X., Zhu, D., 2017. Micropore clogging by leachable pyrogenic organic carbon: A new perspective on sorption irreversibility and kinetics of hydrophobic organic contaminants to black carbon. Environmental Pollution 220, pp. 1349-1358.

Wang, D., Li, C., Parikh, S.J., Scow, K.M., 2019. Impact of biochar on water retention of two agricultural soils – A multi-scale analysis. Geoderma 340, pp. 185-191.

Wang, J., Xia, K., Waigi, M.G., Gao, Y., Odinga, E.S., Ling, W., Liu, J., 2018. Application of biochar to soils may result in plant contamination and human cancer risk due to exposure of polycyclic aromatic hydrocarbons. Environment International 121, pp. 169-177.

Wang, L., O'Connor, D., Rinklebe, J., Ok, Y.S., Tsang, D.C.W., Shen, Z., Hou, D., 2020. Biochar Aging: Mechanisms, Physicochemical Changes, Assessment, And Implications for Field Applications. Environmental Science & Technology.

Wang, P., Yin, Y., Guo, Y., Wang, C., 2016a. Preponderant adsorption for chlorpyrifos over atrazine by wheat straw-derived biochar: experimental and theoretical studies. RSC Advances 6, pp. 10615-10624.

Wang, S., Guo, X., Wang, K., Luo, Z., 2011. Influence of the interaction of components on the pyrolysis behavior of biomass. Journal of Analytical and Applied Pyrolysis 91, pp. 183-189.

Wang, X., Sato, T., Xing, B., 2006. Competitive Sorption of Pyrene on Wood Chars. Environmental Science & Technology 40, pp. 3267-3272.

Wang, Z., Han, L., Sun, K., Jin, J., Ro, K.S., Libra, J.A., Liu, X., Xing, B., 2016b. Sorption of four hydrophobic organic contaminants by biochars derived from maize straw, wood dust and swine manure at different pyrolytic temperatures. Chemosphere 144, pp. 285-291.

Wang, Z., Liu, G., Zheng, H., Li, F., Ngo, H.H., Guo, W., Liu, C., Chen, L., Xing, B., 2015. Investigating the mechanisms of biochar's removal of lead from solution. Bioresource Technology 177, pp. 308-317.

Weber, K., Quicker, P., 2016. Eigenschaften von Biomassekarbonisaten. in: Weber, K., Quicker, P. (Eds.). Biokohle: Herstellung, Eigenschaften und Verwendung von Biomassekarbonisaten. Springer Vieweg, Wiesbaden, p. 202.

Weber, K., Quicker, P., 2018. Properties of biochar. Fuel 217, pp. 240-261.

Weber, W.J., 1984. Evolution of a Technology. Journal of Environmental Engineering 110, pp. 899-917.

Weber, W.J., Huang, W., Yu, H., 1998. Hysteresis in the sorption and desorption of hydrophobic organic contaminants by soils and sediments: 2. Effects of soil organic matter heterogeneity. Journal of Contaminant Hydrology 31, pp. 149-165.

Woolf, D., Amonette, J.E., Street-Perrott, F.A., Lehmann, J., Joseph, S., 2010. Sustainable biochar to mitigate global climate change. Nature Communications 1, p. 56.

Wu, H., Che, X., Ding, Z., Hu, X., Creamer, A.E., Chen, H., Gao, B., 2016. Release of soluble elements from biochars derived from various biomass feedstocks. Environmental Science and Pollution Research 23, pp. 1905-1915.

Wu, H., Yip, K., Kong, Z., Li, C.-Z., Liu, D., Yu, Y., Gao, X., 2011. Removal and Recycling of Inherent Inorganic Nutrient Species in Mallee Biomass and Derived Biochars by Water Leaching. Industrial & Engineering Chemistry Research 50, pp. 12143-12151.

Wu, L., Li, B., Bi, E., 2017. Effect of molecular dissociation and sorbent carbonization on bisolute sorption of pharmaceuticals by biochars. Water, Air, and Soil Pollution 228, p. 242.

Wu, P., Ata-Ul-Karim, S.T., Singh, B.P., Wang, H., Wu, T., Liu, C., Fang, G., Zhou, D., Wang, Y., Chen, W., 2019. A scientometric review of biochar research in the past 20 years (1998–2018). Biochar 1.

Wu, W., Jiang, W., Zhang, W., Lin, D., Yang, K., 2013. Influence of Functional Groups on Desorption of Organic Compounds from Carbon Nanotubes into Water: Insight into Desorption Hysteresis. Environmental Science & Technology 47, pp. 8373-8382.

Xia, G., Ball, W.P., 1999. Adsorption-Partitioning Uptake of Nine Low-Polarity Organic Chemicals on a Natural Sorbent. Environmental Science & Technology 33, pp. 262-269.

Xiao, F., Pignatello, J.J., 2015. Interactions of triazine herbicides with biochar: Steric and electronic effects. Water Research 80, pp. 179-188.

Xiao, X., Chen, B., Chen, Z., Zhu, L., Schnoor, J.L., 2018. Insight into Multiple and Multilevel Structures of Biochars and Their Potential Environmental Applications: A Critical Review. Environmental Science & Technology 52, pp. 5027-5047.

Xiao, X., Chen, Z., Chen, B., 2016. H/C atomic ratio as a smart linkage between pyrolytic temperatures, aromatic clusters and sorption properties of biochars derived from diverse precursory materials. Scientific Reports 6, p. 22644.

Xiao, X., Ulrich, B.A., Chen, B., Higgins, C.P., 2017. Sorption of Poly- and Perfluoroalkyl Substances (PFASs) Relevant to Aqueous Film-Forming Foam (AFFF)-Impacted Groundwater by Biochars and Activated Carbon. Environmental Science & Technology 51, pp. 6342-6351.

Xie, T., Reddy, K.R., Wang, C., Yargicoglu, E., Spokas, K., 2015. Characteristics and Applications of Biochar for Environmental Remediation: A Review. Critical Reviews in Environmental Science and Technology 45, pp. 939-969.

Xie, T., Sadasivam, B.Y., Reddy, K.R., Wang, C., Spokas, K., 2016. Review of the Effects of Biochar Amendment on Soil Properties and Carbon Sequestration. Journal of Hazardous, Toxic, and Radioactive Waste 20, p. 04015013.

Xu, R.-k., Xiao, S.-c., Yuan, J.-h., Zhao, A.-z., 2011. Adsorption of methyl violet from aqueous solutions by the biochars derived from crop residues. Bioresource Technology 102, pp. 10293-10298.

Xu, T., Lou, L., Luo, L., Cao, R., Duan, D., Chen, Y., 2012. Effect of bamboo biochar on pentachlorophenol leachability and bioavailability in agricultural soil. Science of the Total Environment 414, pp. 727-731.

Xu, X., Zhao, Y., Sima, J., Zhao, L., Mašek, O., Cao, X., 2017. Indispensable role of biochar-inherent mineral constituents in its environmental applications: A review. Bioresource Technology 241, pp. 887-899.

Xu, Y., Chen, B., 2013. Investigation of thermodynamic parameters in the pyrolysis conversion of biomass and manure to biochars using thermogravimetric analysis. Bioresource Technology 146, pp. 485-493.

Yadav, K., Tyagi, M., Kumari, S., Jagadevan, S., 2019. Influence of Process Parameters on Optimization of Biochar Fuel Characteristics Derived from Rice Husk: a Promising Alternative Solid Fuel. BioEnergy Research 12, pp. 1052-1065.

Yang, H., Yan, R., Chen, H., Lee, D.H., Zheng, C., 2007. Characteristics of hemicellulose, cellulose and lignin pyrolysis. Fuel 86, pp. 1781-1788.

Yang, H., Yan, R., Chen, H., Zheng, C., Lee, D.H., Liang, D.T., 2006a. In-Depth Investigation of Biomass Pyrolysis Based on Three Major Components: Hemicellulose, Cellulose and Lignin. Energy & Fuels 20, pp. 388-393.

Yang, Y., Sheng, G., Huang, M., 2006b. Bioavailability of diuron in soil containing wheat-straw-derived char. Science of the Total Environment 354, pp. 170-178.

Yang, Y., Sun, K., Han, L., Jin, J., Sun, H., Yang, Y., Xing, B., 2018. Effect of minerals on the stability of biochar. Chemosphere 204, pp. 310-317.

Yao, F.X., Arbestain, M.C., Virgel, S., Blanco, F., Arostegui, J., Maciá-Agulló, J.A., Macías, F., 2010. Simulated geochemical weathering of a mineral ash-rich biochar in a modified Soxhlet reactor. Chemosphere 80, pp. 724-732.

Yu, X., Pan, L., Ying, G., Kookana, R.S., 2010. Enhanced and irreversible sorption of pesticide pyrimethanil by soil amended with biochars. Journal of Environmental Sciences 22, pp. 615-620.

Yuan, J.-H., Xu, R.-K., Zhang, H., 2011. The forms of alkalis in the biochar produced from crop residues at different temperatures. Bioresource Technology 102, pp. 3488-3497.

Yuan, Y., Li, J., Dai, H., 2021. Microcystin-LR sorption and desorption by diverse biochars: Capabilities, and elucidating mechanisms from novel insights of sorption domains and site energy distribution. Science of the Total Environment 754, p. 141921.

Zhang, D., Pan, B., Wu, M., Zhang, H., Peng, H., Ning, P., Xing, B., 2012. Cosorption of organic chemicals with different properties: Their shared and different sorption sites. Environmental Pollution 160, pp. 178-184.

Zhang, P., Sheng, G., Wolf, D.C., Feng, Y., 2004. Reduced Biodegradation of Benzonitrile in Soil Containing Wheat-Residue-Derived Ash. Journal of Environmental Quality 33, pp. 868-872.

Zhang, S., Mao, G., Crittenden, J., Liu, X., Du, H., 2017. Groundwater remediation from the past to the future: A bibliometric analysis. Water Research 119, pp. 114-125.

Zhang, Z., Zhu, Z., Shen, B., Liu, L., 2019. Insights into biochar and hydrochar production and applications: A review. Energy 171, pp. 581-598.

Zhao, L., Cao, X., Mašek, O., Zimmerman, A., 2013a. Heterogeneity of biochar properties as a function of feedstock sources and production temperatures. Journal of Hazardous materials 256–257, pp. 1-9.

Zhao, L., Cao, X., Wang, Q., Yang, F., Xu, S., 2013b. Mineral Constituents Profile of Biochar Derived from Diversified Waste Biomasses: Implications for Agricultural Applications. Journal of Environmental Quality 42, pp. 545-552.

Zheng, H., Wang, Z., Zhao, J., Herbert, S., Xing, B., 2013. Sorption of antibiotic sulfamethoxazole varies with biochars produced at different temperatures. Environmental Pollution 181, pp. 60-67.

Zheng, W., Guo, M., Chow, T., Bennett, D.N., Rajagopalan, N., 2010. Sorption properties of greenwaste biochar for two triazine pesticides. Journal of Hazardous materials 181, pp. 121-126.

Zhu, D., Pignatello, J.J., 2005. Characterization of Aromatic Compound Sorptive Interactions with Black Carbon (Charcoal) Assisted by Graphite as a Model. Environmental Science & Technology 39, pp. 2033-2041.

Zhu, X., Chen, B., Zhu, L., Xing, B., 2017. Effects and mechanisms of biochar-microbe interactions in soil improvement and pollution remediation: A review. Environmental Pollution 227, pp. 98-115.

Zielińska, A., Oleszczuk, P., Charmas, B., Skubiszewska-Zięba, J., Pasieczna-Patkowska, S., 2015. Effect of sewage sludge properties on the biochar characteristic. Journal of Analytical and Applied Pyrolysis 112, pp. 201-213.

Appendix

Appendix A1: Details on the Web of Science bibliographic search

The bibliographic search was conducted in the "Web of Science Core Collection" using the advanced search mode. For the document type, the option "all document types" was selected. Results were restricted to items published in English language only. The search was limited to research items published starting from the year 1995 until 2020 ("PY = 1995-2020"). In combination with the publishing year, the database was screened for selected topics using different search terms using the "*Topic"* field ("TS = Topic"; comprising title, abstract, keywords, keywords plus). The following five search queries were used:

1, PY=1995-2020

2, PY=1995-2020 AND TS=biochar

3, PY=1995-2020 AND TS=(biochar AND soil)

4, PY=1995-2020 AND TS=(biochar AND remediation)

5, PY=1995-2020 AND TS=(biochar AND *sorption)

The results obtained from search query 1, ("PY=1995-2020") were used for normalization, resulting in the fraction of items listed in the "Web of Science Core Collection".

Appendix A2: Additional figures

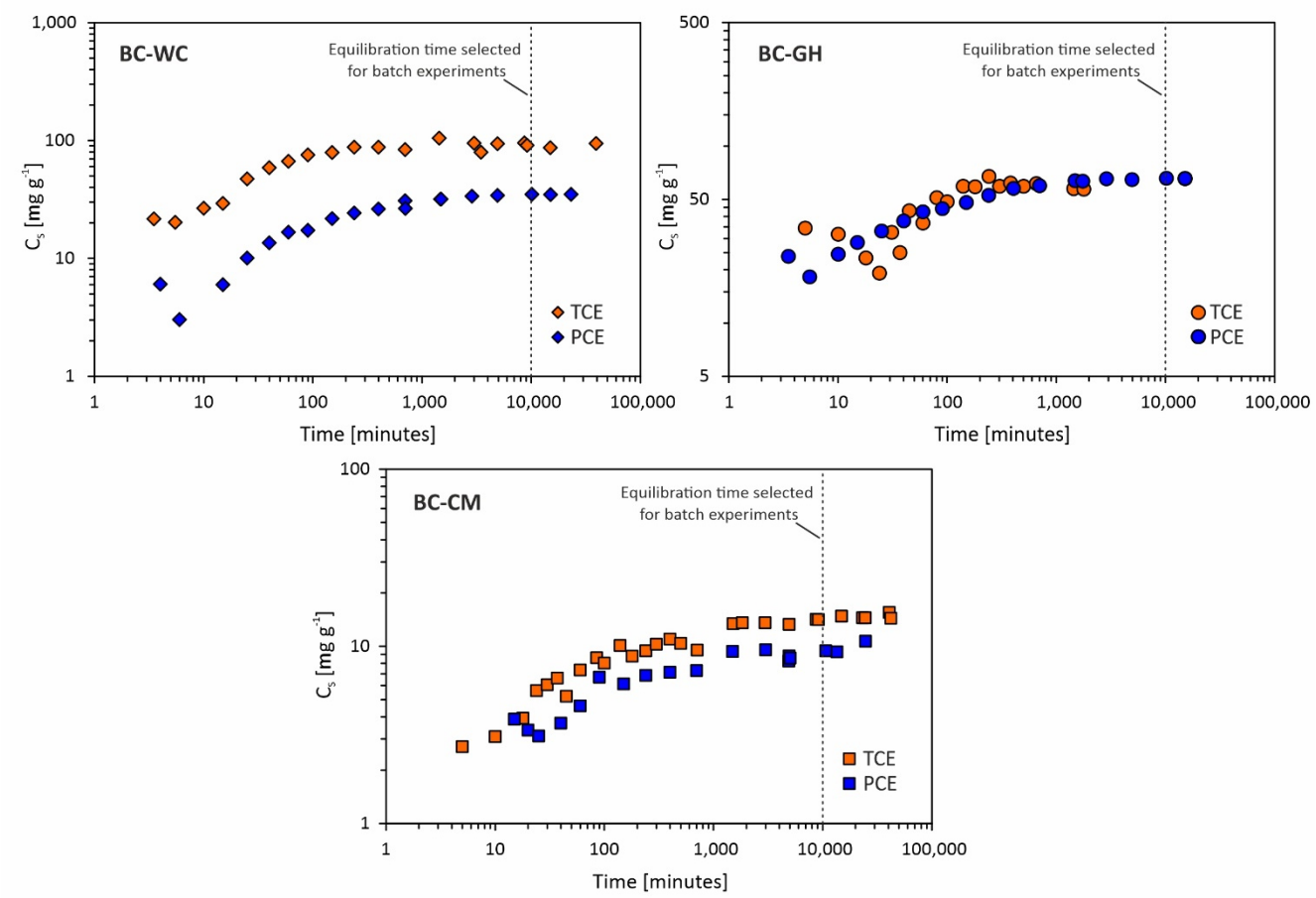

Figure A 1: Plot of C_S [mg g^{-1}] versus time [minutes] showing exemplary data of preliminary experiments performed to select a suitable equilibration time for the batch experiments.

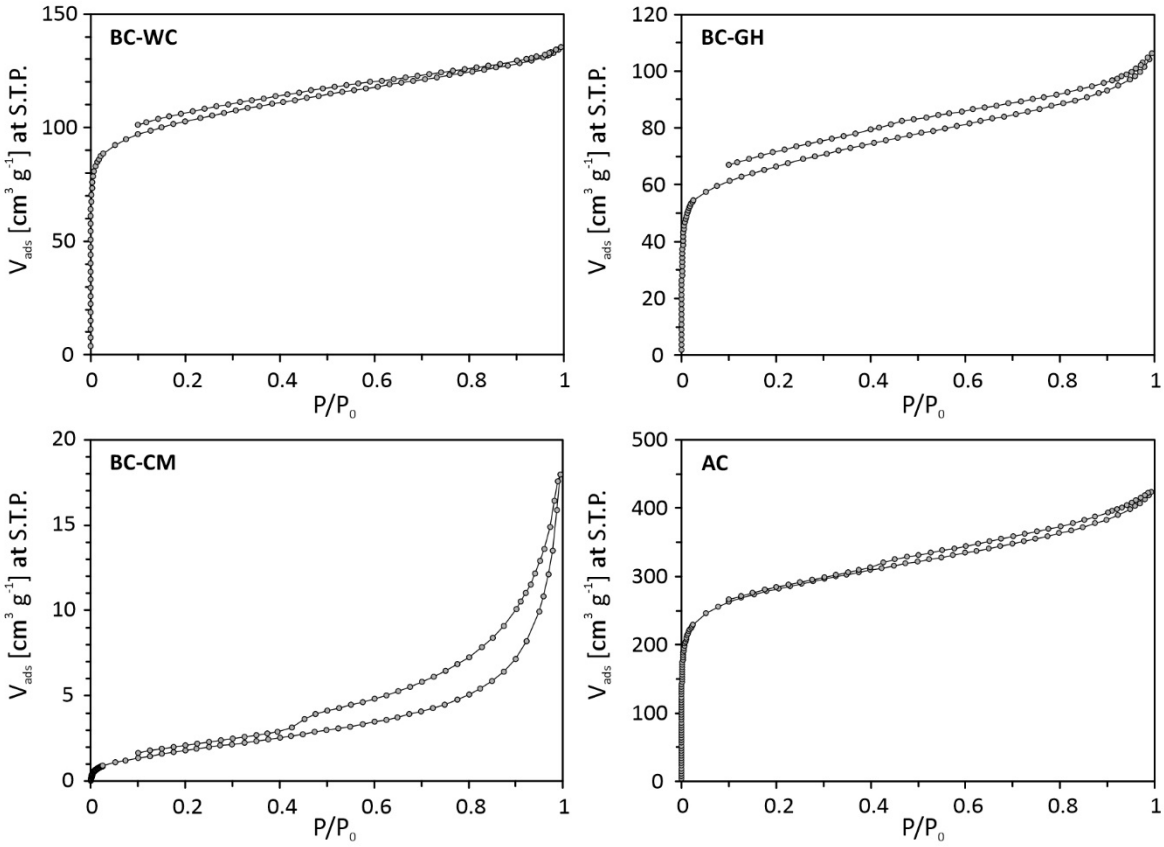

Figure A 2: Plot of the argon adsorption BET-isotherms for the determination of the specific surface area of the original sorbents (BC-WC, BC-GH, BC-CM, and AC).

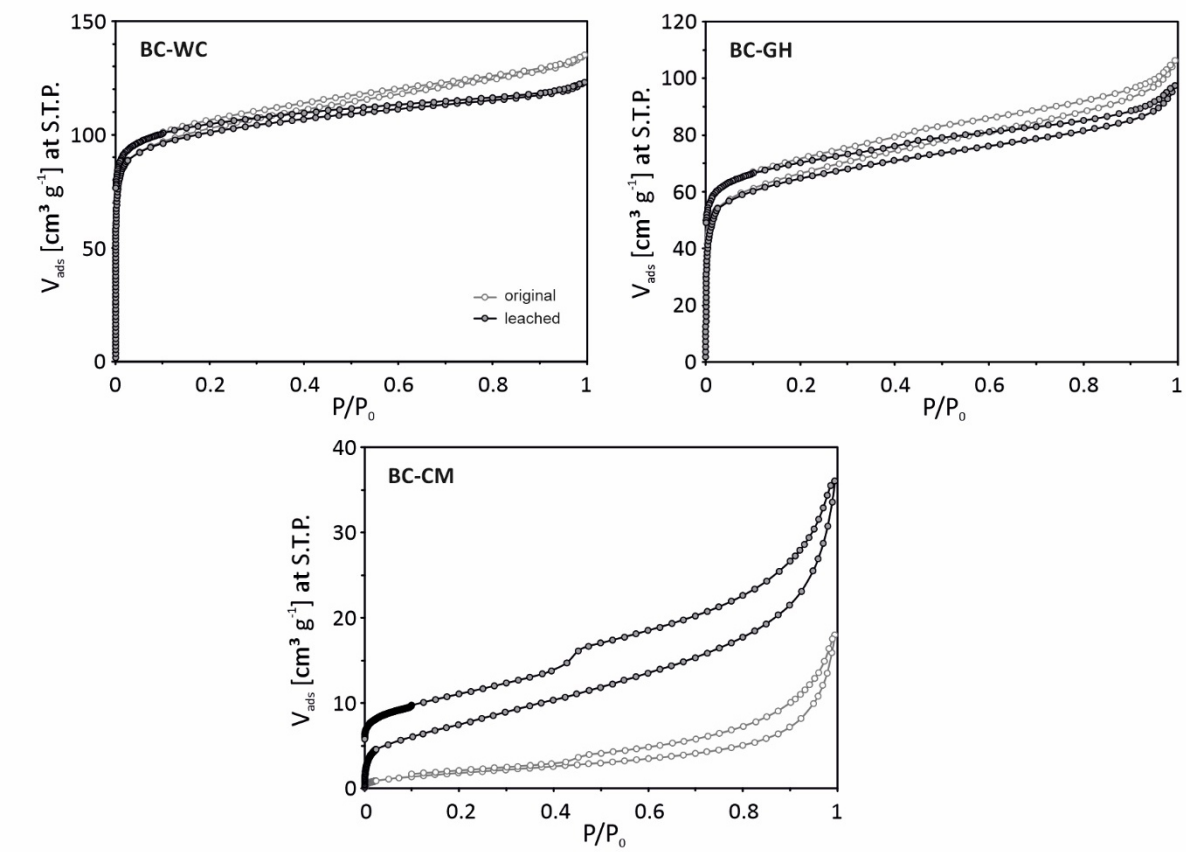

Figure A 3: Plot of the argon adsorption BET-isotherms for the determination of the specific surface area of the leached biochars (BC-WC, BC-GH, and BC-CM).

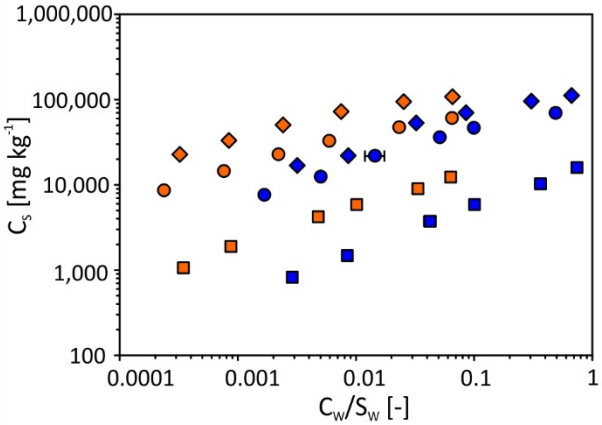

Figure A 4: Sorption isotherms of TCE (orange) and PCE (blue) on the three leached biochars normalized to the water solubility (S_W) plotted on a log-log scale. Different symbols refer to sorbents as follows: ♦ BC-WC, ● BC-GH, and ■ BC-CM. Data points represent the mean of triplicate samples. All error bars are within symbol size.

Appendix A3: Additional raw data

Table A 1: Raw data for the single compound sorption isotherm of TCE on BC-CM.

Initial concentration C_0 [mg L^{-1}] and sorbent mass used [g]	Replicate	C_W [mg L^{-1}]	C_S [mg kg^{-1}]
1.7 mg L^{-1}, 0.07 g	1	1.18	1,175
	2	1.16	1,163
	3	1.17	1,169
1.7 mg L^{-1}, 0.026 g	1	2.03	2,025
	2	2.05	2,052
	3	2.05	2,049
22 mg L^{-1}, 0.27 g	1	3.24	3,237
	2	3.25	3,249
	3	3.25	3,248
22 mg L^{-1}, 0.12 g	1	4.73	4,732
	2	4.81	4,810
	3	4.79	4,789
110 mg L^{-1}, 0.5 g	1	7.54	7,538
	2	7.77	7,770
	3	7.87	7,870
110 mg L^{-1}, 0.15 g	1	11.2	11,212
	2	10.9	10,880
	3	10.7	10,654

Table A 2: Raw data for the single compound sorption isotherm of TCE on BC-GH.

Initial concentration C_0 [mg L^{-1}] and sorbent mass used [g]	Replicate	C_W [mg L^{-1}]	C_S [mg kg^{-1}]
1.7 mg L^{-1}, 9.3 mg	1	0.331	8,322
	2	0.342	8,270
	3	0.336	8,298
1.7 mg L^{-1}, 3.7 mg	1	0.912	13,214
	2	0.951	12,675
	3	0.947	12,699
22 mg L^{-1}, 0.041 g	1	3.29	22,501
	2	3.33	22,556
	3	3.29	22,448
22 mg L^{-1}, 0.019 g	1	9.16	33,816
	2	9.77	32,571
	3	9.42	32,633
110 mg L^{-1}, 0.088 g	1	30.5	45,077
	2	30.9	44,904
	3	30.5	44,899
110 mg L^{-1}, 0.028 g	1	77.5	57,323
	2	75.0	62,414
	3	77.7	56,611

Table A 3: Raw data for the single compound sorption isotherm of TCE on BC-WC.

Initial concentration C_0 [mg L^{-1}] and sorbent mass used [g]	Replicate	C_W [mg L^{-1}]	C_S [mg kg^{-1}]
1.7 mg L^{-1}, 3.5 mg	1	0.434	20,485
	2	0.431	20,638
	3	0.428	20,956
1.7 mg L^{-1}, 1.5 mg	1	0.988	29,690
	2	0.992	29,742
	3	0.970	30,348
22 mg L^{-1}, 0.019 g	1	3.94	48,016
	2	3.46	49,808
	3	3.55	49,575
22 mg L^{-1}, 9.8 mg	1	9.07	66,866
	2	9.20	66,075
	3	9.46	64,890
110 mg L^{-1}, 0.047 g	1	29.6	88,955
	2	29.9	89,200
	3	31.2	87,592
110 mg L^{-1}, 0.016 g	1	79.0	105,984
	2	82.4	97,927
	3	82.1	97,514

Table A 4: Raw data for the single compound sorption isotherm of TCE on AC.

Initial concentration C_0 [mg L^{-1}] and sorbent mass used [g]	Replicate	C_W [mg L^{-1}]	C_S [mg kg^{-1}]
1.7 mg L^{-1}, 1.1 mg	1	0.396	69,619
	2	0.380	71,312
	3	0.405	70,548
1.7 mg L^{-1}, 0.5 mg	1	1.03	93,078
	2	1.00	92,731
	3	1.02	93,329
22 mg L^{-1}, 5.5 mg	1	3.00	164,180
	2	2.96	165,079
	3	2.91	165,477
22 mg L^{-1}, 2.7 mg	1	8.74	231,014
	2	8.74	229,327
	3	8.96	225,050
110 mg L^{-1}, 12.5 mg	1	30.2	339,616
	2	29.4	343,657
	3	30.0	341,024
110 mg L^{-1}, 4 mg	1	82.3	418,938
	2	81.3	427,655
	3	80.4	440,794

Table A 5: Raw data for the single compound sorption isotherm of PCE on BC-CM.

Initial concentration C_0 [mg L^{-1}] and sorbent mass used [g]	Replicate	C_W [mg L^{-1}]	C_S [mg kg^{-1}]
1.7 mg L^{-1}, 0.111 g	1	0.364	761
	2	0.463	715
	3	0.364	760
1.7 mg L^{-1}, 0.036 g	1	1.02	1,434
	2	1.00	1,476
	3	1.04	1,416
22 mg L^{-1}, 0.312 g	1	4.82	3,178
	2	4.41	3,245
	3	4.82	3,177
22 mg L^{-1}, 0.126 g	1	11.5	5,209
	2	11.1	5,363
	3	11.6	5,177
110 mg L^{-1}, 0.48 g	1	45.2	7,731
	2	41.8	8,094
	3	42.2	8,040
110 mg L^{-1}, 0.129 g	1	87.2	12,416
	2	87.8	12,210
	3	88.6	11,933

Table A 6: Raw data for the single compound sorption isotherm of PCE on BC-GH.

Initial concentration C_0 [mg L^{-1}] and sorbent mass used [g]	Replicate	C_W [mg L^{-1}]	C_S [mg kg^{-1}]
1.7 mg L^{-1}, 11 mg	1	0.359	6,986
	2	0.374	6,917
	3	0.381	6,874
1.7 mg L^{-1}, 4.5 mg	1	0.903	10,705
	2	1.01	9,517
	3	0.971	9,950
22 mg L^{-1}, 0.052 g	1	1.92	20,126
	2	2.18	19,886
	3	1.92	20,050
22 mg L^{-1}, 0.026 g	1	7.44	30,178
	2	7.22	30,139
	3	7.10	30,610
110 mg L^{-1}, 0.119 g	1	20.4	39,607
	2	16.3	41,373
	3	17.1	40,904
110 mg L^{-1}, 0.039 g	1	68.1	58,764
	2	69.6	56,670
	3	70.8	55,022

Table A 7: Raw data for the single compound sorption isotherm of PCE on BC-WC.

Initial concentration C_0 [mg L^{-1}] and sorbent mass used [g]	Replicate	C_W [mg L^{-1}]	C_S [mg kg^{-1}]
1.7 mg L^{-1}, 4.3 mg	1	0.641	14,489
	2	0.591	15,052
	3	0.715	13,617
1.7 mg L^{-1}, 1.8 mg	1	1.34	15,581
	2	1.36	14,895
	3	1.30	16,537
22 mg L^{-1}, 0.021 g	1	1.22	18,909
	2	1.30	16,503
	3	1.30	16,621
22 mg L^{-1}, 10.1 mg	1	4.42	41,400
	2	4.83	40,839
	3	6.02	38,266
110 mg L^{-1}, 0.046 g	1	11.8	53,493
	2	11.6	54,124
	3	12.6	49,407
110 mg L^{-1}, 0.016 g	1	43.8	74,601
	2	43.6	75,146
	3	43.4	75,096

Table A 8: Raw data for the single compound sorption isotherm of PCE on AC.

Initial concentration C_0 [mg L^{-1}] and sorbent mass used [g]	Replicate	C_W [mg L^{-1}]	C_S [mg kg^{-1}]
1.7 mg L^{-1}, 0.67 mg	1	0.204	131,237
	2	0.215	129,104
	3	0.193	131,657
1.7 mg L^{-1}, 0.25 mg	1	0.519	184,953
	2	0.574	186,042
	3	0.538	187,369
22 mg L^{-1}, 3.2 mg	1	1.93	340,345
	2	1.82	340,987
	3	1.76	342,670
22 mg L^{-1}, 1.7 mg	1	9.50	430,635
	2	9.23	437,976
	3	9.30	433,655
110 mg L^{-1}, 8.1 mg	1	36.8	526,299
	2	36.4	528,654
	3	37.2	523,610
110 mg L^{-1}, 2.8 mg	1	85.5	640,974
	2	89.2	574,042
	3	85.5	640,904

Table A 9: Raw data for the bi-solute sorption isotherm of TCE and PCE on BC-CM.

Initial concentration C_0 [mg L^{-1}] and sorbent mass used [g]	Replicate	TCE		PCE	
		C_W [mg L^{-1}]	C_S [mg kg^{-1}]	C_W [mg L^{-1}]	C_S [mg kg^{-1}]
1.7 mg L^{-1}, 0.077 g	1	0.347	854	0.420	845
	2	0.349	852	0.421	844
	3	0.392	826	0.466	816
1.7 mg L^{-1}, 0.031 g	1	0.885	1,256	0.953	1,241
	2	0.904	1,241	0.990	1,197
	3	0.910	1,239	0.993	1,200
22 mg L^{-1}, 0.323 g	1	5.00	3,055	5.01	3,276
	2	6.04	2,897	6.17	3,098
	3	6.74	2,782	6.72	3,009
22 mg L^{-1}, 0.155 g	1	11.4	4,363	10.9	4,981
	2	12.5	3,970	12.2	4,536
	3	11.8	4,194	11.6	4,731
110 mg L^{-1}, 0.705 g	1	35.9	6,021	30.9	6,760
	2	44.9	5,359	39.5	6,124
	3	38.5	5,832	32.5	6,641
110 mg L^{-1}, 0.227 g	1	84.1	8,000	75.7	11,039
	2	83.5	8,139	74.8	11,232
	3	84.9	7,831	76.0	10,957

Table A 10: Raw data for the bi-solute sorption isotherm of TCE and PCE on BC-GH.

Initial concentration C_0 [mg L^{-1}] and sorbent mass used [g]	Replicate	TCE		PCE	
		C_W [mg L^{-1}]	C_S [mg kg^{-1}]	C_W [mg L^{-1}]	C_S [mg kg^{-1}]
1.7 mg L^{-1}, 7.5 mg	1	0.559	9,124	0.491	10,013
	2	0.526	9,290	0.450	10,229
	3	0.529	9,256	0.448	10,225
1.7 mg L^{-1}, 3.7 mg	1	1.04	12,015	0.990	13,593
	2	1.03	11,990	0.961	13,828
	3	1.11	11,110	1.02	13,138
22 mg L^{-1}, 0.045 g	1	5.80	20,427	4.04	24,001
	2	5.75	20,616	4.08	24,118
	3	5.80	20,564	3.96	24,248
22 mg L^{-1}, 0.025 g	1	11.9	24,656	9.95	31,549
	2	12.1	23,994	10.1	30,870
	3	12.5	23,435	10.3	30,852
110 mg L^{-1}, 0.129 g	1	36.5	32,337	26.2	38,399
	2	35.9	32,777	26.9	38,366
	3	37.3	32,220	27.6	38,079
110 mg L^{-1}, 0.046 g	1	85.8	36,778	77.1	51,848
	2	83.9	39,081	75.9	53,513
	3	81.2	41,713	71.9	57,464

Table A 11: Raw data for the bi-solute sorption isotherm of TCE and PCE on BC-WC.

Initial concentration C_0 [mg L^{-1}] and sorbent mass used [g]	Replicate	TCE		PCE	
		C_W [mg L^{-1}]	C_S [mg kg^{-1}]	C_W [mg L^{-1}]	C_S [mg kg^{-1}]
1.7 mg L^{-1}, 3.2 mg	1	0.462	20,783	0.465	21,374
	2	0.491	20,600	0.493	21,209
	3	0.473	20,569	0.481	21,075
1.7 mg L^{-1}, 1.6 mg	1	0.952	27,133	1.00	26,876
	2	0.943	27,428	0.992	27,156
	3	0.963	26,214	1.06	24,399
22 mg L^{-1}, 0.023 g	1	4.77	40,631	4.31	43,553
	2	5.01	40,249	4.64	42,973
	3	5.01	40,189	5.61	40,800
22 mg L^{-1}, 0.0135 g	1	10.6	46,455	9.66	53,038
	2	10.3	47,250	9.36	53,838
	3	10.5	47,100	9.55	53,586
110 mg L^{-1}, 0.073 g	1	29.3	56,040	26.2	60,302
	2	29.2	56,369	23.0	62,722
	3	29.2	56,369	25.1	61,317
110 mg L^{-1}, 0.028 g	1	79.6	56,546	73.8	72,383
	2	75.5	62,558	70.9	76,007
	3	75.6	62,831	70.5	77,200

Table A 12: Raw data for the bi-solute sorption isotherm of TCE and PCE on AC.

Initial concentration C_0 [mg L^{-1}] and sorbent mass used [g]	Replicate	TCE		PCE	
		C_W [mg L^{-1}]	C_S [mg kg^{-1}]	C_W [mg L^{-1}]	C_S [mg kg^{-1}]
2.2 mg L^{-1}, 1.25 mg	1	0.765	56,589	0.114	83,469
	2	0.782	56,623	0.114	84,488
	3	0.832	54,451	0.162	82,323
2.2 mg L^{-1}, 0.52 mg	1	1.62	53,360	0.592	152,437
	2	1.64	51,672	0.546	158,962
	3	1.65	51,446	0.527	160,751
22 mg L^{-1}, 3.5 mg	1	14.0	126,968	3.41	276,912
	2	13.5	133,368	3.14	279,111
	3	14.0	127,169	3.24	278,406
22 mg L^{-1}, 2.0 mg	1	19.1	97,745	8.93	351,005
	2	19.3	92,860	8.93	352,408
	3	19.3	93,541	8.96	350,173
110 mg L^{-1}, 12 g	1	75.8	141,497	24.1	358,723
	2	73.4	150,296	23.3	359,184
	3	75.5	141,973	24.3	355,840
110 mg L^{-1}, 4.1 g	1	102.5	89,077	71.7	476,360
	2	100.6	111,817	71.0	479,494
	3	96.3	166,020	67.8	523,882

Table A 13: Raw data for the single sorption isotherm of TCE on leached BC-CM.

Initial concentration C_0 [mg L^{-1}] and sorbent mass used [g]	Replicate	C_W [mg L^{-1}]	C_S [mg kg^{-1}]
1.7 mg L^{-1}, 0.071 g	1	0.387	1,018
	2	0.403	1,069
	3	0.344	1,104
1.7 mg L^{-1}, 0.026 g	1	0.929	1,937
	2	0.940	1,916
	3	0.994	1,826
22 mg L^{-1}, 0.21 g	1	4.96	4,277
	2	5.22	4,216
	3	5.49	4,149
22 mg L^{-1}, 0.11 g	1	11.3	5,723
	2	10.9	5,924
	3	10.9	5,969
110 mg L^{-1}, 0.45 g	1	35.7	9,147
	2	38.5	8,818
	3	35.5	9,154
110 mg L^{-1}, 0.20 g	1	68.3	12,653
	2	69.7	12,173
	3	69.4	12,293

Table A 14: Raw data for the single compound sorption isotherm of TCE on leached BC-GH.

Initial concentration C_0 [mg L^{-1}] and sorbent mass used [g]	Replicate	C_W [mg L^{-1}]	C_S [mg kg^{-1}]
1.7 mg L^{-1}, 9.5 mg	1	0.263	8,567
	2	0.257	8,585
	3	0.262	8,540
1.7 mg L^{-1}, 3.6 mg	1	0.797	14,942
	2	0.862	14,125
	3	0.857	14,098
22 mg L^{-1}, 0.045 g	1	2.54	22,522
	2	2.41	22,715
	3	2.33	22,862
22 mg L^{-1}, 0.025 g	1	6.33	32,784
	2	6.68	32,357
	3	6.59	32,399
110 mg L^{-1}, 0.09 g	1	24.9	47,346
	2	24.9	47,451
	3	26.9	46,302
110 mg L^{-1}, 0.032 g	1	69.6	63,298
	2	72.2	59,059
	3	72.9	58,606

Table A 15: Raw data for the single compound sorption isotherm of TCE on leached BC-WC.

Initial concentration C_0 [mg L^{-1}] and sorbent mass used [g]	Replicate	C_W [mg L^{-1}]	C_S [mg kg^{-1}]
1.7 mg L^{-1}, 3.5 mg	1	0.371	22,592
	2	0.318	23,261
	3	0.368	22,460
1.7 mg L^{-1}, 1.5 mg	1	0.894	34,128
	2	0.908	33,314
	3	0.947	32,206
22 mg L^{-1}, 0.02 g	1	2.65	50,620
	2	2.78	50,306
	3	2.48	50,786
22 mg L^{-1}, 0.01 g	1	8.08	72,427
	2	8.25	71,610
	3	8.21	73,236
110 mg L^{-1}, 0.046 g	1	27.9	94,221
	2	27.3	95,106
	3	27.8	94,606
110 mg L^{-1}, 0.02 g	1	71.2	109,334
	2	72.9	105,690
	3	71.0	109,417

Table A 16: Raw data for the single compound sorption isotherm of PCE on leached BC-CM.

Initial concentration C_0 [mg L^{-1}] and sorbent mass used [g]	Replicate	C_W [mg L^{-1}]	C_S [mg kg^{-1}]
1.9 mg L^{-1}, 0.125 g	1	0.413	824
	2	0.404	827
	3	0.405	824
1.9 mg L^{-1}, 0.043 g	1	1.18	1,501
	2	1.18	1,499
	3	1.21	1,443
19.8 mg L^{-1}, 0.279 g	1	5.55	3,822
	2	5.47	3,819
	3	6.94	3,562
19.8 mg L^{-1}, 0107 g	1	14.2	5,880
	2	14.0	5,964
	3	14.4	5,754
108 mg L^{-1}, 0.45 g	1	53.5	10,077
	2	51.3	10,326
	3	49.5	10,530
108 mg L^{-1}, 0.125 g	1	106.6	15,240
	2	105.8	15,571
	3	101.6	17,273

Table A 17: Raw data for the single compound sorption isotherm of PCE on leached BC-GH.

Initial concentration C_0 [mg L^{-1}] and sorbent mass used [g]	Replicate	C_W [mg L^{-1}]	C_S [mg kg^{-1}]
1.9 mg L^{-1}, 12.9 mg	1	0.212	7,682
	2	0.261	7,497
	3	0.241	7,563
1.9 mg L^{-1}, 5.7 mg	1	0.691	12,573
	2	0.717	12,351
	3	0.733	12,214
19.8 mg L^{-1}, 0.047 g	1	2.36	21,412
	2	1.49	22,387
	3	2.32	21,454
19.8 mg L^{-1}, 0.021 g	1	6.95	36,571
	2	6.91	36,665
	3	8.01	34,209
108 mg L^{-1}, 0.115 g	1	13.4	46,679
	2	14.2	46,194
	3	14.8	45,939
108 mg L^{-1}, 0.037 g	1	69.1	69,246
	2	68.8	70,043
	3	70.4	68,056

Table A 18: Raw data for the single compound sorption isotherm of PCE on leached BC-WC.

Initial concentration C_0 [mg L^{-1}] and sorbent mass used [g]	Replicate	C_W [mg L^{-1}]	C_S [mg kg^{-1}]
1.9 mg L^{-1}, 5.0 mg	1	0.476	16,624
	2	0.371	17,727
	3	0.500	16,376
1.9 mg L^{-1}, 2.1 mg	1	1.33	18,980
	2	1.16	23,365
	3	1.14	23,795
19.8 mg L^{-1}, 0.018 g	1	4.83	52,922
	2	4.47	53,328
	3	4.39	53,843
19.8 mg L^{-1}, 8.35 mg	1	12.1	70,537
	2	12.0	69,751
	3	12.1	70,658
108 mg L^{-1}, 0.044 g	1	42.9	95,967
	2	44.0	95,223
	3	42.2	97,045
108 mg L^{-1}, 0.015 g	1	94.5	111,513
	2	94.7	109,639
	3	93.7	114,461

Table A 19: Summarized raw data of the leachate analysis of the three biochars analyzed with ion chromatography.

Sorbent	BC-CM			BC-GH			BC-WC		
Replicate	1	2	3	1	2	3	1	2	3
Biochar mass [g]	1.49	1.51	1.50	1.49	1.48	1.48	1.48	1.49	1.49
Leachate Vol. [mL]	65.22	65.36	64.40	62.47	62.12	64.78	61.35	62.76	62.96
pH [-]	10.2	10.1	10.2	8.3	8.3	8.3	8.8	8.8	8.9
EC [µS cm^{-1}]	3,670	3,740	3,860	592	609	596	153	145	143
DOC [mg L^{-1}]	618.97	647.23	632.21	59.61	56.01	57.29	33.04	40.09	36.53
K^+ [mg L^{-1}]	717.10	729.57	758.66	176.35	179.12	173.21	14.49	13.89	13.27
Na^+ [mg L^{-1}]	228.17	230.27	236.48	8.89	7.56	7.37	3.91	3.64	3.55
Ca^{2+} [mg L^{-1}]	12.63	9.96	7.49	2.04	2.15	2.28	1.64	1.81	1.78
Mg^{2+} [mg L^{-1}]	1.04	1.91	1.65	1.23	1.35	1.41	0.70	0.67	0.61
NH_4^+ [mg L^{-1}]	0.84	1.04	0.92	0.13	0.15	0.19	0.03	0.01	<dl
PO_4^{3-} [mg L^{-1}]	36.17	33.10	37.04	124.99	125.22	123.23	1.55	1.52	1.47
SO_4^{2-} [mg L^{-1}]	100.96	105.74	105.99	26.76	27.60	26.51	4.62	4.69	4.47
NO_3^- [mg L^{-1}]	<dl	1.29	0.67	0.64	0.59	0.57	0.26	0.46	0.22
NO_2^- [mg L^{-1}]	0.21	0.50	0.24	0.02	0.02	0.02	0.01	0.01	0.01
Cl^- [mg L^{-1}]	539.69	565.04	573.57	26.49	23.94	23.18	2.64	1.89	1.96
Br^- [mg L^{-1}]	1.97	2.05	2.13	0.84	0.76	0.72	0.18	0.18	0.17
F^- [mg L^{-1}]	4.74	5.53	4.92	0.21	0.19	0.17	0.08	0.08	0.08

<dl: below limit of detection

Table A 20: Selected data for biochar leaching from the literature. All ions are given in mg g^{-1} (partly recalculated from original data).

Reference	Feedstock	Pyrolysis temp. [°C]	Leaching method	K^+	Na^+	Ca^{2+}	Mg^{2+}	Cl^-	P	PO_4^{3-}	S	SO_4^{2-}	N	NH_4^+-N	NO_3^--N
Yao et al., 2010	Sewage sludge	550	Soxhlet extractor at 30°C for 300 hours; flowrate: 30 mL every 6 min.	0.95		6.9	0.54		4						
	Poultry matter	250		0.08		8.28	0.38		0.17						
		300		0.01		8.96	0.46		0.10						
		350		0.00		8.57	0.21		0.03						
		400		0.01		8.01	0.26		0.02						
Kloss et al., 2012	Straw	400	Leaching of 2 g biochar with 40 mL of water; mixture was allowed to stand overnight, than shaken for 1 hour, and centrifuged.	10.20	0.02	0.24	0.09	6.30		0.45		1.30			
		460		13.50	0.01	0.71	0.21	4.70		0.68		1.42			
		525		18.20	0.02	0.19	0.04	5.60		0.66		1.38			
	Spruce	400		1.20	0.02	0.46	0.11	0.08		0.44		0.06			
		460		1.30	0.01	0.36	0.03	0.06		0.10		0.04			
		525		1.60	0.01	0.18	0.03	0.17		0.20		0.04			
	Poplar	400		2.50	0.01	1.10	0.25	0.01		0.04		0.10			
		460		2.50	0.01	0.44	0.10	0.02		0.02		0.08			
		525		1.70	0.01	0.23	0.04	0.01		0.06		0.04			
Wu et al., 2016	Peanut Hull	600	Leaching of 0.5 g biochar with 25 mL of deionized water in 50 mL centrifuge tubes at room temperature; samples shaken on an orbital shaker for 24 hours and then centrifuged.	3.50	0.03	0.52	0.14		0.17						
	Hickory wood chips	600		1.17	0.03	0.20	0.07		0.01						
	Spanish moss	600		4.59	1.79	0.36	0.10		0.03						
	Pine needle	600		0.34	0.08	0.54	0.09		0.09						
	Bagasse	600		1.97	0.05	0.43	0.13		0.04						
	Sugar beet tailings	600		7.17	1.19	0.58	0.51		0.11						
	Mixed animal waste	600		7.10	1.30	0.49	0.05		0.90						
	Biosolid	600		0.20	0.09	2.21	0.31		0.80						

Reference	Feedstock	Pyrolysis temp. [°C]	Leaching method	K^+	Na^+	Ca^{2+}	Mg^{2+}	Cl^-	P	PO_4^{3-}	S	SO_4^{2-}	N	NH_4^+-N	NO_3^--N
Graber et al., 2010	Citrus wood		Leaching of biochars with double distilled water (1:10 w/w) by stirring at 25°C for 30 min.	2.74	2.34	0.08	0.03	3.24	0.01		0.61			0.0006	0.0002
Spokas at al., 2014	Switchgrass	500	Leaching of 5 g oven-dried biochar with distilled water [1:20 (w/w)] in 125 mL polyethylene bottles; shaken on a reciprocating shaker (60 rpm) for 24 hours.	0.08	0.13	0.09	0.04	0.05	0.02		0.02			0.002	0.005
	Poultry litter	350		20.24	4.42	0.33	0.10	8.23	0.11		3.38			0.03	0.005
	Coconut shell	900		0.57	0.16	0.04	0.03	0.06	0.12		0.02			0.005	0.02
	Pine chip	350		8.06	0.28	0.06	0.23	0.13	3.30		0.10			0.10	0.07
	Pine chip/poultry litter	350		20.94	0.19	0.09	0.04	0.29	1.30		0.35			0.01	0.01
	Pine chip	700		0.63	0.15	1.33	0.05	0.05	0.02		0.02			0	0.01
	Hardwood	500		0.72	0.14	0.05	0.11	0.05	0.41		0.01			0.002	0.01
	Macadamia nut shell	500		0.02	0.10	0.09	0.00	0.04	0.00		0.01			0.002	0.005
Zhao et al., 2013	Cow manure	500	Leaching of biochar with deionized water at a solid to liquid ratio of 1:1200 (w/v) for 16 hours at room temperature.	0.87		0.06	0.03		0.03				0.031		
	Pig manure	500		2.56		0.002	0.25		1.92				0.008		
	Chicken manure	500		5.33		0.07	0.04		0.10				0.006		
	Sawdust	500		1.18		0.03	0.01		0.03				0.013		
	Tree leaf	500		1.20		0.16	0.08		0.004						
	Grass	500		10.44		0.08	0.04		0.06				0.035		
	Rice straw	500		13.52		0.01	0.02		0.21				0.013		
	Wheat straw	500		19.83		0.17	0.05		0.04						
	Peanut shell	500		1.86		0.03	0.03		0.02						
	Corncob	500		10.38		0.01	0.01		0.10						

Reference	Feedstock	Pyrolysis temp. [°C]	Leaching method	K^+	Na^+	Ca^{2+}	Mg^{2+}	Cl^-	P	PO_4^{3-}	S	SO_4^{2-}	N	NH_4^+-N	NO_3^--N
	Rice hull	500		1.37		0.03	0.09		0.38						
	Sugarcane	500		2.97		0.01	0.03		0.08						
	Polly seed hull	500		6.89		0.05	0.06		0.08				0.002		
	Shrimp hull	500		1.86		0.02	0.04		0.28						
	Bone dregs	500		10.38		0	0.0005		0.37				0.298		
	Eggshell	500		1.37		0.05	0.01		0.002						
	Chlorella	500		31.52		0.12	0.10		0.15						
	Waterweeds	500		12.26		0.03	0.03		0.15						
	Waste paper	500		0.0002		0.11	0.10		0.001						
	Wastewater sludge	500		0.16		1.15	0.06		0.002				0.073		

Table A 21: Total TCE mass extracted for each consecutive extraction step from pre-loaded sorbents.

Sorbent	TCE [mg extracted]											
	AC			BC-WC			BC-GH			BC-CM		
Replicate	1	2	3	1	2	3	1	2	3	1	2	3
	0.01 S_w											
Water-1	0.54	0.25	020	0.13	0.17	0.20	0.09	0.08	0.15	0.01	0.06	0.06
Water-2	0.73	0.80	0.94	0.31	0.30	0.36	0.29	0.10	0.35	0.02	0.05	0.03
Methanol	14.1	8.24	14.1	6.33	8.38	7.62	5.06	3.30	3.96	0.37	0.27	0.42
Toluene	15.4	12.6	22.8	0.66	2.40	2.71	1.74	1.89	1.93	0.15	0.19	0.25
n-hexane	6.63	7.42	8.40	3.99	0.98	1.26	0.66	1.19	0.56	0.09	0.10	0.14
	0.1 S_w											
Water-1	1.79	2.16	2.12	1.28	- [a]	0.61	0.64	0.69	0.77	0.84	0.76	0.84
Water-2	1.06	1.81	1.74	0.91	- [a]	0.80	0.37	0.80	0.83	0.26	0.20	0.10
Methanol	34.2	33.1	31.9	11.9	- [a]	15.7	13.0	10.3	8.00	1.96	1.76	1.06
Toluene	31.2	32.3	30.0	4.19	- [a]	3.27	4.16	2.53	2.81	0.50	0.47	0.44
n-hexane	17.2	16.2	18.1	2.09	- [a]	1.65	1.69	0.89	0.88	0.18	0.13	0.17
	S_w											
Water-1	8.32	- [b]	- [b]	4.51	- [b]	- [b]	4.02	- [b]	- [b]	6.89	- [b]	- [b]
Water-2	7.20	- [b]	- [b]	1.98	- [b]	- [b]	2.04	- [b]	- [b]	1.88	- [b]	- [b]
Methanol	48.3	- [b]	- [b]	10.1	- [b]	- [b]	8.18	- [b]	- [b]	3.73	- [b]	- [b]
Toluene	49.9	- [b]	- [b]	7.38	- [b]	- [b]	5.91	- [b]	- [b]	2.62	- [b]	- [b]
n-hexane	18.8	- [b]	- [b]	3.27	- [b]	- [b]	2.37	- [b]	- [b]	0.68	- [b]	- [b]

[a] Sample lost during extraction.

[b] Only one replicate performed.

Table A 22: Total PCE mass extracted for each consecutive extraction step from pre-loaded sorbents.

Sorbent	PCE [mg extracted]											
	AC			BC-WC			BC-GH			BC-CM		
Replicate	**1**	**2**	**3**	**1**	**2**	**3**	**1**	**2**	**3**	**1**	**2**	**3**
						0.01 S_W						
Water-1	0.39	0.35	0.29	0.02	0.01	0.01	0.05	0.02	0.02	0.02	0.02	0.01
Water-2	0.58	0.45	0.58	0.05	0.01	0.07	0.07	0.05	0.08	0.02	0.01	0.03
Methanol	6.69	4.54	11.6	0.69	0.71	1.18	0.86	0.90	1.08	0.21	0.22	0.16
Toluene	36.9	37.5	44.7	0.57	0.59	0.52	0.52	0.32	0.42	0.07	0.11	0.10
n-hexane	7.83	10.2	6.18	0.29	0.34	0.27	0.31	0.37	0.32	0.03	0.03	0.03
						0.1 S_W						
Water-1	1.42	1.95	2.11	0.14	0.09	0.07	0.11	0.39	0.11	0.13	0.13	0.12
Water-2	1.60	2.06	2.81	0.34	0.11	0.13	0.11	0.27	0.08	0.05	0.05	0.06
Methanol	24.7	31.7	25.0	2.49	2.71	2.57	2.39	2.80	1.94	0.47	0.71	0.48
Toluene	20.6	20.9	15.7	1.25	1.29	1.37	1.00	1.26	0.83	0.30	0.30	0.27
n-hexane	13.8	12.2	16.4	0.62	0.70	0.66	0.49	0.75	0.59	0.14	0.10	0.11
						S_W						
Water-1	6.06	- [a]	- [a]	0.59	- [a]	- [a]	1.99	- [a]	- [a]	1.54	- [a]	- [a]
Water-2	2.25	- [a]	- [a]	0.76	- [a]	- [a]	1.52	- [a]	- [a]	0.67	- [a]	- [a]
Methanol	37.0	- [a]	- [a]	8.71	- [a]	- [a]	7.30	- [a]	- [a]	5.52	- [a]	- [a]
Toluene	55.1	- [a]	- [a]	3.96	- [a]	- [a]	3.96	- [a]	- [a]	1.70	- [a]	- [a]
n-hexane	21.9	- [a]	- [a]	1.96	- [a]	- [a]	1.26	- [a]	- [a]	0.19	- [a]	- [a]

[a] Only one replicate performed.